

# Thermodynamic stabilities of complex phases and their assemblages in Ag-Te, Ag- Bi-S and Ag-Cu-S systems

---

Fiseha Tesfaye

# Thermodynamic stabilities of complex phases and their assemblages in Ag-Te, Ag-Bi-S and Ag-Cu-S systems

**Fiseha Tesfaye**

A doctoral dissertation completed for the degree of Doctor of Science (Technology) to be defended, with the permission of the Aalto University School of Chemical Technology, at a public examination held at the lecture hall V1 of the school (Espoo, Finland) on August 15th 2014 at noon.

**Aalto University**  
**School of Chemical Technology**  
**Department of Materials Science and Engineering**  
**Metallurgical Thermodynamics and Modelling Research Group**

**Supervising professor**

Professor Pekka Taskinen

**Thesis advisor**

Professor Pekka Taskinen

**Preliminary examiners**

Professor Geir Martin Haarberg, Norwegian University of Science and Technology (NTNU), Norway

Professor Andres Öpik, Tallinn University of Technology, Estonia

**Opponent**

Professor Bogusław Zbigniew Onderka, AGH University of Science and Technology, Poland

Aalto University publication series

**DOCTORAL DISSERTATIONS** 100/2014

© Fiseha Tesfaye

ISBN 978-952-60-5763-7

ISBN 978-952-60-5764-4 (pdf)

ISSN-L 1799-4934

ISSN 1799-4934 (printed)

ISSN 1799-4942 (pdf)

<http://urn.fi/URN:ISBN:978-952-60-5764-4>

Unigrafia Oy

Helsinki 2014

Finland

Publication orders (printed book):

[fiseha.tesfaye@aalto.fi](mailto:fiseha.tesfaye@aalto.fi)

[http://materials.aalto.fi/en/research/groups/metallurgical\\_thermodynamics\\_and\\_modelling/](http://materials.aalto.fi/en/research/groups/metallurgical_thermodynamics_and_modelling/)

**Author**

Fiseha Tesfaye

**Name of the doctoral dissertation**

Thermodynamic stabilities of complex phases and their assemblages in Ag-Te, Ag-Bi-S and Ag-Cu-S systems

**Publisher** School of Chemical Technology**Unit** Department of Materials Science and Engineering**Series** Aalto University publication series DOCTORAL DISSERTATIONS 100/2014**Field of research** Metallurgy**Manuscript submitted** 2 May 2014**Date of the defence** 15 August 2014**Permission to publish granted (date)** 17 June 2014**Language** English **Monograph** **Article dissertation (summary + original articles)****Abstract**

Currently, most of the available sulphide ores are low-grades and also becoming increasingly complex. The complex groups of ores can constitute anything from trace amounts to major proportions of minerals; such as tellurides, sulphides and sulfosalts. Among these minerals, the silver-based tellurides and sulfosalts are commonly encountered in ores for the production of base and precious metals. However, unlike the binary sulphides, their thermodynamic properties are poorly known. Recently, the silver-based chalcogenides have also emerged as promising novel functional materials for many applications. Therefore, accurate thermodynamic data concerning the silver-based chalcogenides determined within this thesis have considerable fundamental and practical importance in many aspects of extractive and physical metallurgy.

To acquire thermodynamic data the solid state EMF method was used. The method has been improved for more accurate thermodynamic measurements as well as to overcome experimental challenges in the presence of volatile components. State-of-the-art equipment has been utilized and a new philosophy for constructing the galvanic cell and a new experimental arrangement to control the temperature gradient over the galvanic EMF cell were employed. The thermodynamic measurements on the phases of interest were conducted below  $T = 700$  K.

Based on the experimental results, thermodynamic properties of equilibrium phase assemblages in the two-phase regions of the Ag-Te system have been explicitly determined. New experimental data were also obtained and used to determine eutectic, eutectoidic decomposition and phase transition temperatures. In the Ag-Bi-S system, thermodynamic properties of pavonite, matildite and schapbachite at bismuth- and sulphur-saturation conditions have been determined. Prior to this work, the effects of saturation of sulphur and bismuth on the thermodynamics of the ternary phases were not known distinctively. In addition, new experimental thermodynamic data of the ternary phases over wide temperature ranges were obtained. Thermodynamic properties of the other silver-based phases of interest, stromeyerite and the solid solution  $(\text{Ag,Cu})_2\text{S}_{\text{SS}}$ , were also studied. For the first time, thermodynamic properties of the solid solution were experimentally determined. The experimental data obtained within this thesis together with the selected literature data enabled the determination of accurate thermodynamic functions for 36 selected equilibrium reactions.

**Keywords** silver-based phases, solid solubility, equilibrium, electrochemistry, thermodynamic and thermochemical properties

**ISBN (printed)** 978-952-60-5763-7**ISBN (pdf)** 978-952-60-5764-4**ISSN-L** 1799-4934**ISSN (printed)** 1799-4934**ISSN (pdf)** 1799-4942**Location of publisher** Helsinki**Location of printing** Helsinki**Year** 2014**Pages** 137**urn** <http://urn.fi/URN:ISBN:978-952-60-5764-4>



**Tekijä**

Fiseha Tesfaye

**Väitöskirjan nimi**

Kompleksifaasiin termodynaamiset stabiilisuudet systeemeissä Ag-Te, Ag-Bi-S ja Ag-Cu-S

**Julkaisija** Kemian tekniikan korkeakoulu**Yksikkö** Materiaalitekniikan laitos**Sarja** Aalto University publication series DOCTORAL DISSERTATIONS 100/2014**Tutkimusala** Metallurgia**Käsitteilyajankohdan pvm** 02.05.2014**Väitöspäivä** 15.08.2014**Julkaisuluvan myöntämispäivä** 17.06.2014**Kieli** Englanti **Monografia** **Yhdistelmäväitöskirja (yhteenvedo-osa + erillisartikkelit)****Tiivistelmä**

Suurin osa nykyisin saatavilla olevista sulfidisista malmeista ovat heikkolaatuisia ja entistä kompleksisempia. Kompleksiset sulfidimalmilaadut sisältävät hivenainejäämiä sekä merkittäviä mineraalipitoisuuksia, kuten tellurideja, sulfideja ja sulfosuoloja. Näistä mineraaleista hopeapohjaiset telluridit ja sulfosuolat esiintyvät yleisimmin perus- ja jalometallien valmistusprosesseissa. Toisin kuin binääristen sulfidien tapauksessa, näiden mineraalien termodynaamiset ominaisuudet ovat vielä huonosti tunnettuja. Hiljattain hopeapohjaiset kalkogeenidit ovat osoittautuneet lupaavaksi tutkimuskohteeksi etsittäessä uusia funktionaalisia materiaaleja erilaisiin teknisiin sovelluksiin. Tässä väitöstyössä tutkittujen hopeapohjaisten kalkogeenidien termodynaamisten ominaisuuksien määrittäminen on näin ollen tärkeää monilla prosessimetallurgian ja fysikaalisen metallurgian osa-alueilla. Hopeapohjaisten kalkogeenidien tarkkojen termodynaamisten ominaisuuksien määrittämiseksi käytettiin EMF-menetelmää. Kyseinen menetelmä on kehitetty termodynaamisten datan tarkkaan mittaamiseen ja se soveltuu myös haastavien helposti haihtuvien aineiden tutkimukseen. Tässä väitöstyössä on käytetty nykyistä huipputasoa edustavaa tutkimuslaitteistoa ja galvaanisten kennojen kokoamiseen on käytetty uutta menetelmää. Tutkimusmenetelmä perustuu uudelleen koelaitteistoon, jolla voidaan hallita galvaanisen EMF-kennon lämpötilagradientin käyttäytymistä. Tutkittujen faasiin termodynaamisten ominaisuuksien mittaukset on tehty alle 700 K lämpötilassa. Ag-Te-systeemin faasitasapainokoostumuksien termodynaamiset ominaisuudet kaksifaasi-alueella on määritetty selkeästi. Systeemistä saatiin uutta kokeellista tietoa ja väitöstyössä on määritetty eutektoidinen hajoamispiste sekä systeemin faasiinmuutoslämpötilat. Ag-Bi-S-systeemissä pavoniitin, matildiitin ja schapbaciitin termodynaamiset ominaisuudet vismutin ja rikin saturaatio-olosuhteissa määriteltiin kokeellisesti. Ennen tätä tutkimusta rikki- ja vismutti-saturaation vaikutukset ternääriseen systeemin faasiin termodynaamisten ominaisuuksien kannalta eivät ole olleet selkeästi tiedossa. Lisäksi saatiin uutta kokeellista termodynaamista tietoa ternääriseen systeemin faaseista laajalla lämpötila-alueella. Myös muiden mielenkiinnon kohteena olevien hopeapohjaisten faasiin, kuten stromeyriitin ja  $(\text{Ag,Cu})_2\text{S}_{12}$  kiinteän liuoksen termodynaamisia ominaisuuksia on tutkittu. Tämän kiinteän liuoksen termodynaamisia ominaisuuksia on tutkittu kokeellisesti ensimmäistä kertaa. Tässä väitöstyössä saatu kokeellinen sekä kirjallisuudesta valittu tieto ovat mahdollistaneet 36 valitun tasapainoreaktion termodynaamisten funktioiden määrittämisen.

**Avainsanat** hopea-pohjaiset faasit, kiinteä liukoisuus, tasapainotila, sähkökemian, termodynaamiset ja kemialliset ominaisuudet

**ISBN (painettu)** 978-952-60-5763-7**ISBN (pdf)** 978-952-60-5764-4**ISSN-L** 1799-4934**ISSN (painettu)** 1799-4934**ISSN (pdf)** 1799-4942**Julkaisupaikka** Helsinki**Painopaikka** Helsinki**Vuosi** 2014**Sivumäärä** 137**urn** <http://urn.fi/URN:ISBN:978-952-60-5764-4>



# Preface

The research work presented in this doctoral thesis was conducted at Aalto University School of Chemical Technology, in the research group of Metallurgical Thermodynamics and Modelling (TDM), between May 2010 and December 2013.

First of all, I would like to express my deepest appreciation to my supervisor and advisor, Professor Pekka Taskinen. His world-class expertise in the field of metallurgy has been a great source of learning and professional inspiration for me. I feel privileged in having him as my supervisor.

This Ph.D. project work has been conducted with the support of Improved Sulphide Smelting (ISS) – a project of the FIMECC-ELEMET programme and Tekes – the Finnish Funding Agency for Technology and Innovation. The ISS project was also supported financially by Outotec (Finland) Oy, Boliden Harjavalta, Boliden Kokkola, and Norilsk Nickel Finland Oy. The Academy of Finland via the Graduate School of Advanced Materials and Processes (AMP) at Aalto University has also provided financial support. Technology Industries of Finland Centennial Foundation has covered two travel costs for presenting my research results in international conferences. All financial supports provided by these groups are greatly appreciated.

Members of the ISS steering group are acknowledged for their encouragement and interest towards my work. The current and previous doctoral candidates of the TDM research group are thanked for their mutual co-operation. M.Sc.(Tech.) Markus Aspiala and M.Sc.(Tech.) Hanna Viitala above all are thanked for their assistance with the experiments. Thanks also to the workshop personnel in the Department of Materials Science and Engineering for the help provided in building the experimental setups.

My thanks also go to Dr. Marko Kekkonen and Dr. David Lloyd for their interest and proofreading of this compendium. I would also like to thank Professor Michael Gasik for his guidance and advice at the beginning of my doctoral studies, and Professor Guven Akdogan from Stellenbosch University, RSA, for his encouragement and advice.

My workmates in the research groups TDM, MTG and MVT are acknowledged for their help, support and pleasant working environment.

Finally, the warmest thanks to my parents and my wife Anne for their love, trust and encouragement, my daughter Tina for being the most wonderful and caring creature in the universe, and who gives purpose to everything I do.

Espoo, 2 May 2014

Fiseha Tesfaye

# List of publications

This doctoral dissertation consists of a summary and of the following publications which are referred to in the text by their corresponding Roman numerals. The original publications are found in Appendices [I–VI].

- [I] **F. Tesfaye**, P. Taskinen, M. Aspiala, D. Feng, “Experimental thermodynamic study of intermetallic phases in the binary Ag-Te system by an improved EMF method,” *Intermetallics* 34 (2013) 56–62.
- [II] **F. Tesfaye**, P. Taskinen, M. Aspiala, “Thermodynamic investigation of intermetallic phases in the binary system Ag-Te,” in: J. Harre, U. Waschki (Eds.), *Proceedings of European Metallurgical Conference EMC 2011*, vol. 3, Düsseldorf, Germany, 2011, pp. 1111–1124. ISBN: 978-394027638-4
- [III] **F. Tesfaye**, P. Taskinen, “Experimental thermodynamic study of the equilibrium phase  $\text{AgBi}_3\text{S}_5$  by an improved EMF method,” *Thermochim. Acta* 562 (2013) 75–83.
- [IV] **F. Tesfaye**, P. Taskinen, “Electrochemical study of the thermodynamic properties of matildite ( $\beta\text{-AgBiS}_2$ ) in different temperature and compositional ranges,” *J. Solid State Electrochem.* 18 (2014) 1683–1694.
- [V] **F. Tesfaye**, P. Taskinen, “Experimentally determined thermodynamic properties of schapbachite ( $\alpha\text{-AgBiS}_2$ ) below  $T = 700$  K,” *J. Chem. Thermodyn.* 70 (2014) 219–226.
- [VI] **F. Tesfaye**, P. Taskinen, “Thermodynamic properties of equilibrium phases in the Ag-Cu-S system below 500 K: experimental study,” in: J. Yurko, L. Zhang, A. Allanore, C. Wang, J.S. Spangenberg, R.E. Kirchain, J.P. Downey, L.D. May (Eds.), *EPD Congress 2014*, John Wiley and Sons, Inc., Hoboken, NJ, USA, 2014, pp. 185–193.

## Author’s contribution

In all publications [I–VI], the author defined the research plan together with the co-authors. The author improved the experimental method, carried out all experimental work and wrote the first version of the manuscripts. The final versions were prepared by the author based on the input from the co-authors.

# List of abbreviations and symbols

## Abbreviations

EMF	Electromotive Force
EDS	Energy Dispersive Spectrometer
SEM	Scanning Electron Microscope
PRT	Platinum Resistance Thermometer

## Symbols

L	liquid
g	gas
$T$	temperature [K]
$T_{tr}$	phase transformation temperature [K]
$T_m$	melting temperature [K]
$P$	pressure [atm]
$\Delta_r H^\circ$	standard enthalpy of reaction [ $\text{kJ}\cdot\text{mol}^{-1}$ ]
$\Delta_f H^\circ$	standard enthalpy of formation [ $\text{kJ}\cdot\text{mol}^{-1}$ ]
$\Delta_{mix} H^\circ$	standard enthalpy of mixing [ $\text{kJ}\cdot\text{mol}^{-1}$ ]
$\Delta_{tr} H^\circ$	standard enthalpy of phase transition [ $\text{kJ}\cdot\text{mol}^{-1}$ ]
$S^\circ$	standard entropy of the pure substances [ $\text{kJ}\cdot(\text{K}\cdot\text{mol})^{-1}$ ]
$\Delta_r S^\circ$	standard entropy of reaction [ $\text{kJ}\cdot(\text{K}\cdot\text{mol})^{-1}$ ]
$\Delta_f S^\circ$	standard entropy of formation [ $\text{kJ}\cdot(\text{K}\cdot\text{mol})^{-1}$ ]
$\Delta_{mix} S^\circ$	standard entropy of mixing [ $\text{kJ}\cdot(\text{K}\cdot\text{mol})^{-1}$ ]
$G^\circ$	standard Gibbs energy of the pure substances [ $\text{kJ}\cdot\text{mol}^{-1}$ ]
$\Delta_r G^\circ$	standard Gibbs energy of reaction [ $\text{kJ}\cdot\text{mol}^{-1}$ ]
$\Delta_f G^\circ$	standard Gibbs energy of formation [ $\text{kJ}\cdot\text{mol}^{-1}$ ]
$\Delta_{mix} G^\circ$	standard Gibbs energy of mixing [ $\text{kJ}\cdot\text{mol}^{-1}$ ]
$\Delta_{tr} G^\circ$	standard Gibbs energy of phase transition [ $\text{kJ}\cdot\text{mol}^{-1}$ ]
$\Delta_r c_p$	heat capacity of reaction at constant pressure [ $\text{kJ}\cdot(\text{K}\cdot\text{mol})^{-1}$ ]

$t$	ion transference number
$n$	number of electrons involved in virtual cell reaction
$F$	Faraday constant, $96487 \text{ C}\cdot\text{mol}^{-1}$
$E_{\text{EMF}}$	EMF of a cell [V]
$N$	number of experimental points
$R^2$	coefficient of determination

### **Subscripts and superscripts**

r	reaction
f	formation
tr	transformation
i	species
$x, y, z$	mole fractions
P	at constant pressure/atm
°	standard state
mix	mixing
m	melting
ss	solid solution

# Table of contents

Preface.....	i
List of publications.....	ii
Author's contribution.....	ii
List of abbreviations and symbols.....	v
Table of contents.....	vii
1. Introduction.....	1
1.1 Previous experimental thermodynamic studies.....	2
1.2 Objective of the thesis.....	2
1.3 New scientific contribution.....	3
1.4 Application.....	4
1.5 Structure of the thesis.....	4
2. The EMF method with solid state electrolytes.....	5
2.1 Experimental requirements.....	5
2.2 Ag <sup>+</sup> ion conducting solid electrolytes.....	6
2.2.1 Properties of AgI and RbAg <sub>4</sub> I <sub>5</sub> .....	7
2.3 Thermodynamics of electrochemical cells.....	8
2.3.1 Gibbs energy of formation.....	8
2.3.2 Simplified calculations of $\Delta_rG^\circ$ .....	9
3. Partial phase relations in selected Ag-based systems.....	10
3.1 The binary Ag-Te system.....	10
3.2 The ternary Ag-Bi-S system.....	11
3.3 The ternary Ag-Cu-S system.....	12
4. Experimental section.....	14
4.1 Materials synthesis and characterizations.....	14
4.1.1 Chemical analysis.....	15
4.2 The electrochemical cells.....	15
4.3 Experimental procedures.....	16
4.3.1 Furnaces and measuring devices.....	16
4.3.2 Protective atmosphere.....	17
4.3.3 Temperature and EMF measurements.....	17
5. Results and discussion.....	18
5.1 $E_{EMF}$ values.....	18
5.2 Ag-Te system.....	18

5.2.1	$E_{EMF}$ values (cathode: Ag-Te-phase assemblages) .....	19
5.2.2	Thermodynamic functions of the Ag-tellurides .....	24
5.3	Ag-Bi-S system .....	27
5.3.1	$E_{EMF}$ values (cathode: Ag-Bi-S phase assemblages) .....	28
5.3.2	$\Delta_r G^\circ$ values of reactions including Ag-Bi-sulfosalts .....	32
5.3.3	$\Delta_r G^\circ$ values of pavonite .....	33
5.3.4	$\Delta_r G^\circ$ values of matildite and schapbachite .....	37
5.4	Ag-Cu-S system .....	46
5.4.1	$E_{EMF}$ values (cathode: Ag-Cu-S phase assemblages) .....	46
5.4.2	Thermodynamic functions in Ag-Cu-S system .....	48
6.	Conclusions .....	49
7.	References .....	51

# 1. Introduction

Due to intense mining of high grade metal sulphide ores in the past, currently, the available sulphide ores are poor in valuable metals and are also becoming increasingly complex; such that the production of high grade metals by conventional pyrometallurgical processes is compromised. Consequently, smelters need to modify their operating flow sheets and strategies for processing more complex feed materials economically, while meeting strict environmental regulations [1]. To make appropriate modifications, accurate thermodynamic data of selected phases and phase assemblages which exist in these complex sulphide ores are essential.

The complex group of non-ferrous metal ore minerals varies from trace amounts to major proportions of tellurides, sulphides and sulfosalts. Among the tellurides, silver-tellurides are characteristic minerals and the major carriers of precious metals in epithermal gold deposits, which are sources for about 10 % of gold mining [2]. They also exist as inclusions, intergrowths and overgrowths in sulphide ore minerals for the production of noble and base metals [3–5].

Although sulfosalts rarely form massive ore bodies, they are commonly associated with metal rich sulphide ores for the production of base and precious metals [6]. For instance, silver-bearing sulfosalts are encountered in ores for the production of the base metals and are common sources of silver. Ag-Bi sulphides often occur in many types of hydrothermal Au-Ag ore deposits [7].  $\text{AgBi}_3\text{S}_5$  and  $\text{AgBiS}_2$  are relatively common sulfobismuthide minerals in non-ferrous metal sulphide ores. Among the silver-based sulfosalts, stromeyerite ( $\text{Ag}_{0.9}\text{Cu}_{1.1}\text{S}$ ) is a relatively common ore mineral in most hydrothermal vein and replacement copper deposits [8].

The quaternary Ag–In–Sb–Te system, including the Ag-Te-intermetallic phases, is widely used for making phase-change discs, such as compact rewritable discs (CD-RW) and rewritable digital versatile discs (DVD + RW) [9,10]. Recently, silver-based sulfosalts have also emerged as promising novel functional materials for different applications. For instance,  $\text{AgBi}_3\text{S}_5$  is known for its good thermoelectric properties, particularly, its solid solution  $\text{AgSb}_{0.3}\text{Bi}_{2.7}\text{S}_5$  [11]. The ternary chalcogenide semiconducting compound  $\text{AgBiS}_2$  is under intensive study due to its unique electronic and magnetic properties which can be applied in linear, nonlinear, optoelectronic, and thermoelectric devices as well as optical recording media [12–20]. The solid solution  $(\text{Ag,Cu})_2\text{S}_{8s}$  and ternary chalcogenide compound  $\text{Ag}_{0.9}\text{Cu}_{1.1}\text{S}$  are also under study due to their high ionic conductivity and gradual disorder in the sequential phase transitions [21].

Nevertheless, unlike the binary sulphides, thermodynamic properties of silver-based tellurides and sulfosalts are poorly known. Reliable thermodynamic data are essential for accurate quantitative modelling of the stabilities of tellurides and sulfosalts and their chemical behaviour in the presence of other equilibrium

phases. These accurate thermochemical data can support process improvement, in the extractive metallurgy of valuable metals, as well as product development work, in the design of novel multi-component inorganic functional materials.

## 1.1 Previous experimental thermodynamic studies

Kiukkola [22], Kiukkola and Wagner [23], Valverde [24] as well as Sitte and Brunner [25] have extensively studied the thermodynamic properties of silver-based tellurides using the EMF method and solid state coulometric titration. Recently, Echmaeva and Osadchii [2,26] and Chareev et al. [27] reported the Gibbs energies of formation of  $\text{Ag}_5\text{Te}_3$  (stützite) below  $T = 505$  K, after performing experimental studies by the EMF method. In spite of these investigations, no complete thermodynamic analysis for the entire silver-tellurium system has been undertaken, including the low and intermediate temperature ranges.

Bryndzia and Kleppa [28] determined the enthalpy of formation of  $\text{AgBi}_3\text{S}_5$ ,  $\beta$ - $\text{AgBiS}_2$  and  $\alpha$ - $\text{AgBiS}_2$  at 298.15 K, and the enthalpy of polymorphic phase transition of  $\text{AgBiS}_2$  at 468 K, by the high-temperature direct synthesis calorimetric method. Schmidt et al. [29,30], Shykhyev et al. [31] and, recently, Voronin and Osadchii [7] have studied the thermodynamic properties of  $\text{AgBi}_3\text{S}_5$  and  $\beta$ - $\text{AgBiS}_2$  below  $T = 383$  K, by the EMF method. Craig and Barton [32] estimated the Gibbs energies of formation of  $\alpha$ - $\text{AgBiS}_2$  in the temperature range 544–1074 K, by reanalysing experimental thermodynamic data reported in [6,33,34], with  $\text{S}_2(\text{g})$  as the standard state of sulphur at 1 atm. Neither study reported experimental data which considered each temperature region of the stable phases  $\text{S}(\text{s})$ ,  $\text{S}(\text{L})$ ,  $\text{Bi}(\text{s})$ ,  $\text{Bi}(\text{L})$ , nor thermodynamic properties of the ternary phases at different solubility limits.

## 1.2 Objective of the thesis

For the purpose of compiling accurate thermodynamic databases of the equilibrium binary and ternary phases in the Ag-Te, Ag-Bi-S and Ag-Cu-S systems, only few experimental studies in different temperature and compositional ranges have been published. In addition, this incomplete thermodynamic data reported by different researchers, prior to this work, is inconsistent to some extent. The accuracy of the experimental techniques used has also left some room for improvement. Therefore, the objectives of this thesis were:

1. to improve the EMF method for more accurate thermodynamic measurements of alloys and compounds,
2. to determine accurate experimental thermodynamic properties of selected tellurides and sulfosalts in different temperature regions and solubility limits, and
3. to contribute new experimental thermodynamic data in the selected systems in compositional and temperature ranges that have not been experimentally studied before.

Thermodynamic properties of the silver-tellurium-intermetallic phases have been studied by several researchers. However, no complete thermodynamic analysis for the entire silver-tellurium system has been undertaken, including below  $T = 700$  K. The available experimental thermodynamic data of the silver-based sulfosalts are neither accurate enough nor sufficient to describe their thermodynamic properties over a wider temperature range.

To achieve our goal of compiling accurate thermodynamic data on the phases of interest, the EMF method has been selected as the most appropriate method to study thermodynamic stabilities of the phases. This method has proven to be direct, effective, and most accurate for the determination of Gibbs energies and entropies of reactions [35]. The experimental data obtained together with literature data can be used to derive other standard thermodynamic functions of the studied equilibrium phases or equilibrium reactions involving them.

### 1.3 New scientific contribution

The new scientific information obtained within this thesis consists of an improved EMF method for thermodynamic measurements of alloys and compounds and the experimentally determined thermodynamic properties of equilibrium phases and their assemblages in the Ag-Te, Ag-Bi-S and Ag-Cu-S systems. The EMF method has been improved by introducing unique techniques and state-of-the-art equipment. This improved technique facilitated highly accurate and new thermodynamic measurements.

In the Ag-Te system, new experimental points were obtained and the thermodynamic properties of the stoichiometric equilibrium phase assemblages;  $\text{Ag}_5\text{Te}_3\text{-Te}$ ,  $\text{Ag}_5\text{Te}_3\text{-Ag}_{1.9}\text{Te}$ ,  $\text{Ag}_5\text{Te}_3\text{-Ag}_2\text{Te}$  and  $\text{Ag}_2\text{Te-Ag}_{1.9}\text{Te}$ , have been determined explicitly *in situ* at low and intermediate temperatures. The eutectic temperature of the reaction  $1.3\beta\text{-Ag}_5\text{Te}_3(\text{s}) + 2.1\text{Te} \rightleftharpoons \beta\text{-Ag}_5\text{Te}_3(\text{s}) + 4.5[\text{Ag}_{0.333}\text{Te}_{0.667}](\text{L})$  has been accurately determined and new experimental thermodynamic functions above the eutectic temperature have been obtained.

In the Ag-Bi-S system, the thermodynamic properties of  $\beta\text{-AgBiS}_2$ ,  $\alpha\text{-AgBiS}_2$  and  $\text{AgBi}_3\text{S}_5$  at bismuth- and sulphur-saturation conditions have been experimentally determined. Prior to this work, the effect of saturation of sulphur and bismuth on the thermodynamic properties of the ternary phases were not known. In addition, new experimental thermodynamic data of the ternary phases in temperature ranges that have not been experimentally studied before were determined.

In the Ag-Cu-S system, thermodynamic functions of stromeyerite ( $\text{Ag}_{0.9}\text{Cu}_{1.1}\text{S}$ ) in equilibrium with  $\text{Cu}_{2-x}\text{S}$  and  $\text{CuS}$  have been determined including temperature ranges over which thermodynamic measurements have never been made. For the first time, thermodynamic quantities for the solid solution  $(\text{Ag,Cu})_2\text{S}_{\text{ss}}$  have been experimentally determined.

## 1.4 Application

Industrial raw materials for metals production are becoming increasingly complex. Their behaviour during smelting is difficult to predict without a good knowledge of their thermodynamic properties.

Silver-based tellurides and sulfosalts are relatively common minerals in precious and base metal ores. Thus, smelters are in need of accurate thermochemical data of the complex phase systems, which will be used in modification of operating flow sheets and outlining strategies for processing the complex feed materials economically and in an environmentally friendly manner. The accurate and new thermodynamic properties of several silver-based tellurides and sulfosalts determined in this thesis can contribute to the needed data sets.

The accurately determined thermochemical data can also be used for improved manufacturing of novel inorganic functional materials incorporating the studied chalcogenides. For instance, with accurate thermochemical data of chalcogenides, it is possible to estimate their behaviour in an oxidizing atmosphere, as well as at elevated temperature conditions.

Therefore, accurate and extended knowledge of the thermodynamic properties of the silver-based tellurides and sulfosalts are of considerable fundamental and practical interest in many aspects of extractive and physical metallurgy.

## 1.5 Structure of the thesis

This thesis consists of four scientific peer-reviewed journal publications [I,III–V], two peer-reviewed conference publications [II,VI] and the present compendium. The articles have all been published and are attached in the Appendices [I–VI].

Chapter 2 of the thesis presents the EMF method in solid state electrochemistry studies and gives an insight into basic principles, state-of-the-art and the benefits of the method. Chapter 3 gives an overview of selected phase relations in the studied binary and ternary systems. Phase equilibria studies that do not involve our experimental binary and ternary phases and above  $T = 700$  K are left as outside of the scope of this thesis. Chapter 4 presents a detailed summary of the experiments that have been reported in [I–VI]. The results and discussion are given in Chapter 5, followed by the conclusions in Chapter 6.

## 2. The EMF method with solid state electrolytes

There are three major groups of experimental methods to determine thermodynamic properties of materials. These are calorimetry, vapour pressure measurements and EMF methods. Calorimetry is a very convenient method to determine enthalpy values precisely. In the vapour pressure methods, one usually tries to measure the partial pressures of individual components and to derive from them the thermodynamic activities and partial Gibbs energies. In the case where partial pressures can also be obtained as a function of temperature, this provides a way to calculate partial enthalpies and entropies, although these derived quantities are usually less accurate than the directly measured partial Gibbs energies. Introduced by Kiukkola [22] for solid state thermodynamic studies, the EMF method has proven to be direct, effective, and the most accurate method for determining the Gibbs energies of formation, chemical potentials, thermodynamic activities and partial pressures in equilibrium conditions. Furthermore, the entropies and enthalpies of reactions can be calculated from the temperature dependence of EMF in the cell [36].

Galvanic cells with solid electrolytes for thermodynamic studies consist of a solid electrolyte between the reference and the cathode electrodes [36]. These electrodes are connected to wires, which are usually Pt or Au, for measuring the EMF of the cell. In thermodynamic measurements, the EMF must be measured under open circuit conditions. This is usually assured by the use of high-resistance (above  $R = 10^{10} \Omega$ ) measuring devices, resulting in the measurement of an 'open circuit' potential [35,37]. In all our thermodynamic measurements [I–VI] the EMF was measured with an electrometer which has an input impedance of  $2 \cdot 10^{14} \Omega$ . Application of the EMF method for thermodynamic studies of metallic systems and its basic principles as well as requirements has been recently discussed in detail by a few researchers [35–41].

### 2.1 Experimental requirements

In EMF measurements for the determination of thermodynamic properties, it is important to ascertain the conditions under which the electrolyte shows the best performance. The main problems for successful cell operation are: finding a suitable electrolyte; and the exact identification of the single reversible process occurring at each electrode. The corresponding electrolyte should provide purely ionic conductivity in the temperature range where it is used, i.e., one single ion should be responsible for establishing the potential. A well-defined reversible reaction is required to establish the potential. From a practical point of view, there are several additional requirements [35,37]:

- the equilibrium potential at a given temperature should be established within a reasonable time;

- after temperature changes, the same equilibrium potential has to be established regardless of whether the temperature has been increased or lowered; and
- following polarization of the cell by a potential imposed from outside, again the same equilibrium potential has to be established.

In addition, there are a number of purely experimental requirements that have to be considered, especially in measurements at high temperatures [35,37,41]:

- any reaction between electrodes and electrolyte or between electrodes and lead wires must be negligible,
- if lead wires of different materials are used it is necessary to consider the corresponding thermal-EMF,
- any temperature gradient in the cell should be avoided;
- reactions between crucible materials and electrodes or electrolyte should be excluded,
- concentration changes due to the vapour pressure of the electrodes must be taken into consideration,
- any direct exchange of matter between the two electrodes (e.g., via the gas phase) has to be excluded, and
- any electrical interference between the furnace in which the cell is heated and the cell itself should be avoided, either by a proper winding of the furnace or by appropriate grounding.

Thermal-EMF and temperature gradients can be minimized by using similar lead material at both electrodes and by placing the cell within the constant heating zone of the experimental assembly, respectively [41]. Proper design of the galvanic cells and their flexibility in the furnace while measurements are conducted will also help to minimize temperature differences at both ends of the electrodes, as described in [I,III–V]. In this thesis, all these experimental requirements were fulfilled.

## 2.2 Ag<sup>+</sup> ion conducting solid electrolytes

Solid electrolytes are materials in which the electric current is carried predominantly by ions. They can be oxides, halides, iodides, sulphides and other types of solid materials. Solid electrolytes have gained considerable attention due to their role in various scientific and technological applications as they are being used in electrochemical cells to measure chemical potentials in gases, liquids and solids.

One of the most important criteria for a solid electrolyte to be used in EMF cells for thermodynamic studies is that it should be a purely ionic conductor, or at least has only a negligible contribution of electronic conduction. Thus, if electric current is carried solely by ions, the ion transference number  $t$ , in Equation (1), should be greater than 0.99 at experimental conditions [35,42].

$$t = \frac{\sigma(\text{ion})}{\sigma(\text{ion}) + \sigma(\text{elec})} \quad (1)$$

where  $\sigma(\text{ion})$  is ionic conductivity and  $\sigma(\text{elec})$  is electronic conductivity.

In the thermodynamic studies of silver-based alloys and compounds,  $\text{RbAg}_4\text{I}_5$  and  $\text{AgI}$  are two widely used fast ionic conductors of  $\text{Ag}^+$  ions. These electrolytes were also used in our study by the EMF method. Properties of the solid electrolytes and their usage limits in the EMF method are reviewed in Section 2.2.1.

### 2.2.1 Properties of $\text{AgI}$ and $\text{RbAg}_4\text{I}_5$

At ambient pressure conditions,  $\text{AgI}$  exists in three different crystalline forms;  $\gamma$ - $\text{AgI}$ ,  $\beta$ - $\text{AgI}$  and  $\alpha$ - $\text{AgI}$ . The  $\beta$ -  $\rightarrow$   $\alpha$ - $\text{AgI}$  phase transition temperature is 420 K, which is accompanied by a significant increase in ionic conductivity [43-46]. At the phase transition temperature, the ionic conductivity of  $\alpha$ - $\text{AgI}$  is  $1.31 \text{ S}\cdot\text{cm}^{-1}$  [47]. One of the three crystalline forms of  $\text{RbAg}_4\text{I}_5$ ,  $\alpha$ - $\text{RbAg}_4\text{I}_5$  is thermodynamically stable within the temperature range 209–505 K and can be used as an electrolyte even at room temperatures [45,48]. At 298.15 K,  $\alpha$ - $\text{RbAg}_4\text{I}_5$  shows a high ionic conductivity of  $\sim 0.21 \text{ S}\cdot\text{cm}^{-1}$  [49].

Ionic conductivity in solid electrolytes is usually due to lattice defects, and in  $\text{AgI}$ -based electrolytes these defects are caused by large cation disorders [35,46]. Chemical diffusion occurs in the presence of concentration or chemical potential gradient and it results in net transport of mass. For example, when local differences in stoichiometry equilibrate, metal or non-metal ions and electrons diffuse simultaneously. These phenomena are described by the chemical diffusion coefficient  $D$  [36]. At low-temperatures, the ionic conductivity generally follows the Arrhenius-type temperature dependence [45,46,50].

$\text{AgI}$ -based electrolytes possess a large amount of free sites for the  $\text{Ag}^+$  ions to move. Due to the presence of these excess sites for  $\text{Ag}^+$  ions [51] and quasi-molten state of  $\text{Ag}^+$  ions in the structure [45], as well as the presence of passageways for  $\text{Ag}^+$  ions which are formed by the face-sharing tetrahedral [52];  $\alpha$ - $\text{AgI}$  is a fast ionic conductor of  $\text{Ag}^+$  ions. In  $\alpha$ - $\text{RbAg}_4\text{I}_5$ , iodide ions are arranged in a similar structure as manganese atoms are in  $\beta$ - $\text{Mn}$ , so that one unit cell, which includes  $\text{RbAg}_4\text{I}_5$ , contains 56 tetrahedral sites, such that  $\text{Ag}^+$  ions can move freely in the lattice. The large  $\text{Rb}^+$  ions are surrounded by highly distorted iodide octahedral and are not mobile [47,49].

The ion transference number of  $\alpha$ - $\text{AgI}$ , in the temperature range 420–713 K, is  $1 \pm 0.01$  [53]. Below its melting temperature, at  $T_m = 505 \text{ K}$ ,  $\alpha$ - $\text{RbAg}_4\text{I}_5$  is a high ionic conductor of  $\text{Ag}^+$  ions with negligible electronic conduction [45,54].

Based on various conductivity data and/or EMF data, Patterson [55] has shown that in the electrolytic conduction domain of  $\text{AgI}$ , the chemical potential of silver in  $\text{AgI}$  changes only slightly. Using the compiled thermodynamic data of Barin [56], we calculated activities of silver ( $a_{\text{Ag}}$ ) in  $\text{AgI}$  at  $P_{\text{I}_2(\text{g})} = 1 \text{ atm}$  (for the dissociation reaction  $2\text{AgI} \rightleftharpoons 2\text{Ag} + \text{I}_2(\text{g})$ ), as a function of temperature. According to results from our analysis, the  $a_{\text{Ag}}$  in  $\text{AgI}$  varied between  $2.5\cdot 10^{-9}$  at 420 K,  $1.2\cdot 10^{-7}$  at 500 K and  $3.6\cdot 10^{-5}$  at 700 K. Thus, the chemical potential of silver in  $\text{AgI}$  does not change significantly, in its ionic conduction domain. Therefore, the solid electrolytes  $\text{AgI}$  and  $\text{RbAg}_4\text{I}_5$  can be safely used in their respective pure ionic conduction domains (420–713 K and 298–505 K, respectively) for EMF cells in the experimental thermodynamic studies of silver-based phases.

## 2.3 Thermodynamics of electrochemical cells

For a general galvanic cell with a solid electrolyte and elements A and B:



at equilibrium, the incorporation of  $A^{+n}$  or  $A^{-n}$  at the interface into the cathode or the overall electrochemical reaction of the galvanic cell can be expressed by a virtual electrochemical cell reaction (I).



The amount of work, other than the work for volume expansion, which is necessary for the transfer of one mole of element A in a valence state  $n$  from its pure state into a A-B-compound, is related to the transfer of a charge  $n \cdot F$  by;

$$\mu_A(A - B - \text{compound}(s)) - \mu_A^\circ(A) = -n \cdot F \cdot E_{EMF} \quad (2)$$

or

$$\Delta_r G^\circ = -n \cdot F \cdot E_{EMF} \quad (3)$$

where  $\mu_A$  is the chemical potential of substance A in the A-B-compound(s) and  $\mu_A^\circ$  is the standard chemical potential of substance A in pure substance A, which is 1.

The Gibbs energies of our isobaric equilibrium reactions were calculated directly from the measured  $E_{EMF}$  vs.  $T$  relations, by using the basic thermodynamic Equation (3) of an electrochemical cell. In a similar way, the entropies, enthalpies and heat capacities of the studied virtual reactions were calculated using Equations (4)–(6).

$$\Delta_r S^\circ = -n \cdot F \cdot \left( \frac{\partial E_{EMF}}{\partial T} \right) \quad (4)$$

$$\Delta_r H^\circ = -n \cdot F \cdot \left[ E_{EMF} - \left( \frac{\partial E_{EMF}}{\partial T} \right) \cdot T \right] \quad (5)$$

$$\Delta_r C_p = -n \cdot F \cdot \left( \frac{\partial^2 E_{EMF}}{\partial T^2} \right) \cdot T. \quad (6)$$

### 2.3.1 Gibbs energy of formation

By definition, the reaction of formation of a species M can be written as:



where a, b, m etc are stoichiometric coefficients, and the standard Gibbs energy of formation is:

$$\Delta_f G^\circ = G_{\text{products}}^\circ - G_{\text{reactants}}^\circ = mG_M^\circ - aG_A^\circ - bG_B^\circ - \dots \quad (7)$$

The standard Gibbs energies of formation of the studied multicomponent phases were calculated by combining the Gibbs energies of the virtual electrochemical cell

reactions (calculated according to Equation (3)) and the standard Gibbs energies of the pure components, for which literature data are available. The standard entropies of pure compounds have been calculated by:

$$S_M^\circ = \Delta_f S_M^\circ + S_A^\circ + S_B^\circ + \dots \quad (8)$$

Gibbs energy of phase transition at the transformation temperature  $T_{tr}$  can be expressed by:

$$\Delta_{tr} G^\circ = \Delta_{tr} H^\circ - \left( \frac{\Delta_{tr} H^\circ}{T_{tr}} \right) \cdot T. \quad (9)$$

The high or low temperature experimental points were extrapolated to low or high temperatures, respectively, by using the Gibbs energies of phase transitions expressed by Equation (9).

### 2.3.2 Simplified calculations of $\Delta_f G^\circ$

According to Craig and Barton [32], temperature-dependent standard Gibbs energies of formation of some sulfosalts can be approximated, based on assumption of near-ideal mixing of simple sulphide end members to produce sulfosalts of intermediate composition. In the estimate of Gibbs energy of mixing ( $\Delta_{mix} G^\circ = \Delta_{mix} H^\circ - \Delta_{mix} S^\circ \cdot T$ ), enthalpy of mixing was assumed to be zero. Their approximation formula is:

$$\Delta_f G_{\text{Sulfosalt}}^\circ = \sum_1^n (x_i \Delta_f G_{\text{Sulfide}}^\circ) + \Delta_{mix} H^\circ - [(5.02 \pm 3.35) \cdot R \cdot T \cdot \sum_1^n (x_i \ln x_i)], \quad (10)$$

where  $x_i$  is the mole fraction of the  $i^{\text{th}}$  binary sulphide component. In the case of  $\text{AgBi}_3\text{S}_5$  and  $\beta\text{-AgBiS}_2$ , Bryndzia and Kleppa [28] concluded that the assumption of  $\Delta_{mix} H^\circ = 0 \text{ kJ}\cdot\text{mol}^{-1}$  made by Craig and Barton [32] is reasonable. However, they reported an experimental value of  $\Delta_{mix} H^\circ = 12 \text{ kJ}\cdot\text{mol}^{-1}$  for the high temperature phase  $\alpha\text{-AgBiS}_2$ .

We calculated the  $\Delta_f G^\circ$  values of the studied multi-component phases also by using Equation (10) and thermochemical data of Barin [56]. Comparisons of the results obtained by this approximation method with those of our experimental results are discussed in Chapter 5.

### 3. Partial phase relations in selected Ag-based systems

This chapter summarizes previous phase equilibria studies related to the binary phases of the Ag-Te system and the ternary phases of the Ag-Bi-S and Ag-Cu-S systems. More details of partial phase relations in the studied systems can be found in [I–VI].

#### 3.1 The binary Ag-Te system

The condensed equilibrium phases of the Ag-Te system are the liquid with a miscibility gap and the solid phases: Ag(fcc), Te(cph), and three intermetallic compounds  $\text{Ag}_2\text{Te}$ ,  $\text{Ag}_{1.9}\text{Te}$  and  $\text{Ag}_5\text{Te}_3$  [57]. An enlargement of the two-phase regions  $\text{Ag}_2\text{Te}-\text{Ag}_5\text{Te}_3$ ,  $\text{Ag}_2\text{Te}-\text{Ag}_{1.9}\text{Te}$ ,  $\text{Ag}_{1.9}\text{Te}-\text{Ag}_5\text{Te}_3$  and  $\text{Ag}_5\text{Te}_3-\text{Te}$  in the Ag-Te phase diagram, in which our thermodynamic measurements were performed, is shown in Figure 1. Stützite,  $\text{Ag}_{5 \pm x}\text{Te}_3$ , has a wide homogeneity field, where  $0.23 < x < 0.37$  [2]. The phase diagram presented by Karakaya and Thompson [57] and the experimental studies of Kracek et al. [58] using the XRD and DTA techniques imply that below  $T = 503$  K  $\alpha\text{-Ag}_2\text{Te}$ ,  $\beta\text{-Ag}_2\text{Te}$ ,  $\alpha\text{-Ag}_{1.9}\text{Te}$ ,  $\beta\text{-Ag}_{1.9}\text{Te}$  and  $\alpha\text{-Ag}_5\text{Te}_3$  are the stable phases of the binary Ag-Te system. In this work, all the three Ag-Te-intermetallic phases were synthesized from the pure elements by a method described in Chapter 4.

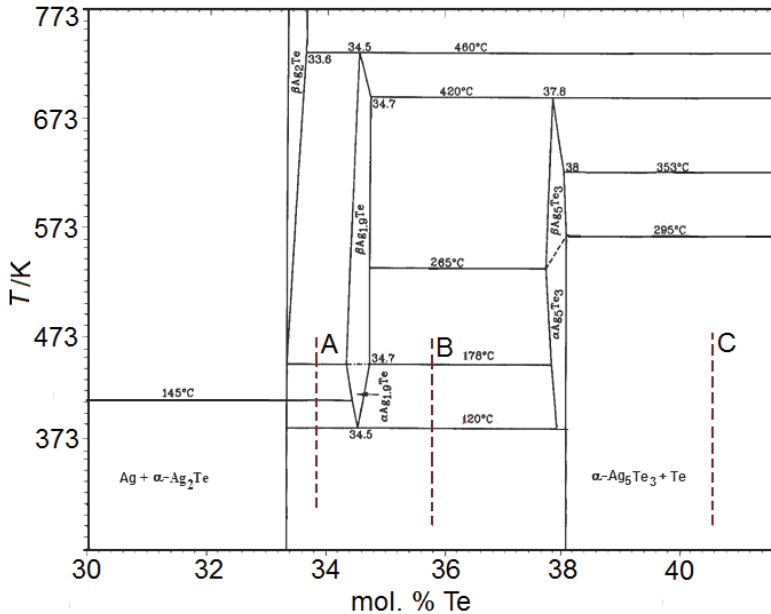


**Figure 1.** A magnified phase diagram of the Ag-Te system (redrawn from [2,57]) with dashed lines showing the compositions and temperature ranges of EMF measurements performed in [I,II].

Phase stabilities in the Ag-Te system have been investigated by several authors, using various experimental techniques. However, solid solubilities in the system are not well-defined. Thermodynamic studies of Sitte and Brunner [25] below  $T = 596$  K suggested that the maximum solubility of Ag into (Te) to be less than 0.7 at. %. The maximum solubility of Te into (Ag) is about  $5 \cdot 10^{-3}$  at. % [59].

Karakaya and Thompson [57] and Gierlotka [60] have made an assessment of this system, based on the available literature data. Experimental thermodynamic data of the binary Ag-Te system were manifested to be incomplete. In order to calculate the whole phase diagram accurately new thermodynamic data are essential. The dashed lines in Figure 1 with notations A, B and C indicate temperature and compositional ranges of the cathode electrodes in the study of thermodynamic properties of Ag-Te-intermetallic compounds that are presented in Chapter 5.

### 3.2 The ternary Ag-Bi-S system

In this thesis, only the ternary phases of the Ag-Bi-S system were experimentally studied. This chapter summarizes phase equilibria studies related to the ternary phases prior to this work. More details of partial phase relations in the Ag-Bi-S system were reviewed in [III–V].

AgBiS<sub>2</sub> was the first ternary phase to be synthesized in the Ag-Bi-S system [61]. Then, Nuffidd [62] reported the existence of an additional sulfosalt, pavonite (AgBi<sub>3</sub>S<sub>5</sub>). Recently, Kim et al. [11] synthesized pavonite with an approximated composition of Ag<sub>0.95</sub>Bi<sub>3.30</sub>S<sub>5</sub>. The composition of pavonite and matildite synthesized in our study, by a method described in Chapter 4, have approximate compositions of Ag<sub>1±0.01</sub>Bi<sub>3.03±0.01</sub>S<sub>5±0.01</sub> and AgBi<sub>0.98±0.02</sub>S<sub>1.95±0.04</sub>, respectively.

An extensive study, below  $T = 1123$  K, conducted by Van Hook [63] and the results of Chang et al. [64] have shown that all the ternary phases exist on the tie line Ag<sub>2</sub>S-Bi<sub>2</sub>S<sub>3</sub>. In contrast to AgBiS<sub>2</sub>, AgBi<sub>3</sub>S<sub>5</sub> is stoichiometric and exists in only one structural form below  $T_m(\text{incongruent}) = 1005 \pm 4$  K [65]. Wu [66], and Gather and Blachnik [67] reported pavonite to melt congruently at  $1018 \pm 5$  K and  $994$  K, respectively. However, Kim et al. [11] reported pavonite (Ag<sub>0.95</sub>Bi<sub>3.30</sub>S<sub>5</sub>) to melt congruently at  $1008$  K. These deviations could be as a result of the differences in the composition of pavonite.

According to Craig [65] the maximum solid solubility limits into AgBi<sub>3</sub>S<sub>5</sub> and the solid solubility of bismuth into AgBiS<sub>2</sub> are less than 1 mol. %. The solid solubility of AgBi<sub>3</sub>S<sub>5</sub> in Bi<sub>2</sub>S<sub>3</sub> is less than 1 wt. %. Above  $T = 473$  K, AgBiS<sub>2</sub> can dissolve an excess of Ag<sub>2</sub>S and Bi<sub>2</sub>S<sub>3</sub> into solid solution [64,65].

The phase relations in the bismuth and sulphur rich corners of the ternary Ag-Bi-S system below  $T = 723$  K are shown in Figure 2, which are illustrated based on Craig's [68] isothermal phase diagram at  $623$  K and the literature information about the phase stabilities in the binary systems [69–75], below  $T = 723$  K.

Below its congruent melting point at  $T_m = 1074 \pm 4$  K, AgBiS<sub>2</sub> exists in two structural forms [65]. The low-temperature phase  $\beta$ -AgBiS<sub>2</sub>, which corresponds to mineral matildite, is hexagonal ( $D_{3d}(5)$ -R3m,  $a = 4.07 \pm 0.02$  Å,  $c = 19.06 \pm 0.05$  Å) and the high temperature phase  $\alpha$ -AgBiS<sub>2</sub> is cubic ( $F_{m3m}$ ,  $a_0 = 5.648 \pm 0.002$  Å)

[76]. Experiments on stoichiometric  $\text{AgBiS}_2$  indicate that the cubic form ( $\alpha$ - $\text{AgBiS}_2$ ) is stable above  $T = 468 \pm 5$  K and coexists with the hexagonal form ( $\beta$ - $\text{AgBiS}_2$ ) in the temperature range from  $468 \pm 5$  K to  $455 \pm 3$  K, and below  $T = 455 \pm 3$  K the hexagonal form is the stable phase [65]. According to Wu [66,77], at temperatures above  $T = 468.15 \pm 5$  K matildite inverts to a cubic PbS-like structure, schapbachite ( $\alpha$ - $\text{AgBiS}_2$ ). The coexistence of schapbachite and matildite ( $\beta$ - $\text{AgBiS}_2$ ) has also been reported in the microspheres and flower-like  $\text{AgBiS}_2$  morphologies synthesized on different templates at  $\sim 453$  K [15, 19]. In the presence of  $\text{Ag}_2\text{S}$  or  $\text{AgBi}_3\text{S}_5$  only the  $\alpha$ - $\text{AgBiS}_2$  occurs above  $T = 455 \pm 3$  K [65].

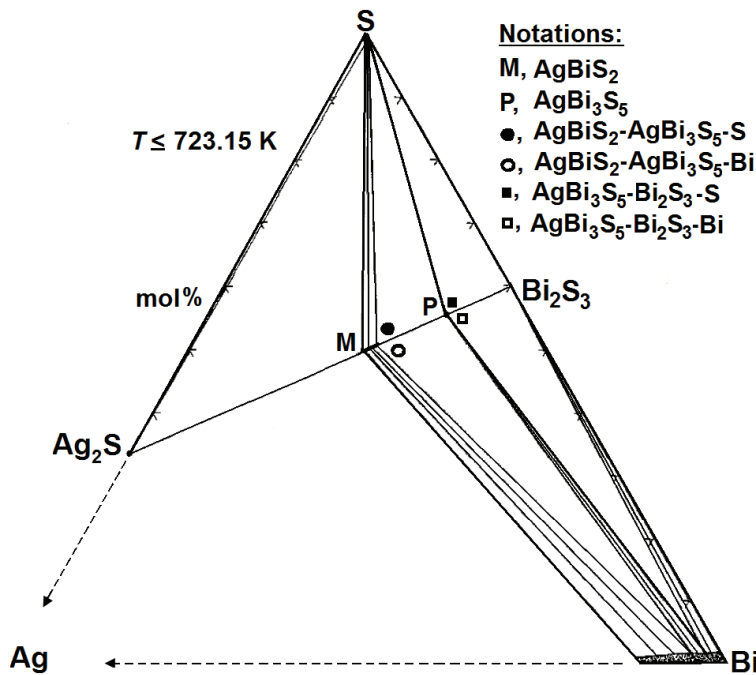


**Figure 2.** Phase diagram of Ag-Bi-S in the Bi- and S-rich regions: Liquid bismuth appears above  $T = 544.592$  K [III, 78]. Solid and open circles and squares indicate compositions of the cathode materials of our chemical cells [III-V].

### 3.3 The ternary Ag-Cu-S system

The orthorhombic compound anilite ( $\text{Cu}_{1.75}\text{S}$ ) is stable up to  $348 \pm 3$  K and the orthorhombic djurleite ( $\text{Cu}_{1.934}\text{S}$ ) is stable up to  $366 \pm 2$  K [79]. The monoclinic low-chalcocite ( $\alpha$ - $\text{Cu}_2\text{S}$ ) is stable up to 376 K and the hexagonal high-chalcocite ( $\beta$ - $\text{Cu}_2\text{S}$ ) is stable in the temperature range 376–708 K [80]. Covellite ( $\text{CuS}$ , hexagonal-R) is stable up to 780 K [79,80].

All the ternary phases of the Ag-Cu-S system exist on the  $\text{Ag}_2\text{S}$ - $\text{Cu}_2\text{S}$  join and are stable only at temperatures below  $T = 392$  K [81,82]. At  $T = 363$  K,  $\text{Ag}_{0.93}\text{Cu}_{1.07}\text{S}$  transforms congruently to the solid solution of  $\text{Cu}_2\text{S}$  and  $\text{Ag}_2\text{S}$  ( $\text{Ag}_y\text{Cu}_{2-y}\text{S}$ , hcp) [82]. At higher temperatures solid solutions  $\text{Ag}_y\text{Cu}_{2-y}\text{S}$ (hcp) and  $\text{Ag}_{2-y}\text{Cu}_y\text{S}$ (bcc) are the dominant phases [81]. According to Skinner [83] and Frueh [84], stromeyerite ( $\text{Ag}_{1-z}\text{Cu}_{1+z}\text{S}$ ) exhibits extended stoichiometric variation of  $0 \leq z \leq 0.1$ . The

$\text{Ag}_{0.89}\text{Cu}_{1.1}\text{S}$  reported by Takuhara et al. [85] as the stable phase of stromeyerite is in agreement with the estimated stoichiometric variation of stromeyerite. We synthesized stromeyerite of composition  $\text{Ag}_{0.9}\text{Cu}_{1.1}\text{S}$  to be used in our galvanic cell, by a method described in Chapter 4. Partial phase relations including the three phase region  $\text{Ag}_{0.9}\text{Cu}_{1.1}\text{S}-\text{Cu}_{2-x}\text{S}-\text{CuS}$  below  $T = 363 \text{ K}$ , in which our experimental composition lies, are shown in Figure 3. More details on the ternary system can be found in [VI].

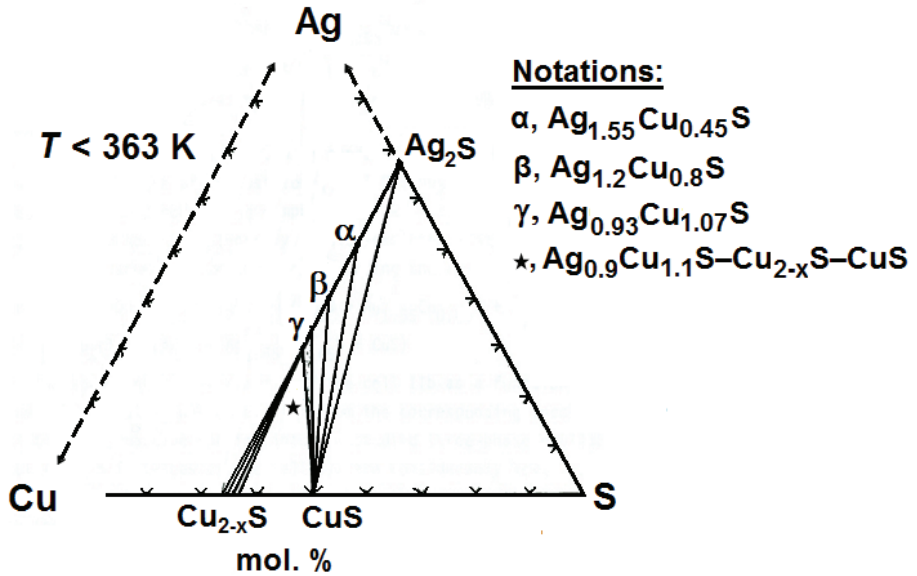


**Figure 3.** A portion of isothermal phase diagram of the ternary Ag-Cu-S system, below  $T = 363 \text{ K}$  [VI]. Solid star indicates the composition of the cathode material in our galvanic cell (M) which is described in Chapter 5.

## 4. Experimental section

The binary phases in the Ag-Te system and the ternary phases in the Ag-Bi-S and Ag-Cu-S systems were synthesized from high purity substances purchased from Alfa Aesar (Germany). The conventional EMF technique has been improved in order to increase measurement accuracies as well as to avoid experimental difficulties in the study of the sulphide systems. An overview of the experimental techniques used in this thesis work is given below. More details of the experimental procedures as well as the state-of-the-art equipment used for temperature and EMF measurements have been described in [I–VI].

### 4.1 Materials synthesis and characterizations

The intermetallic compounds were synthesized from high purity Ag and Te. The pure substances, in a fine powder form, were mixed according to the appropriate stoichiometric compositions of the compounds and poured into alumina crucibles. The alumina crucibles were placed in a vertical tube furnace in flowing  $H_2(g)$  atmosphere, one at a time, and heated above the melting point of Ag ( $T_m = 1235\text{ K}$  [78]). After a dwelling time of 30 minutes the furnace was cooled to the room temperature.

The ternary phases  $AgBi_3S_5$  and  $AgBiS_2$  were synthesized from a mixture of fine powders of high purity  $Ag_2S$  and  $Bi_2S_3$ . The pure binary phases in powder form were mixed in the appropriate composition for each phase, sealed in a separate evacuated fused silica tube and annealed in a muffle furnace at 673 K for three days and at 873 K for twelve days. The ' $AgBi_3S_5$ ' phase was quenched in ice water, while the evacuated silica glass tube was intact, and the ' $AgBiS_2$ ' phase was left to cool slowly in the furnace.

The ternary phase  $Ag_{0.9}Cu_{1.1}S$  was synthesized from a mixture of fine powders of high purity  $Ag_2S$  and  $Cu_2S$ . The pure binary phases in powder form were mixed in the appropriate composition, sealed in an evacuated fused silica tube and annealed in a muffle furnace at 573 K for three days and at 873 K for ten days. In an attempt to homogenize, the sample was heated up to 1173 K and then cooled at a rate of  $4\text{ K}\cdot\text{min}^{-1}$  to 338 K. The sample was then annealed at 338 K for three weeks.

The solid  $RbAg_4I_5$  electrolyte was synthesized by mixing stoichiometric amounts of high purity  $RbI$  and  $AgI$  with water to form a thick fluid paste, and then by drying in a furnace, at a slowly increasing temperature [54]. Finally, the remaining reactant phases were heated in a vacuum furnace at 493 K for about two hours [54] and heated at 433 K for about two days [86], in the same furnace. The glassy greenish yellow material was stored in a vacuum furnace at 343 K before use. The provenance and purity of all the materials used in this thesis are given in Table 1.

**Table 1.** Provenance and purity of the materials used in this thesis work.

Chemical	Mass fraction purity	Source	CAS No.	Form
Bismuth	0.9999	Alfa Aesar (Germany)	7440-69-9	Pieces
Bismuth(III) sulphide	0.99999	Alfa Aesar (Germany)	1345-07-9	Lump
Carbon	0.999995	Alfa Aesar (Germany)	7440-44-0	Powder
Silver	0.999985	Alfa Aesar (Germany)	7440-22-4	Foil
Silver iodide	0.99999	Alfa Aesar (Germany)	7783-96-2	Powder
Silver(I) sulphide	0.999+	Alfa Aesar (Germany)	21548-73-2	Powder
Tellurium	0.99999	Alfa Aesar (Germany)	13494-80-9	Powder
Rubidium iodide	0.998	Alfa Aesar (Germany)	7790-29-6	Powder
Argon	0.99999	AGA (Finland)	2007A7	Compressed gas
Platinum	0.99998	Johnson Matthey, Noble Metals (England)	3085134/002	Wire
Copper (I) sulphide	0.995	Alfa Aesar (Germany)	22205-45-4	Powder
Copper (II) sulphide	0.998	Alfa Aesar (Germany)	1317-40-4	Powder

#### 4.1.1 Chemical analysis

With the combined SEM-EDS analysis, the surface images showing the homogeneity and chemical analysis of each sample of the synthesized phases were obtained. The equipment used within this work was a SEM LEO 1450 scanning electron microscope (Carl Zeiss Microscopy GmbH, Jena, Germany) which includes X-Max type EDS by Oxford Instruments (Abingdon, UK). The results of the element analysis were obtained with INCA-Energy software of Oxford Instruments. The SEM-EDS analyses confirmed the existence of single homogenous multi-component phases, in each case, within compositional ranges that are reported in the literature.

## 4.2 The electrochemical cells

The synthesized phases were ground into fine powders and mechanically well-mixed with additional components before pressing into pellets from 0.0015 kg to 0.005 kg. The synthesized compound  $\text{RbAg}_4\text{I}_5$  and the commercially available AgI were also pressed to obtain electrolyte pellets from 0.0035 kg to 0.005 kg. The cathode and electrolyte pellets were formed by pressing at a pressure of  $\sim 0.1$  GPa. A 1 mm thick silver-foil (Alfa Aesar, 99.9985 % purity) was used as a reference electrode. Small pieces of the silver-foil were cut such that their diameters were much less than that of the electrolyte pellets and pressed together with the electrolyte pellets, as shown in Figure 4.

The electrode and electrolyte pellets were assembled to form the solid state galvanic cells in the configurations represented by cell (ii). In some galvanic cells which incorporated pure bismuth as part of the cathode phase assemblage, high purity graphite pellets were inserted between the platinum lead wire and the cathode material. These additional layers of graphite pellets were introduced to prevent the potential dissolution of platinum into bismuth at our experimental temperatures [87].

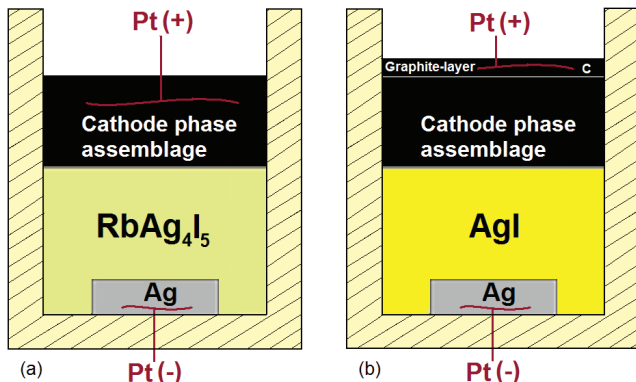


**Figure 4.** Schematic diagram of the structures of the electrochemical cells inside alumina crucibles [III,IV]; (a) materials of the cathode are composed of phase assemblage without pure bismuth and the electrolyte is RbAg<sub>4</sub>I<sub>5</sub>, (b) material of the cathode is composed of the phase assemblages that may or may not include bismuth and the electrolyte is AgI.

### 4.3 Experimental procedures

#### 4.3.1 Furnaces and measuring devices

The stable temperature region inside a Lenton tube furnace was located and, during all EMF measurements, temperatures on both sides of the galvanic cells were measured using two Pt100 sensors (platinum resistance thermometers, PRT). The PRTs, with tolerance class B 1/10 Din, i.e. ± 0.03 K variations at 273 K, according to the manufacturer, were calibrated in a mixture of ice and water at 273 K. The obtained resistance values above 100 Ω (0.02 Ω < 100 – R<sub>0</sub> < 0.03 Ω) were added to a program based on LabVIEW Code from National Instruments that records the temperature values from each PRT.

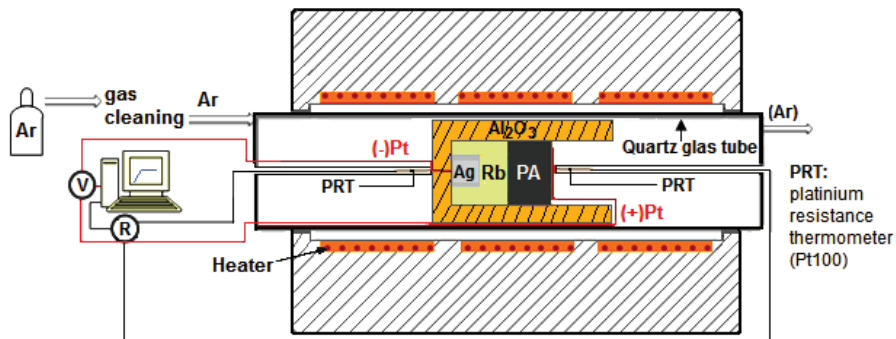


**Figure 5.** Schematic experimental set up for the EMF measurements in a horizontal tube furnace, the thin alumina tubes for holding the PRTs press the solid galvanic cells against the bottom of the alumina crucible to ensure good contact between the interfaces. Notations: PA stands for the cathode phase assemblages and Rb stands for RbAg<sub>4</sub>I<sub>5</sub> or AgI [I,III].

The platinum wires for the EMF measurements and the lead wires from the Pt100 sensors for temperature measurements were connected to a KEITHLEY-6517B-electrometer/high resistance meter and a KEITHLEY-2000-multimeter, respectively. The input impedance of the electrometer for voltage measurements is  $2 \cdot 10^{14} \Omega$ , which allows the cells to function in a reversible way, i.e., no external current is flowing [35]. The measured  $E_{EMF}$  values and temperatures were simultaneously transferred to a computer through IEE-488-GPIB-cable and a KEITHLEY-KUSB-488A USB-to-GPIB interface adapter and the readings were recorded by the program at a rate of two measured values in 5 seconds. A schematic diagram of the experimental setup is shown in Figure 5.

#### 4.3.2 Protective atmosphere

All experiments were run in a gas tight quartz glass tube, in a horizontal tube furnace. The protective atmosphere was Ar(g). The Ar(g), which was supplied as compressed in a cylinder, may contain impurities such as traces of O<sub>2</sub>(g) and H<sub>2</sub>O(g). The impurities can affect electrochemical reactions of the galvanic cells. To avoid the potential impurities effect, pure titanium was selected as a material to trap impurities prior to supply of Ar(g) to the experimental furnaces. Small pieces of chopped titanium plates were put into a separate gas tight tube furnace and Ar(g), which was fed by a DFC-digital mass flow controller (AALBORG-DFC26), was allowed to pass through them at 873 K before reaching the experimental furnaces that contained the electrochemical cell. The gas flow rate during all measurements was  $\sim 27.47 \text{ mL} \cdot \text{min}^{-1}$ . To avoid gaseous substances attacking the reference electrode (pure silver), exiting inert gas flow was directed toward the cathode electrode, as shown in Figure 5.

#### 4.3.3 Temperature and EMF measurements

Most measurements were performed by heating and cooling the cells in steps from 5 K to 20 K. To reach steady state EMF readings took from a few days up to a few weeks. The equilibrium was considered to be reached when the  $E_{EMF}$  values were constant or their variations were not significant ( $\Delta V \leq 0.1 \text{ mV}$ ) and they were oscillating about a certain value for several hours. By manually adjusting the horizontal position of the galvanic cells in the furnace and observing real-time temperature readings from the highly accurate PRTs, temperature difference between the two electrodes, during all measurements, were controlled to be less than 1 K. Thus, any possible thermoelectric effect in the cell EMF is negligible.

Functionality of the experimental system for EMF measurements was tested by measuring the EMF of the symmetric cell Ag | Ag<sup>+</sup> | Ag, which should not result in any measurable potential difference. The equilibrium was considered reproducible when the heating and cooling curves coincided.

## 5. Results and discussion

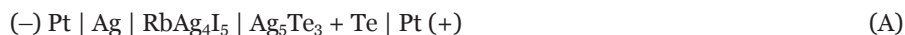
The results obtained within this thesis are presented in Appendices [I–VI], and a summary with discussion is given below. The results are divided into Ag-Te, Ag-Bi-S and Ag-Cu-S systems. Publications [I,II] were the beginning of the experimental study of silver-based systems. All the Ag-Te-intermetallic phases investigated were previously known to some extent, which made it easier to start the experiments. The experimental method was developed continuously in order to obtain as accurate results as possible. Consequently, the accuracies of the thermodynamic properties of the intermetallic compounds were improved and new experimental data were also obtained [I,II]. Publications [III–V] deal with the three principal ternary phases of the Ag-Bi-S-system and publication [VI] deals with selected multicomponent phases of the Ag-Cu-S system. Legends and references in figures presented in this chapter are modified to comply with the flow of information in this compendium, the original figures can be found in Appendices [I–VI]. The errors for the temperatures were calculated based on the errors in least squares regression of  $E_{EMF}$  values on temperature and the temperature differences obtained between the two ends of the galvanic cells. Decimals were rounded to the next whole number.

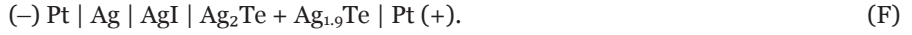
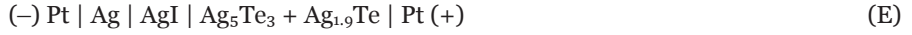
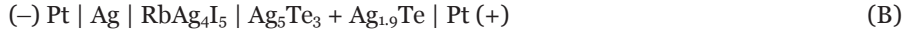
### 5.1 $E_{EMF}$ values

The  $E_{EMF}$  vs.  $T$  relations of the solid + solid and solid + liquid phases reaction in the different temperature regions of stable phases are linear and fit into equations of the type  $E_{EMF} = a + b \cdot T$  [2,23,25,26]. It suggests  $\Delta_r c_p = 0 \text{ kJ} \cdot (\text{K} \cdot \text{mol})^{-1}$  for the virtual cell reactions. Accordingly, analytical expressions for all measured  $E_{EMF}$  values as a function of temperature, in different temperature regions of phase stabilities, were calculated with correlation coefficients close to 1. Cell temperatures used in the calculations are mean values of temperatures measured at both ends of the galvanic cells. As mentioned in Chapter 4, temperature differences between the two electrodes during all measurements were controlled to be less than 1 K.

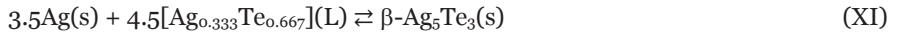
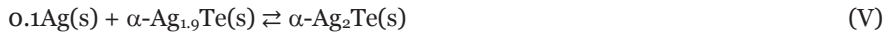
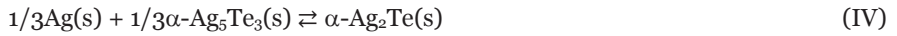
### 5.2 Ag-Te system

In this section, a combined summary of results obtained in the Ag-Te system, which were published in [I,II], is presented. In the Ag-Te system, thermodynamic measurements were conducted in the temperature range 298–690 K. The cell arrangement on which the measurements were conducted can be represented by galvanic cells (A)–(F).





Based on the literature data and the results of this study, the virtual electrochemical cell reactions of galvanic cells (A)–(F) can be explicitly written over temperature regions of the different stable phases as:



### 5.2.1 $E_{\text{EMF}}$ values (cathode: Ag-Te-phase assemblages)

#### *The $\text{Ag}_{1.9}\text{Te}$ – $\text{Ag}_2\text{Te}$ equilibrium (cell (C))*

The  $E_{\text{EMF}}$  values obtained with the galvanic cell (C) decreased sharply with increasing temperature from 388 K to 414 K. The observation is in reasonable agreement with the experimental results reported by Sitte and Brunner [25], as illustrated in Figure 6. However, the experimental points obtained in [I] align on the same line with a smaller scatter than those of Sitte and Brunner [25].

Above  $T = 412$  K, the  $\alpha$ -  $\rightarrow$   $\beta$ -phase transition of  $\text{Ag}_2\text{Te}$  is marked by the angular upward turn of the  $E_{\text{EMF}}$  vs.  $T$  curve. Results reported by Sitte and Brunner [25] as well as the results reported in [II], obtained with galvanic cells in which AgI was used as the solid electrolyte, are in agreement with the results obtained in [I]. However, the experimental points of Sitte and Brunner [25] are fewer and scattered. In extreme case, at  $T \approx 415$  K, their  $E_{\text{EMF}}$  values are 10 mV higher.

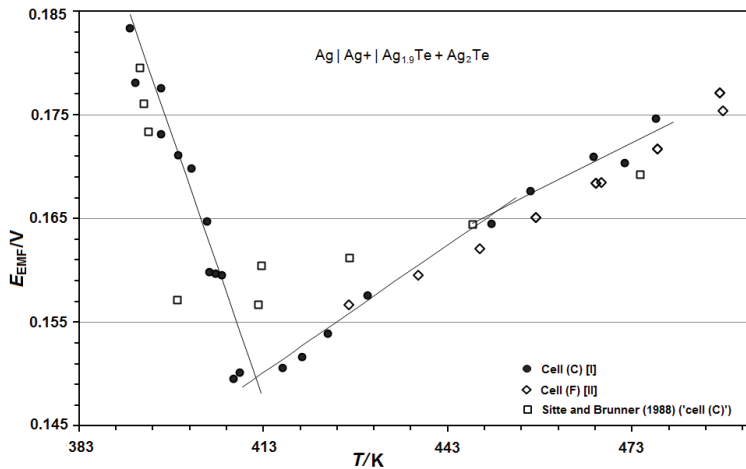


**Figure 6.**  $E_{EMF}$  vs.  $T$  relations obtained with the galvanic cell (C) together with the literature values, the least squares regression lines of  $E_{EMF}$  values on cell temperatures of publication [I] are shown with solid lines.

#### *The $Ag_2Te$ – $Ag_{1.9}Te$ – $Ag_5Te_3$ equilibrium (cells (B) and (C))*

Figure 7 shows the results of the  $Ag_5Te_3$ – $Ag_{1.9}Te$  and  $Ag_2Te$ – $Ag_{1.9}Te$  phase equilibria, from this work [I,II] and from the previous authors [2,25]. Below  $T = 388$  K, the obtained  $E_{EMF}$  vs.  $T$  relations with galvanic cells (B) and (C) [I] are in good agreement with the available literature values [2,25].

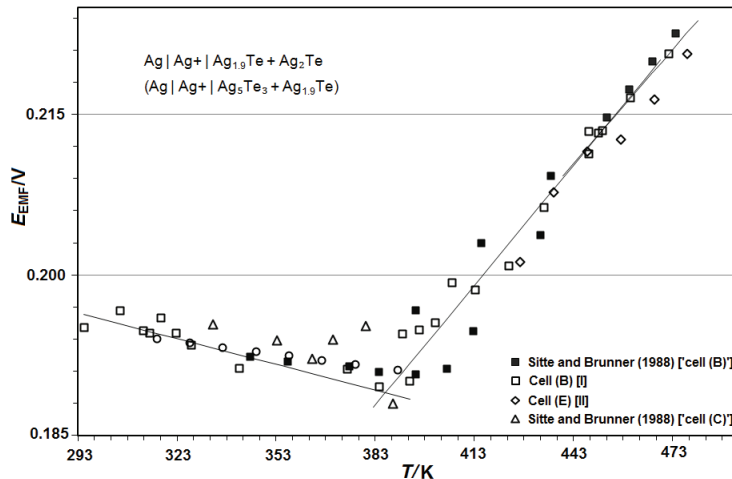


**Figure 7.** The  $E_{EMF}$  vs.  $T$  relations obtained on the galvanic cells (B) and (C) with the previous literature values, the least squares regression lines of  $E_{EMF}$  values on cell temperatures of publication [I] are shown with solid lines.

Below  $T = 393$  K, the EMF and temperature relations obtained using galvanic cells (B) and (C) are comparable and also coincide well with the results reported by Echmaeva and Osadchii [2] and Sitte and Brunner [25]. The results reported by Echmaeva and Osadchii [2], in which the two-phase composition (similar to the composition in cell (C)) was used as the cathode material directly, are in good

agreement with the results obtained in [I]. However, the results of Sitte and Brunner [25] show slightly higher  $E_{EMF}$  values for the same temperature range, as displayed in Figure 7.

Above  $T = 388$  K, the results obtained in this study lie on the least square line of Sitte's and Brunner's [25] experimental points. In the temperature range 426–470 K, the results obtained in [II] are in good agreement with the results obtained in [I], with different cell arrangement.

#### The $Ag_5Te_3 - Te$ equilibrium

Figure 8 shows the results for  $Ag_5Te_3$ -Te equilibrium of this study [I,II] and from the previous authors [25–27]. Above  $T = 426$  K, the results obtained in this study with AgI electrolyte [I] and  $RbAg_4I_5$  electrolyte [II] cells are in good agreement. Above  $T = 388$  K, the results reported by Echmaeva and Osadchii [26], Sitte and Brunner [25] and Chareev et al. [27] are also in agreement with the results obtained in [I]. The  $E_{EMF}$  vs.  $T$  results reported by Chareev et al. [27], which start at about 333 K, are slightly lower (from 3.48 mV to 0.01 mV) below  $T = 382$  K and slightly higher (from 3.5 to 0.7 mV) above  $T = 382$  K.

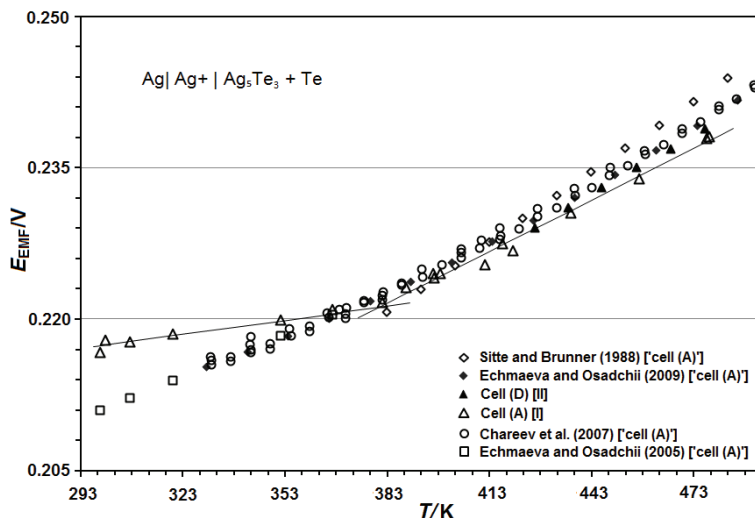


**Figure 8.**  $E_{EMF}$  vs.  $T$  relations obtained with the galvanic cells (A) and (D), together with the literature values [25–27]. The linear least square lines of the present work are shown with solid lines [I].

Below  $T = 358$  K the results reported by Echmaeva and Osadchii [26] are lower than the current observations from 5.7 mV to 1 mV, with the difference decreasing as the temperature increases. This deviation may also be attributed to the shift in the furnace peak temperatures, which in turn increase the temperature gradients along the cell. In the experimental work that resulted in publication [I], temperatures at both ends of the electrodes were simultaneously measured by the Pt100 sensors and these effects were noted and the necessary adjustments were made, as discussed in Chapter 4.

### The $\text{Ag}_2\text{Te}-\text{Ag}_{1.9}\text{Te}-\text{Ag}_5\text{Te}_3-\text{Te}$ equilibria

The  $E_{\text{EMF}}$  vs.  $T$  plots obtained through the linear least square fitting of the experimental points in [I] are summarized in Figure 9. A combined result of the electrochemical measurements in [I,II] are shown in Figure 10.

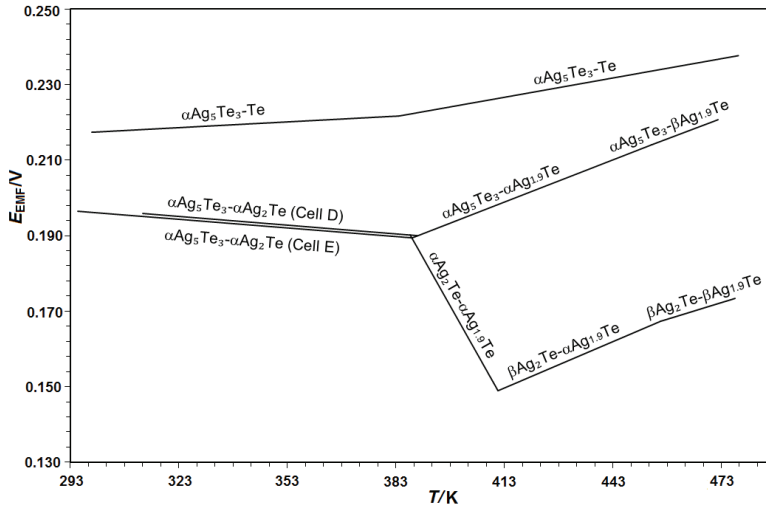


**Figure 9.**  $E_{\text{EMF}}$  vs.  $T$  plots obtained through least square fitting of the experimental data obtained in [I].

The results obtained with galvanic cell (C) in the temperature range 388–413 K show that the formation of the intermediate phase  $\text{Ag}_{1.9}\text{Te}$  is indicated by a sudden decrease of the  $E_{\text{EMF}}$  values with increasing temperature, as illustrated in Figure 9. This behaviour is in agreement with the experimental results reported by Sitte and Brunner [25]. Above  $T = 411$  K, the  $\alpha$ -  $\rightarrow$   $\beta$ - $\text{Ag}_2\text{Te}$  phase transition is indicated by the change of the slope in the  $E_{\text{EMF}}$  vs.  $T$  plot.

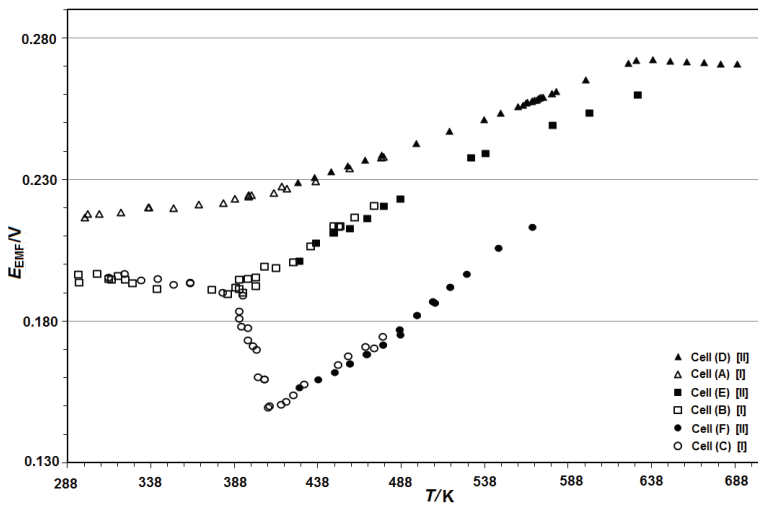


**Figure 10.** A summary of the  $E_{\text{EMF}}$  vs.  $T$  relations obtained with galvanic cells (A)–(C) [I,II].

The change in the slope of the  $E_{EMF}$  vs.  $T$  plot at about 451 K, as shown in Figure 9, is because of the phase transition  $\alpha$ -  $\rightarrow$   $\beta$ - $Ag_{1.9}Te$ . Over the two-phase region  $Ag_5Te_3$ - $Ag_{1.9}Te$ , the slope of  $E_{EMF}$  vs.  $T$  plot is also decreased at about 453 K, which obviously is caused by the phase transition of  $\alpha$ -  $\rightarrow$   $\beta$ - $Ag_{1.9}Te$ . In the temperature range 473–593 K, the two-phase region of  $Ag_{1.9}Te$ - $Ag_2Te$  exhibits a smooth linear  $E_{EMF}$  vs.  $T$  relation, as shown in Figure 10.

Figure 11 illustrates the  $E_{EMF}$  vs.  $T$  plot obtained with galvanic cell (D) and the literature values. The results obtained show a tendency for a larger scatter with increasing temperature. At lower temperatures all reported  $E_{EMF}$  values, particularly, the results of Echmaeva and Osadchii [2], are in good agreement with the results obtained in [II].

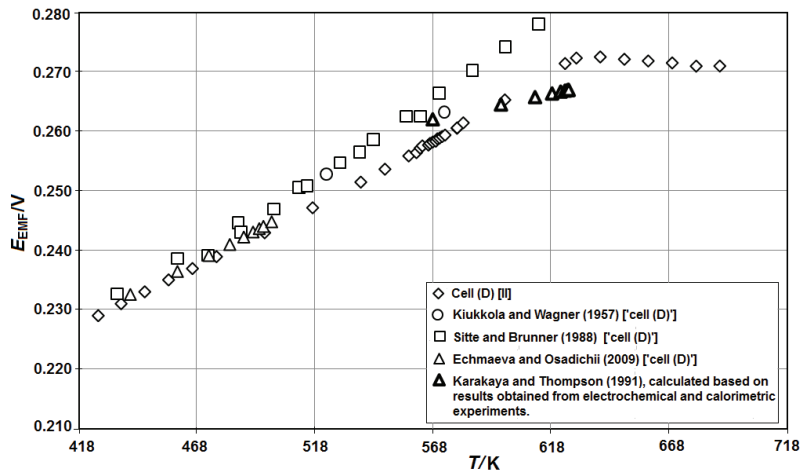


**Figure 11.**  $E_{EMF}$  vs.  $T$  plot obtained with galvanic cell (D) together with the literature values [II].

Below  $T = 568$  K, the  $E_{EMF}$  measured in the two-phase region  $Ag_5Te_3$ - $Te$  is increasing along with temperature, as shown in Figures 10 and 11. At about 382 K, the  $E_{EMF}$  vs.  $T$  plot turns upward with increasing temperature. A similar effect can also be observed in the works of [2,26]. This could be an indication for the particular case where  $\Delta_r c_p \neq 0$   $\text{kJ}\cdot(\text{K}\cdot\text{mol})^{-1}$ , as expressed by Echmaeva and Osadchii [2]. Future phase characterization works for this particular compositional and temperature range may confirm the solid phase relations that are involved in this reaction.

The slight bending of the  $E_{EMF}$  vs.  $T$  plot at about 568 K, as shown in Figure 10, can be interpreted to have been caused by the phase transition  $\alpha$ -  $\rightarrow$   $\beta$ - $Ag_5Te_3$ . In the temperature range 629–689 K the  $E_{EMF}$  vs.  $T$  relation flattens out, as shown in Figures 10 and 11. This is an indication of crossing the eutectic temperature, which according to these results exists at 629.6 K.

#### *Analytical forms of $E_{EMF}$ and $T_{tr}$*

The linear equations obtained for the  $E_{EMF}$  vs.  $T$  relations in [I,II] are compiled in Table 2.

By solving selected equations in Table 2 simultaneously, the temperature at which eutectoid decomposition of  $\alpha\text{-Ag}_{1.9}\text{Te} \rightleftharpoons 0.1\alpha\text{-Ag}_5\text{Te}_3 + 0.7\alpha\text{-Ag}_2\text{Te}$ , involving  $E_{\text{EMF}}$  values obtained with galvanic cells (C) and (F), is found to be  $390 \pm 3$  K. This is in the range of the eutectoid decomposition temperature reported by Kracek et al. [58],  $393 \pm 15$  K. The phase transition temperature for  $\alpha \rightarrow \beta\text{-Ag}_2\text{Te}$ , at  $\alpha\text{-Ag}_{1.9}\text{Te}$  saturation, is determined to be  $412 \pm 2$  K and that of  $\alpha \rightarrow \beta\text{-Ag}_{1.9}\text{Te}$  is  $451 \pm 3$  K. The former is in good agreement with the results reported by Mustafaev et al. [88], 410 K, and both values are in fair agreement with the results of Kracek et al. [58]. However, the phase transition temperature of  $\alpha \rightarrow \beta\text{-Ag}_2\text{Te}$ , at silver saturation, reported by Kracek et al. [58] ( $T_{\text{tr}} = 418 \pm 3$  K) is slightly higher. The slightly lower temperature of phase transition observed in this and Mustafaev's et al. [88] study is consistent with Frueh's [89] observation that the phase transformation temperature of  $\alpha \rightarrow \beta\text{-Ag}_2\text{Te}$  is slightly higher at the saturation of silver. The phase transition temperatures of  $\alpha \rightleftharpoons \beta\text{-Ag}_5\text{Te}_3$ , 568 K and  $\alpha \rightleftharpoons \beta\text{-[Ag}_{1.9}\text{Te} + \text{Ag}_2\text{Te}]$ , 450.52 K and eutectic temperature through the reaction  $1.3\beta\text{-Ag}_5\text{Te}_3 + 2.1\text{Te} \rightleftharpoons \beta\text{-Ag}_5\text{Te}_3 + 4.5[\text{Ag}_{0.333}\text{Te}_{0.667}](\text{L})$ , 629.73 K, were obtained. The eutectic temperature obtained in this study is 3.6 K higher than the value given in the assessment of Karakaya and Thompson [57], which is mainly based on the experimental DTA data of Kracek et al. [58].

**Table 2.** Values of the coefficients a and b, which were calculated by least squares linear regression of  $E_{\text{EMF}}$  values on temperature-values in the two-phase regions of the Ag-Te system [I,II].

Equilibrium phases	$E_{\text{EMF}}(\text{mV}) = a + b \cdot T$			T/K	N	Ref.
	a	$b \cdot 10^{-2}$	$R^2$			
$\alpha\text{-Ag}_5\text{Te}_3 + \text{Te}$	201.53	5.27	0.9652	298–382	7	[I]
	156.69	16.95	0.9893	382–477	12	[I]
	141.02	20.58	0.9995	426–569	18	[II]
$\beta\text{-Ag}_5\text{Te}_3 + \text{Te}$	124.32	23.52	0.9994	570–625	10	[II]
$\beta\text{-Ag}_5\text{Te}_3 + \text{L}(\text{Ag}_{0.333}\text{Te}_{0.667})$	289.56	-2.72	0.9210	628–690	7	[II]
$\alpha\text{-Ag}_5\text{Te}_3 + \alpha\text{-Ag}_2\text{Te}$ (in galvanic cell (C))	220.37	-7.83	0.9138	366–376	7	[I]
$\alpha\text{-Ag}_5\text{Te}_3 + \alpha\text{-Ag}_2\text{Te}$ (in galvanic cell (B))	219.44	-8.00	0.8763	377–498	10	[I]
$\alpha\text{-Ag}_2\text{Te} + \alpha\text{-Ag}_{1.9}\text{Te}$	854.00	-170.59	0.9358	391–409	12	[I]
	48.37	25.36	1.0000	426–448	3	[II]
$\beta\text{-Ag}_2\text{Te} + \alpha\text{-Ag}_{1.9}\text{Te}$	-19.254	41.00	0.9845	419–450	4	[I]
$\beta\text{-Ag}_2\text{Te} + \beta\text{-Ag}_{1.9}\text{Te}$	30.698	29.94	0.8263	456–477	4	[I]
	-46.00	46.3	1.0000	457–567	13	[II]
$\alpha\text{-Ag}_5\text{Te}_3 + \alpha\text{-Ag}_{1.9}\text{Te}$	44.893	37.31	0.9608	394–451	11	[I]
$\alpha\text{-Ag}_5\text{Te}_3 + \beta\text{-Ag}_{1.9}\text{Te}$	53.467	35.42	0.9999	452–472	3	[I]
$\beta\text{-Ag}_5\text{Te}_3 + \beta\text{-Ag}_{1.9}\text{Te}$	127.8	21.0	0.9987	578–630	3	[II]

### 5.2.2 Thermodynamic functions of the Ag-tellurides

Electrochemical studies of the thermodynamic properties related to the solid intermetallic phases in the Ag-Te system have been previously made by several researchers [2,25–27]. A comparison of experimental thermodynamic properties determined in this work [I,II] with those available in the literature is compiled in Table 3.

**Table 3.** Summary of experimentally determined standard thermodynamic functions for the reactions (III)–(XII). The standard states are: Ag(fcc) and Te(hex) [I,II].

Reaction	$\Delta_r G^\circ/\text{J}\cdot\text{mol}^{-1}$	$\Delta_r H^\circ/\text{J}\cdot\text{mol}^{-1}$	$\Delta_r S^\circ/\text{J}\cdot(\text{K}\cdot\text{mol})^{-1}$	T/K	Ref.
(III)	$-97222.7 \pm 720 - (25.42 \pm 2) \cdot T$	$-97222.7 \pm 720$	$25.42 \pm 2$	299–382	[I]
	$-81700 - 66.8 \cdot T$	$-81700.00$	$66.80$	298–385	[26]
	$-75590.8 \pm 1296 - (81.8 \pm 3) \cdot T$	$-75590.8 \pm 1296$	$81.8 \pm 3$	382–477	[I]
	$-124220 + 750.99 \cdot T - 118.87 \cdot T \cdot \ln T$	$-124220 + 1383.11 \cdot T - 237.74 \cdot T \cdot \ln T$	$632.12 - 118.87 \cdot \ln T$	298–500	[2]
	$-70612.2 \pm 922 - (94.7 \pm 2) \cdot T$	$-70612.2 \pm 922$	$94.7 \pm 2$	410–500	[27]
	$-63593 \pm 724 - (111.9 \pm 24) \cdot T$	$-63593 \pm 724$	$111.9 \pm 24$	383–563	[25]
	$-51870 \pm 724 - (134.1 \pm 15) \cdot T$	$-51870 \pm 724$	$134.1 \pm 15$	473–613	[25]
	$-68031.3 \pm 256 - (99.3 \pm 0.5) \cdot T$	$-68031.3 \pm 256$	$99.3 \pm 0.5$	426–568	[II]
(IV)	$-7072.5 \pm 124 + (2.5 \pm 0.4) \cdot T$	$-7072.5 \pm 124$	$-2.5 \pm 0.4$	295–384	[I]
(V)	$-15065.2 \pm 1122 + (30.2 \pm 3) \cdot T$	$-15065.2 \pm 1122$	$-30.2 \pm 3$	391–409	[I]
(VI)	$188.5 \pm 153 - (7.2 \pm 0.4) \cdot T$	$188.5 \pm 153$	$7.2 \pm 0.4$	419–450	[I]
(VII)	$-300.5 \pm 38 - (5.3 \pm 0.1) \cdot T$	$-300.5 \pm 38$	$5.3 \pm 0.1$	456–477	[I]
(VIII)	$-1004.4 \pm 232 - (8.4 \pm 0.6) \cdot T$	$-1004.4 \pm 232$	$8.4 \pm 0.6$	393–451	[I]
(IX)	$-1196.2 \pm 37 - (7.9 \pm 0.1) \cdot T$	$-1196.2 \pm 37$	$7.9 \pm 0.1$	452–472	[I]
	$-1004.3 \pm 43 - (8.4 \pm 0.3) \cdot T$	$-1004.3 \pm 43$	$8.4 \pm 0.3$	453–533	[25]
(X)	$-59974.8 \pm 574 - (113.5 \pm 1) \cdot T$	$-59974.8 \pm 574$	$113.5 \pm 1$	569–624	[II]
(XI)	$-97783.2 \pm 1089 + (9.2 \pm 2) \cdot T$	$-97783.2 \pm 1089$	$-9.2 \pm 2$	629–690	[II]
(XII)	$-2859.5 \pm 103 - (4.7 \pm 0.2) \cdot T$	$-2859.5 \pm 103$	$4.7 \pm 0.2$	579–630	[II]
	$-2340.7 \pm 38 - (5.7 \pm 0.2) \cdot T$	$-2340.7 \pm 38$	$5.7 \pm 0.2$	543–593	[25]

**Table 4.** Standard thermodynamic functions for the formation reactions of the intermetallic phases. The calculations are solely based on experimental results within this thesis. The standard states are: Ag(fcc) and Te(hex) [I,II].

Phase	$\Delta_r G^\circ/\text{J}\cdot\text{mol}^{-1}$	$\Delta_r H^\circ/\text{J}\cdot\text{mol}^{-1}$	$\Delta_r S^\circ/\text{J}\cdot(\text{K}\cdot\text{mol})^{-1}$	T/K
$\alpha\text{-Ag}_5\text{Te}_3(\text{s})$	$-97222.7 \pm 720 - (25.4 \pm 2) \cdot T$	$-97222.7 \pm 720$	$25.4 \pm 2.0$	299–382
	$-75590.8 \pm 1296 - (81.8 \pm 3) \cdot T$	$-75590.8 \pm 1296$	$81.8 \pm 3.0$	382–477
$\alpha\text{-Ag}_2\text{Te}(\text{s})$	$-39480 \pm 240 - (6.0 \pm 0.7) \cdot T$	$-39480.0 \pm 240$	$6.0 \pm 0.7$	299–382
$\beta\text{-Ag}_2\text{Te}(\text{s})$	$-26012.9 \pm 1858 - (42.8 \pm 9) \cdot T$	$-26012.9 \pm 1858$	$42.8 \pm 9.0$	419–450
$\alpha\text{-Ag}_{1.9}\text{Te}(\text{s})$	$-26201.3 \pm 1117 - (35.6 \pm 2) \cdot T$	$-26201.3 \pm 1117$	$35.6 \pm 2.0$	393–451
$\beta\text{-Ag}_{1.5}\text{Te}(\text{s})$	$-26393.2 \pm 470 - (35.2 \pm 1) \cdot T$	$-26393.2 \pm 470$	$35.2 \pm 1.0$	452–472

The standard Gibbs energies of formation of the intermetallic phase  $\text{Ag}_5\text{Te}_3$ , as given in Table 3, were directly calculated from the measured  $E_{\text{EMF}}$  values obtained with galvanic cell (A), according to Equation (3). Standard Gibbs energies of formations of the intermetallic phases  $\text{Ag}_{1.9}\text{Te}$  and  $\text{Ag}_2\text{Te}$  were calculated by combining the  $E_{\text{EMF}}$  values obtained with galvanic cells (A)–(C). For instance, the standard Gibbs energies of formation of the intermetallic phase  $\text{Ag}_2\text{Te}$  were calculated by combining the experimentally determined standard Gibbs energies

of formation of reaction (III) and Gibbs energies of reaction (IV). Results of the determined standard Gibbs energies of formations of the three intermetallic phases are compiled in Table 4.

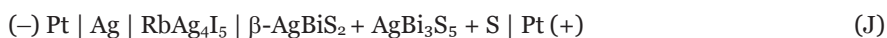
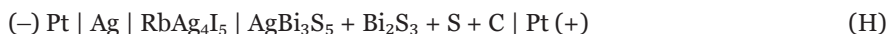
The determined standard Gibbs energies of formations of the intermediate phase  $\text{Ag}_2\text{Te}$  in [I] are in fair agreement with the results given in the literature [56]. For instance;  $\Delta_f G^\circ(\alpha\text{-Ag}_2\text{Te}, 300 \text{ K}) = -41.6 \text{ kJ}\cdot\text{mol}^{-1}$  and  $\Delta_f G^\circ(\beta\text{-Ag}_2\text{Te}, 421 \text{ K}) = -44.10 \text{ kJ}\cdot\text{mol}^{-1}$ , which were reviewed by Barin [56], are both consistent with the values determined in [I];  $\Delta_f G^\circ(\alpha\text{-Ag}_2\text{Te}, 300 \text{ K}) = -41.3 \pm 0.5 \text{ kJ}\cdot\text{mol}^{-1}$  and  $\Delta_f G^\circ(\beta\text{-Ag}_2\text{Te}, 421 \text{ K}) = -44.0 \pm 5.5 \text{ kJ}\cdot\text{mol}^{-1}$ , respectively. Mustafaev et al. [88], Reinhold [90] and Takahashi [91] studied the thermodynamic properties of  $\alpha\text{-Ag}_2\text{Te}$  by the EMF method. Their results at 298.15 K;  $\Delta_f G^\circ(\alpha\text{-Ag}_2\text{Te}) = -36.6 \pm 0.3 \text{ kJ}\cdot\text{mol}^{-1}$  [88],  $\Delta_f G^\circ(\alpha\text{-Ag}_2\text{Te}) = -44.2 \text{ kJ}\cdot\text{mol}^{-1}$  [90] and  $\Delta_f G^\circ(\alpha\text{-Ag}_2\text{Te}) = -41.4 \text{ kJ}\cdot\text{mol}^{-1}$  [91] are in fair agreement with the result obtained in [I],  $\Delta_f G^\circ(\alpha\text{-Ag}_2\text{Te}) = -40.1 \pm 0.3 \text{ kJ}\cdot\text{mol}^{-1}$ . Mustafaev et al. [88] reported  $\Delta_f G^\circ(\beta\text{-Ag}_2\text{Te}, 432 \text{ K}) = -39.4 \pm 0.2 \text{ kJ}\cdot\text{mol}^{-1}$ , the corresponding value calculated in [I] is  $\Delta_f G^\circ(\beta\text{-Ag}_2\text{Te}, 432 \text{ K}) = -44.5 \pm 5.7 \text{ kJ}\cdot\text{mol}^{-1}$ . Despite the fact that  $-\Delta_f G^\circ(432 \text{ K}, \beta\text{-Ag}_2\text{Te})$  is slightly higher in [I], their reported  $\Delta_f S^\circ(\beta\text{-Ag}_2\text{Te}, 432 \text{ K}) = 42.5 \pm 2.2 \text{ kJ}\cdot(\text{K}\cdot\text{mol})^{-1}$  is in good agreement with the result observed in [I] in the temperature range 419–450 K,  $\Delta_f S^\circ(\beta\text{-Ag}_2\text{Te}) = 42.8 \pm 9.0 \text{ kJ}\cdot(\text{K}\cdot\text{mol})^{-1}$ . The calorimetric study by Pool [92] resulted in  $\Delta_f H^\circ(\alpha\text{-Ag}_2\text{Te}, 273 \text{ K}) = -36.0 \text{ kJ}\cdot\text{mol}^{-1}$ . His value is in reasonable agreement with the result observed in [I] over the temperature range 299–382 K,  $\Delta_f H^\circ(\alpha\text{-Ag}_2\text{Te}) = -39.5 \pm 0.24 \text{ kJ}\cdot\text{mol}^{-1}$ .

Sitte and Brunner [25] determined the standard Gibbs energies of formations of the intermetallic compounds in the Ag-Te system as well as the activities of silver and tellurium in the two-phase regions at 473 K. Their reported value for the standard Gibbs energies of formation of the intermediate phase  $\text{Ag}_2\text{Te}$ ,  $\Delta_f G^\circ(\text{Ag}_2\text{Te}, 473 \text{ K}) = -45.3 \pm 0.1 \text{ kJ}\cdot\text{mol}^{-1}$ , is slightly more positive than the value obtained in [I],  $\Delta_f G^\circ(\text{Ag}_2\text{Te}, 473 \text{ K}) = -46.3 \text{ kJ}\cdot\text{mol}^{-1}$ . However, their reported value for the standard Gibbs energies of formation of the intermediate phase  $\text{Ag}_5\text{Te}_3$ ,  $\Delta_f G^\circ(\text{Ag}_{1.625}\text{Te}, 473 \text{ K}) = -37.7 \pm 0.1 \text{ kJ}\cdot\text{mol}^{-1}$ , as well as the result obtained by Bonnacaze et al. [93],  $\Delta_f G^\circ(\text{Ag}_{1.62}\text{Te}, 435 \text{ K}) = -36.0 \text{ kJ}\cdot\text{mol}^{-1}$ , are consistent with the result obtained in [I],  $\Delta_f G^\circ(\text{Ag}_{1.625}\text{Te}, 473 \text{ K}) = -37.14 \text{ kJ}\cdot\text{mol}^{-1}$ . From dissociation pressure measurements by a Knudsen effusion method, Mills [94] calculated the standard enthalpy of formation of stützite to be  $\Delta_f H^\circ(\text{Ag}_{1.64}\text{Te}, 298.15 \text{ K},) = -29.7 \pm 5.0 \text{ kJ}\cdot\text{mol}^{-1}$ , the corresponding value determined in [I] is  $\Delta_f H^\circ(\text{Ag}_{1.64}\text{Te}, 298.15 \text{ K}) = -31.9 \pm 0.24 \text{ kJ}\cdot\text{mol}^{-1}$ . Gobec and Sitte [95] calculated the enthalpy of formation of stützite, on the basis of the Miedema model presented by Eichler et al. [96], to be  $\Delta_f H^\circ(\text{Ag}_{1.667}\text{Te}, 298.15 \text{ K}) = -24.2 \text{ kJ}\cdot\text{mol}^{-1}$ ; this value is off by about  $8 \text{ kJ}\cdot\text{mol}^{-1}$  from the result obtained in [I],  $\Delta_f H^\circ(\text{Ag}_{1.667}\text{Te}, 298.15 \text{ K}) = -32.4 \pm 0.24 \text{ kJ}\cdot\text{mol}^{-1}$ . Results reported by Echmaeva and Osadchii [2],  $\Delta_f H^\circ(\text{Ag}_5\text{Te}_3, 298.15 \text{ K}) = -88.78 \pm 3.4 \text{ kJ}\cdot\text{mol}^{-1}$ , and Abbasov and Mustafaev [97],  $\Delta_f H^\circ(\text{Ag}_5\text{Te}_3, 298.15 \text{ K},) = -89.29 \text{ kJ}\cdot\text{mol}^{-1}$ , are in a fair agreement with the result obtained in [I],  $\Delta_f H^\circ(\text{Ag}_5\text{Te}_3, 298.15 \text{ K}) = -97.2 \pm 0.7 \text{ kJ}\cdot\text{mol}^{-1}$ . As a result of the vapour pressure measurements, Mills [94] reported  $\Delta_f H^\circ(\text{Ag}_5\text{Te}_3, 298.15 \text{ K},) = -98.7 \text{ kJ}\cdot\text{mol}^{-1}$ . His value is in good agreement with the result obtained in [I]. Castanet et al. [98] determined  $\Delta_f H^\circ(523 \text{ K}, \alpha\text{-Ag}_5\text{Te}_3) = -67.6 \text{ kJ}\cdot\text{mol}^{-1}$ , by the calorimetric method, this value is in reasonable agreement with the value

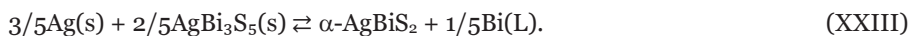
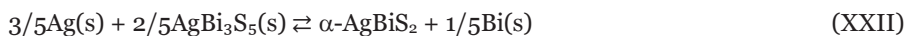
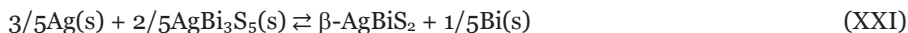
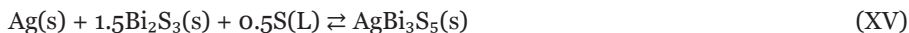
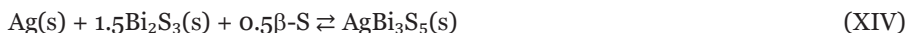
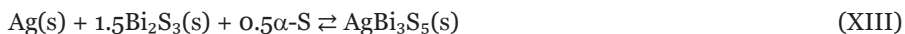
determined in [I] in the temperature range 382–477 K,  $\Delta_f H^\circ(\alpha\text{-Ag}_5\text{Te}_3) = -75.6 \pm 1.3 \text{ kJ}\cdot\text{mol}^{-1}$ .

### 5.3 Ag-Bi-S system

In this section, a combined summary of results obtained in the Ag-Bi-S system, which are published in [III–V], is presented. In the Ag-Bi-S system, thermodynamic measurements were conducted in the temperature range 299–699 K. The cell arrangement on which the measurements were conducted can be represented by galvanic cells (G)–(K).



Based on the literature data and the results observed in [III–V], the virtual electrochemical cell reactions of galvanic cells (G)–(K) can be explicitly written over temperature regions of the different stable phases as:



For simplicity reasons, we express pavonite, matildite and schapbachite in equilibrium with bismuth or sulphur as stoichiometric  $\text{AgBi}_3\text{S}_5$ ,  $\beta\text{-AgBiS}_2$  and  $\alpha\text{-AgBiS}_2$ , respectively, in all reactions within this thesis. According to Craig [65], the

maximum solid solubilities into  $\text{AgBi}_3\text{S}_5$  and solid solubility of bismuth into  $\text{AgBi}_{1+x}\text{S}_2$  are less than 1 mol. %. The solid solubility limits of sulphur into the ternary phases have not been numerically reported, however, the extent of the solid solubility at 623 K can be seen in Figure 2.

### 5.3.1 $E_{\text{EMF}}$ values (cathode: Ag-Bi-S phase assemblages)

The EMF-measurements conducted on galvanic cell (G) have shown very long equilibration times and failed at higher temperatures [III]. To improve this sluggish experimental period, graphite powder was added into the phase assemblage for study (cell (H)). The galvanic cells which contained graphite (5, 7, 9 and 12 wt. % C) resulted in a steady EMF readings in most cases in less than a week. The results obtained on the galvanic cells (G) and (H) are shown in Figure 12. As also noted by Schmidt et al. [29], the addition of graphite altered the  $E_{\text{EMF}}$  values. However, as reported by Schmidt et al. [29] with a suggestion of further studies, the pattern in which the  $E_{\text{EMF}}$  values were altered consistently in accordance with the amount of added graphite was not observed in [III]. Addition of 5, 9 and 12 wt. % C to the cathode phase assemblage of cell (G) (i.e., cell (H)) resulted in an increase of approximately the same  $E_{\text{EMF}}$  values, as shown in Figure 12. The increase in  $E_{\text{EMF}}$  values due to the addition of graphite may indicate that the presence of graphite, which was assumed to be inert from the chemical reactions point of view, not only improved the electronic conductivity in the cathode materials, but may have also caused side reactions to take part in the overall chemical cell reactions. The results obtained with galvanic cell (H) incorporating graphite may only be considered as indirect measurements. More experimental work should be done to elucidate the effect of graphite addition on the  $E_{\text{EMF}}$  values.

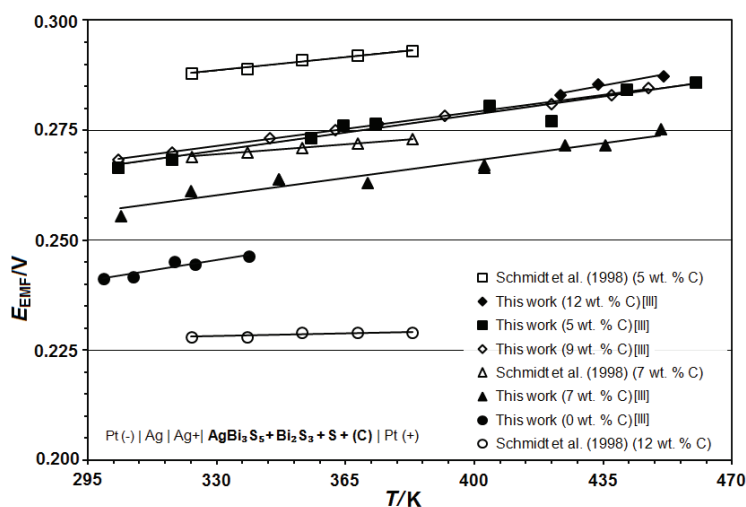


**Figure 12.** A summary of the  $E_{\text{EMF}}$  vs.  $T$  relations obtained with galvanic cells (G) and (H) together with the literature values, the least square fitting of the experimental points are shown with solid lines [III].

Measurements conducted on galvanic cell (I) have also shown long equilibration times. At 492.69 K, it took up to three weeks to reach equilibrium. The results obtained with galvanic cell (I) are shown in Figure 13.

As can be seen in Figure 13, in the temperature range 492.7–528 K the  $E_{EMF}$  values increased slightly with increasing temperature. Above  $T = 548$  K, the slope of the  $E_{EMF}$  vs.  $T$  plot turned upward remarkably. This is an indication for a significant phase change in the cathode phase assemblage [III].

The measured  $E_{EMF}$  values with galvanic cells (J) and (K) at different temperatures are shown in Figures 14 and 15, respectively.

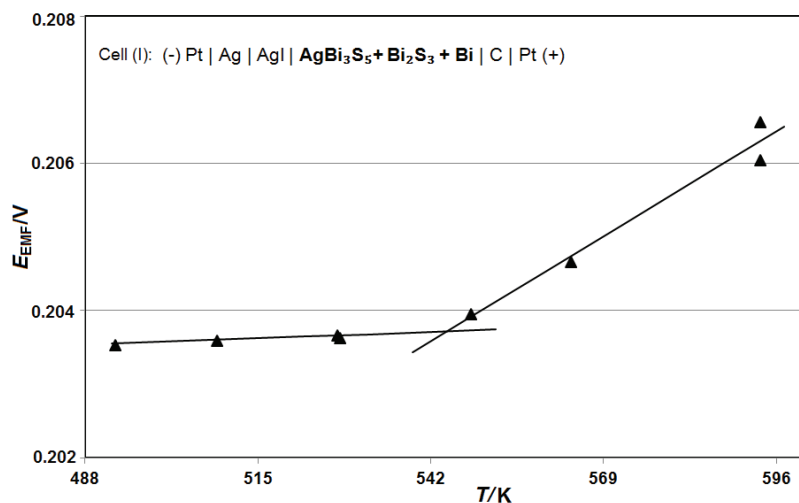


**Figure 13.**  $E_{EMF}$  vs.  $T$  relations obtained with galvanic cell (I), the least square fitting of the experimental points are shown with solid lines. Literature values for the same EMF cell and temperature range are not available [III].

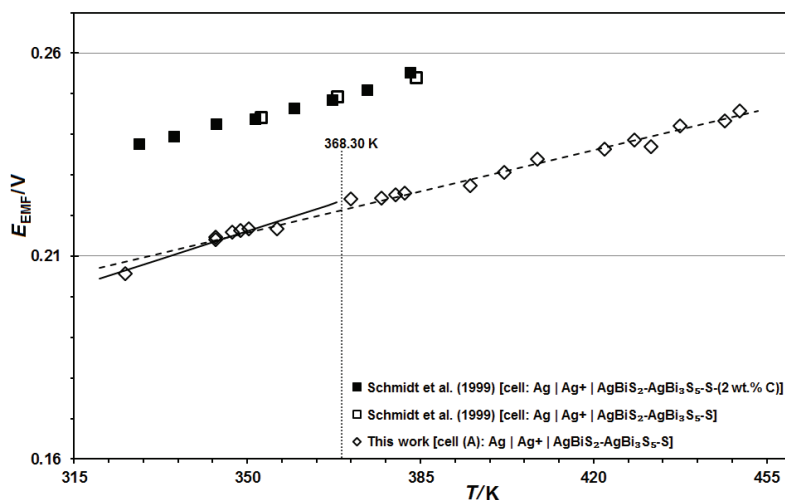


**Figure 14.**  $E_{EMF}$  vs.  $T$  relations obtained with galvanic cell (J) together with the literature values, the least squares regression lines of  $E_{EMF}$  values on cell temperatures of this work are shown with solid and dashed lines [IV].

Below  $T = 390$  K, as shown in Figure 14, the  $E_{EMF}$  values obtained in [IV] are approximately 0.027 V less than the values reported by Schmidt et al. [30]. Most of their experimental points were obtained from galvanic cells which had additional 2 wt. % C in the cathode material. In the earlier study [III], we observed that galvanic cells (H) with cathode materials incorporating different compositions of graphite ( $AgBi_3S_5-Bi_2S_3-S$ -(0...12 wt. % C)) result in different  $E_{EMF}$  values at the same temperatures. Schmidt et al.'s [29] previous work also suggested that  $E_{EMF}$  values from galvanic cells containing graphite as an additional constituent of the cathode material are different from graphite free cathodes of the same materials, for poorly defined reasons. Thus, the presence of graphite may have increased their  $E_{EMF}$  values. Recently, Voronin and Osadchii [7] have measured the EMF of a galvanic cell similar to that of our cell (K), for which the measured  $E_{EMF}$  values are shown in Figure 15. However, they report  $E_{EMF}$  values within the temperature range 303–403 K; furthermore, their cathode ( $Ag-Bi-S$  phase assemblages) incorporated 15 wt. % C. Therefore, our results shown in Figure 15 could not be directly compared with their results.

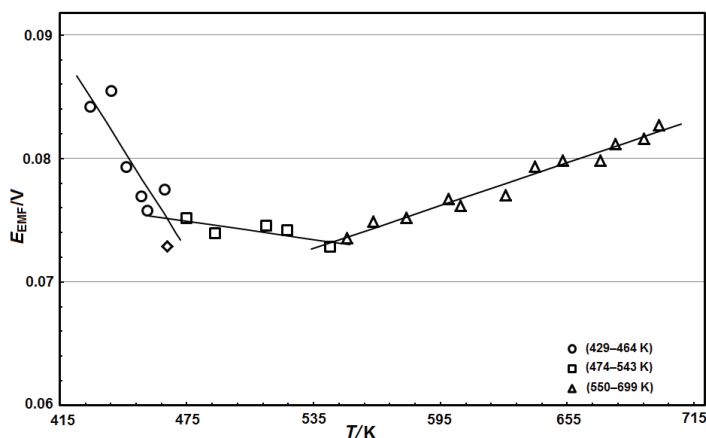


**Figure 15.** A summary of the  $E_{EMF}$  vs.  $T$  relations obtained with galvanic cell (K), the least square fitting of the experimental points are shown with solid lines. The open diamond point was not included in the calculations. No literature values for the same cell and temperature range are available [V].

Least squares regression of all measured  $E_{EMF}$  values on temperatures of cell (J), which is shown with a dashed line in Figure 14, indicate that  $E_{EMF}$  values increase with increasing temperature. According to the literature, sulphur undergoes polymorphic phase transition at  $T_{tr} = 368.30$  K [56,65,99]. Based on this information least squares regression of the measured  $E_{EMF}$  values on temperatures of cell (J) were also made within the experimental temperature range 325–356 K, as shown with a solid line in Figure 14. The slope of the dashed line is relatively lower than that of the solid line. This could be as a result of phase transformation and melting of sulphur in the cathode material (the phase assemblage  $\beta-AgBiS_2-AgBi_3S_5-S$ ) after crossing the phase transformation temperature  $T_{tr}(\text{sulphur}) \approx 368.30$  K. Linear analyses taking three  $E_{EMF}$  vs.  $T$  values obtained with galvanic cell

(K), at a time, did not show any angular turn on the curve for the whole experimental values, as shown in Figure 15.

The EMF measurements conducted on galvanic cell (K) also showed long equilibration times. For instance, at 429 K and 673 K, it took about 15 days and 3 days to reach equilibrium, respectively. The results obtained from galvanic cell (K) are shown graphically in Figure 15.

As can be seen in Figure 15, in the temperature range 429–464 K the  $E_{EMF}$  values decreased with increasing temperature. Above  $T = 474$  K, the slope of the  $E_{EMF}$  vs.  $T$  curve turned upward remarkably. Above  $T = 550$  K, the  $E_{EMF}$  vs.  $T$  curve turned again noticeably upward and the EMF increased with increasing temperature. As also observed in previous studies [I–IV] and [2,25,100], the discontinuities in the slope of the  $E_{EMF}$  vs.  $T$  curve are considered to be due to phase transitions in the cathode phase assemblage  $AgBiS_2$ - $AgBi_3S_5$ -Bi [V].

#### *Analytical forms of $E_{EMF}$ and $T_{tr}$*

The calculated equations for the temperature dependence of  $E_{EMF}$  values obtained with galvanic cells (G)–(K), for different concentrations of graphite are compiled in Table 5.

**Table 5.** Values of the coefficients a and b obtained through linear least square analysis of the measured EMF and temperature values with the galvanic cells (G)–(K) [III–V].

Galvanic Cell	Wt. % C	$E_{EMF}(mV) = a + b \cdot T$			T/K	N	Ref.
		a	b·10 <sup>-2</sup>	R <sup>2</sup>			
cell (G)	-	199.93	13.81	0.8843	299–338	5	[III]
cell (H)	5	231.37	11.81	0.9328	303–460	9	[III]
cell (H)	7	223.48	11.14	0.9203	303–451	11	[III]
cell (H)	9	235.06	11.03	0.9983	303–448	9	[III]
cell (H)	12	221.40	14.67	0.9504	423–452	3	[III]
cell (J)	-	73.79	39.25	0.933	325–356	7	[IV]
cell (K)	-	210.68	-29.86	0.733	429–464	6	[IV,V]
cell (K)	-	84.20	-2.69	0.610	474–543	5	[V]
cell (K)	-	34.88	6.37	0.970	550–699	12	[V]
cell (I)	-	202.08	0.30	0.9079	492–528	4	[III]
cell (I)	-	174.96	5.281	0.9682	548–594	4	[III]

By solving simultaneously the selected equations in Table 5, which were calculated from the results obtained with galvanic cell (K), the phase transition temperatures in the experimental temperature range 429–699 K were found to be  $465.6 \pm 5$  K and  $544.0 \pm 4$  K [V]. And, by solving simultaneously other selected equations in Table 5, which were separately obtained with galvanic cell (I), phase change temperature in the temperature range 492–594 K was found to be  $544.5 \pm 3.8$  K [III]. These temperatures are in good agreement with the literature values of  $\beta \rightarrow \alpha$ - $AgBiS_2$  polymorphic phase transition temperature,  $468.7 \pm 5$  K [65,66,77], and the melting point of bismuth, 543–544.6 K [65,78,87]. The lower polymorphic phase transition temperature from  $\beta$ - to  $\alpha$ - $AgBiS_2$  obtained in [V], compared to previous observations [65,66,77], may be a result of excess bismuth in our experimental phase. This phase transition temperature lowering effect of bismuth

saturation is in reasonable agreement with the conclusion made by Craig [65], i.e., in the presence of  $\text{AgBi}_3\text{S}_5$ , the phase transition temperature of the coexisting phase  $\text{AgBiS}_2$  is lower.

### 5.3.2 $\Delta_r G^\circ$ values of reactions including Ag-Bi-sulfosalts

The Gibbs energies of reactions (XIII), (XVI)–(XVIII) and (XXI)–(XXIII) were calculated directly from the measured  $E_{\text{EMF}}$  vs.  $T$  values according to Equation (3). The results obtained for each reaction are expressed by Equations (11)–(17), respectively.

$$\Delta_{\text{r(XIII)}}G^\circ = -19.291 - 13.30 \cdot 10^{-3} \cdot T \quad (299\text{--}338 \text{ K}) \quad (11)$$

$$\Delta_{\text{r(XVI)}}G^\circ = -19.498 - 0.2895 \cdot 10^{-3} \cdot T \quad (492\text{--}528 \text{ K}) \quad (12)$$

$$\Delta_{\text{r(XVII)}}G^\circ = -16.881 - 5.0953 \cdot 10^{-3} \cdot T \quad (548\text{--}594 \text{ K}) \quad (13)$$

$$\Delta_{\text{r(XVIII)}}G^\circ = -4.75 \pm 1.1 - (25.25 \pm 3.0) \cdot 10^{-3} \cdot T \quad (325\text{--}356 \text{ K}) \quad (14)$$

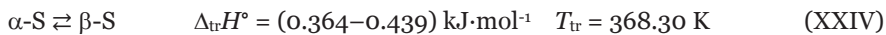
$$\Delta_{\text{r(XXI)}}G^\circ = -12.19 \pm 2.3 + (17.26 \pm 5.2) \times 10^{-3} \cdot T \quad (429\text{--}464 \text{ K}) \quad (15)$$

$$\Delta_{\text{r(XXII)}}G^\circ = -4.87 \pm 0.37 + (1.56 \pm 0.7) \cdot 10^{-3} \cdot T \quad (474\text{--}543 \text{ K}) \quad (16)$$

$$\Delta_{\text{r(XXIII)}}G^\circ = -2.02 \pm 0.13 - (3.69 \pm 0.2) \cdot 10^{-3} \cdot T \quad (550\text{--}699 \text{ K}). \quad (17)$$

The enthalpy of melting of bismuth can be calculated from Equations (12) and (13). In the absence of accurate data on the solubility of bismuth in pavonite at different temperatures, the mole fraction of bismuth in a bismuth-saturated pavonite can only be estimated based on Craig's [65] assumption that the maximum solid solubility into  $\text{AgBi}_3\text{S}_5$  is less 1 mol. %. Accordingly, by considering the number of moles of bismuth in reactions (XVI) and (XVII) as well as the possible solubility of bismuth (0.18...0.99 mol. %) into  $\text{AgBi}_3\text{S}_5$ , reactions (XVI) and (XVII) can be re-expressed as:  $\text{Ag} + 5/3\text{Bi}_2\text{S}_3 \rightleftharpoons \text{AgBi}_{3+x}\text{S}_5 + (1-3 \cdot x/3) \cdot \text{Bi(s,L)}$ . Based on these solubility ranges and the errors while calculating the least squares regression Equations (12) and (13);  $\Delta_{\text{melt}}H^\circ(\text{Bi})$  was calculated to be  $9.41 \pm 2.4 \text{ kJ}\cdot\text{mol}^{-1}$  [III]. The values are in agreement with those reported in [56,99,101–104], 8.5–11.3  $\text{kJ}\cdot\text{mol}^{-1}$ .

According to thermochemical data compiled in [56,99], pure sulphur undergoes polymorphic phase transition and melting over the experimental temperature range 298–450 K [IV]. Consequently, Gibbs energies of phase transition and melting of sulphur that should be considered above  $T_{\text{tr}} = 368.30 \text{ K}$  were calculated according to Equation (9) using thermodynamic values of [56,99] in reactions (XXIV) and (XXV).



Thus, the low temperature experimental values from galvanic cell (J), over the temperature range 325–356 K, were extrapolated to high-temperatures, with  $\beta$ -S and S(L) as standard states, using reactions (XXIV) and (XXV) and Equation (9). The least squares analysis yields Equations (18) and (19) of reactions (XIX) and (XX), respectively.

$$\Delta_{r(\text{XIX})}G^\circ = -4.61 \pm 1.1 - (25.61 \pm 3.0) \times 10^{-3} \cdot T \quad (371\text{--}382 \text{ K}) \quad (18)$$

$$\Delta_{r(\text{XX})}G^\circ = -4.04 \pm 1.1 - (27.09 \pm 3.0) \times 10^{-3} \cdot T \quad (395\text{--}450 \text{ K}). \quad (19)$$

Considering bismuth as the only phase that dissolves into  $\text{AgBiS}_2$  in the studied phase assemblage  $\text{AgBiS}_2\text{-AgBi}_3\text{S}_5\text{-Bi}$ , the enthalpy of phase transformation of  $\beta\text{-AgBi}_{1+x}\text{S}_2$  to  $\alpha\text{-AgBi}_{1+x}\text{S}_2$  can be calculated from Equations (15) and (16). As the solid solubility of silver into bismuth is negligible at the experimental temperatures [69,70]; the enthalpy of melting of bismuth can also be calculated from Equations (16) and (17). Including the errors while calculating the least squares regression Equations (15)–(17);  $\Delta_{\text{tr}}H^{\beta \rightarrow \alpha}(\text{AgBi}_{1+x}\text{S}_2)$  was found to be  $7.3 \pm 2.1 \text{ kJ}\cdot\text{mol}^{-1}$  and that of  $\Delta_{\text{melt}}H^{\text{Bi(s)} \rightarrow \text{Bi(L)}}$  was found to be  $12.9 \pm 1.3 \text{ kJ}\cdot\text{mol}^{-1}$ . The errors for the enthalpy values were also calculated based on the errors in least square fitting of the experimental data and the measured temperature differences between the two electrodes during the measurements.

The average  $\Delta_{\text{melt}}H^{\text{Bi(s)} \rightarrow \text{Bi(L)}}$  value estimated in [V] is slightly higher than the average value,  $9.41 \pm 2.4 \text{ kJ}\cdot\text{mol}^{-1}$ , estimated in a different phase assemblage as reported in [III]. However, it is in a reasonable agreement with the compiled values reported in [99], from  $8.95 \text{ kJ}\cdot\text{mol}^{-1}$  to  $12.33 \text{ kJ}\cdot\text{mol}^{-1}$ . The  $\Delta_{\text{tr}}H^{\beta \rightarrow \alpha}(\text{AgBi}_{1+x}\text{S}_2)$  value estimated in [V] is also in agreement with the only available literature value  $\Delta_{\text{tr}}H^{\beta \rightarrow \alpha}(\text{AgBiS}_2) = 10.5 \pm 4.6 \text{ kJ}\cdot\text{mol}^{-1}$  reported in [28].

### 5.3.3 $\Delta_f G^\circ$ values of pavonite

By interpolating the  $\Delta_f G^\circ(\text{Bi}_2\text{S}_3)$  values compiled in [56] at the experimental temperatures and combining those with the determined  $\Delta_r G^\circ$  values of reactions (XIII)–(XVII), in the temperature range 299–594 K, the Gibbs energies of formation of pavonite were calculated [III]. The interpolation of  $\Delta_f G^\circ(\text{Bi}_2\text{S}_3)$  vs.  $T$  data of [56] at the experimental temperatures were done in three temperature regions; 298–300 K, 400–500 K and 600–700 K, taking into account the temperature regions in which  $\alpha$ -S,  $\beta$ -S, S(L), Bi(s) and Bi(L) are the stable phases. The calculations yield  $\Delta_f G^\circ('AgBi_3S_5')$  values in different temperature regions:

$$\Delta_f G^\circ_{\text{AgBi}_3\text{S}_5'} = -233.92 \pm 0.88 + (0.50 \pm 2.78) \cdot 10^{-3} \cdot T \quad (299\text{--}338 \text{ K}) \quad (20)$$

$$\Delta_f G^\circ_{\text{AgBi}_3\text{S}_5'} = -271.76 \pm 0.04 + (50.51 \pm 0.07) \cdot 10^{-3} \cdot T \quad (492\text{--}528 \text{ K}) \quad (21)$$

$$\Delta_f G^\circ_{\text{AgBi}_3\text{S}_5'} = -318.69 \pm 0.37 + (137.10 \pm 0.65) \cdot 10^{-3} \cdot T \quad (548\text{--}594 \text{ K}). \quad (22)$$

In the temperature range 299–594 K, in which EMF measurements with galvanic cell (I) were conducted, pure sulphur and bismuth undergo phase transition and melting [56,65,78,99,105,106]. Therefore, the high temperature experimental data

in which  $\beta$ -S, S(L) and Bi(L) are stable phases were extrapolated to low temperatures with  $\alpha$ -S and Bi(s) as standard states by reactions (XXIV)–(XXVI) and Equation (9) [III]:

$$\Delta_f G^\circ_{\text{AgBi}_3\text{S}_5'} = -268.65 \pm 6.9 + (37.1 \pm 13.5) \cdot 10^{-3} \cdot T \quad (299\text{--}369 \text{ K}). \quad (23)$$

The  $\Delta_{\text{tr}} G^\circ$  values considered at each temperature above  $T_{\text{tr}}(\text{sulphur}) = 368.30 \text{ K}$  and  $T_{\text{melt}}(\text{bismuth}) = 544.50 \text{ K}$  were calculated using the literature data reported in [78,99,56,107,108], as well as the estimated  $\Delta_{\text{melt}} H(\text{Bi})$  in [III] and Equation (9). The errors were calculated by taking into account the different values of the enthalpies of phase transition and melting of sulphur and bismuth [56,78,99,107,108], including the estimated values in [III], and the errors in least square fitting of the experimental data. Differences in the literature values of the phase transition temperatures of bismuth and sulphur [56,65,78,99,105,106] are small and insignificant in the  $\Delta_{\text{tr}} G^\circ$  calculations.

As can be seen in Figure 16, the standard Gibbs energies of formation of pavonite calculated through the analysis of results obtained with galvanic cell (G) are more positive than those of the standard Gibbs energies obtained with galvanic cell (I). The observed differences in  $\Delta_f G^\circ$  values can be interpreted as the difference between thermodynamic properties of pavonite saturated with sulphur (Equation (20)) and bismuth (Equation (23)). As the results expressed in Equations (20) and (23) indicate, pavonite saturated with bismuth ( $\text{AgBi}_{3+x}\text{S}_5$ ;  $0 < x < 0.14$ ) is more stable than that of pavonite saturated with sulphur ( $\text{AgBi}_3\text{S}_{5+y}$ ).

The standard Gibbs energies of pavonite were also calculated by the Craig and Barton [32] approximation method. By interpolating the standard Gibbs energies of the pure binary sulphides  $\text{Bi}_2\text{S}_3$  and  $\text{Ag}_2\text{S}$  given in [56] at the experimental temperatures and using those values in Equation (10), Equations (24)–(26) were obtained:

$$\Delta_f G^\circ_{\text{AgBi}_3\text{S}_5'} = -230.94 + (-10.4 \pm 7.3) \cdot 10^{-3} \cdot T \quad (299\text{--}338 \text{ K}) \quad (24)$$

$$\Delta_f G^\circ_{\text{AgBi}_3\text{S}_5'} = -244.27 + (23.9 \pm 7.3) \cdot 10^{-3} \cdot T \quad (492\text{--}528 \text{ K}) \quad (25)$$

$$\Delta_f G^\circ_{\text{AgBi}_3\text{S}_5'} = -287.66 + (103.3 \pm 7.3) \cdot 10^{-3} \cdot T \quad (548\text{--}594 \text{ K}). \quad (26)$$

As can be seen in Figure 17, the experimentally determined values in the temperature range 299–338 K are in very good agreement with the calculated values according to the Craig and Barton [32] approximation method.

$\Delta_f G^\circ$  vs.  $T$  relation of Equation (24) indicates,  $\Delta_f H^\circ(\text{AgBi}_3\text{S}_5, 298.15 \text{ K})$  obtained by the Craig and Barton [32] approximation method,  $-230.94 \text{ kJ}\cdot\text{mol}^{-1}$ , is in fair agreement with the results obtained in [III],  $-233.92 \pm 0.88 \text{ kJ}\cdot\text{mol}^{-1}$ , according to Equation (20). The  $\Delta_f H^\circ(\text{AgBi}_3\text{S}_5, 298.15 \text{ K})$  value obtained from the  $\Delta_f G^\circ$  vs.  $T$  relation in Equation (23), for the bismuth-saturated pavonite ( $\text{AgBi}_{3+x}\text{S}_5$ ;  $0 < x < 0.14$ ),  $-268.65 \pm 6.92 \text{ kJ}\cdot\text{mol}^{-1}$ , is clearly more negative than the value calculated for the stoichiometric  $\text{AgBi}_3\text{S}_5$ ,  $-230.94 \text{ kJ}\cdot\text{mol}^{-1}$ .

$\Delta_f S^\circ(\text{AgBi}_3\text{S}_5, 298.15 \text{ K}) = 10.4 \pm 7.3 \text{ J}\cdot(\text{K}\cdot\text{mol})^{-1}$  which was calculated from the  $\Delta_f G^\circ$  vs.  $T$  relation in Equation (24), is slightly more positive than the result observed through the analysis of  $\Delta_f G^\circ$  vs.  $T$  relation in Equation (20),  $-0.5 \pm 2.78$

$\text{J}\cdot(\text{K}\cdot\text{mol})^{-1}$ . It also deviates largely from  $\Delta_f S^\circ(\text{AgBi}_{3+x}\text{S}_5, 298.15 \text{ K})$  calculated for bismuth-saturated pavonite according to the  $\Delta_f G^\circ$  vs.  $T$  relation of Equation (23),  $-37.1 \pm 13.5 \text{ J}\cdot(\text{K}\cdot\text{mol})^{-1}$ .

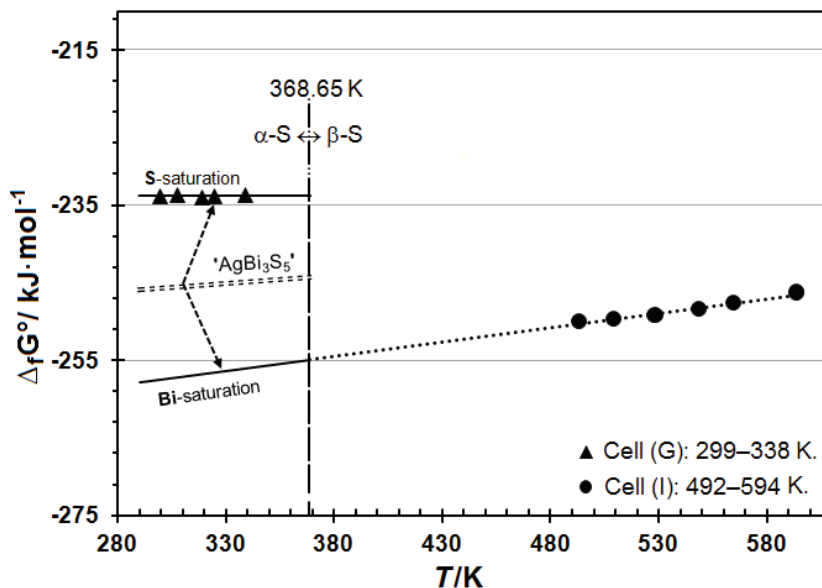


**Figure 16.** A summary of  $\Delta_f G^\circ('AgBi_3S_5')$  vs.  $T$  determined in [III] at bismuth and sulphur saturations. Solid circles and triangles are the experimental data obtained with galvanic cell (G) and (I), respectively. Solid lines indicate extrapolation of the calculated least squares lines (according to Equations (20) and (23)), for each experimental data set. Standard states; Ag(fcc), Bi(rho) and S(ortho).

In the temperature range 492–594 K, differences between the calculated (Equations (25) and (26)) and experimentally determined (Equations (21) and (22)) Gibbs energies of formation of pavonite are large; with the differences slightly decreasing as the temperature increases. The average deviation between the calculated and experimentally determined  $\Delta_f G^\circ(\text{AgBi}_3\text{S}_5)$  values at the experimental temperatures is about  $12.7 \pm 4 \text{ kJ}\cdot\text{mol}^{-1}$  [III]. Craig and Barton [32] mentioned that their approximation is a gross estimate based on the earlier experimental work of [6,33,34] on more than twenty different sulfosalts. Nevertheless, the magnitude of the observed deviation emanates from the differences in the thermodynamic properties of the stoichiometric pavonite ( $\text{AgBi}_3\text{S}_5$ ) and bismuth-saturated pavonite ( $\text{AgBi}_{3+x}\text{S}_5$ ;  $0 < x < 0.14$ ) studied in the temperature range 492–594 K [III].

The  $\Delta_f H^\circ(\text{AgBi}_3\text{S}_5, 298.15 \text{ K})$  value determined from the  $E_{EMF}$  vs.  $T$  relations obtained with galvanic cell (G) is  $-233.92 \pm 0.9 \text{ kJ}\cdot\text{mol}^{-1}$ . The average value for the derived thermodynamic functions by the galvanic cell (I) from higher temperatures, according to Equation (23), is  $-268.7 \pm 6.9 \text{ kJ}\cdot\text{mol}^{-1}$ . The former is close to  $-219.3 \text{ kJ}\cdot\text{mol}^{-1}$  of 'stoichiometric' pavonite determined by Schmidt et al. [29] by the EMF-method and the average value  $-219.6 \pm 4.2 \text{ kJ}\cdot\text{mol}^{-1}$  determined by Bryndzia and Kleppa [28] by a calorimetric method. As in galvanic cell (G) of [III], the cathode material of Schmidt et al. [29] also contained pure sulphur as the

third constituent, indicating that the pavonite studied was also sulphur-saturated. Hence, a fair agreement of  $\Delta_f H^\circ(\text{AgBi}_3\text{S}_5, 298.15 \text{ K})$  was observed in [III] and their work, due to different compositions of pavonite.

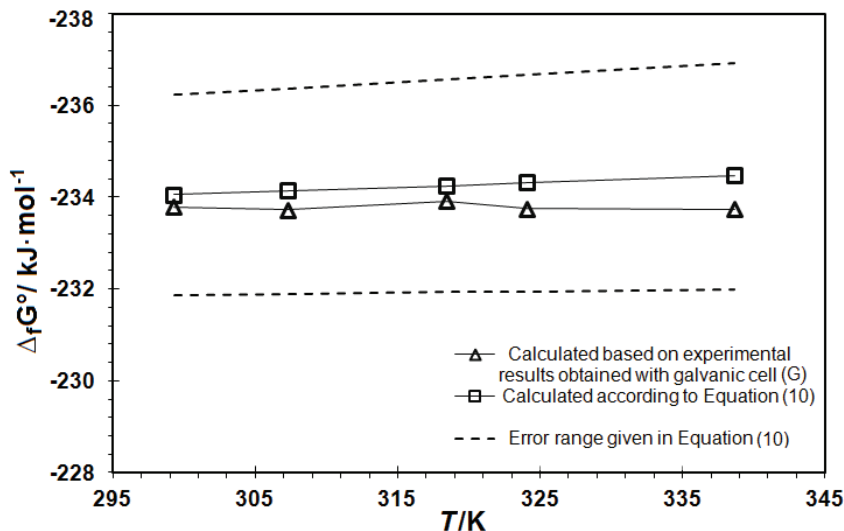


**Figure 17.**  $\Delta_f G^\circ$  vs.  $T$  diagram showing the agreement between the experimentally determined values and the calculated values, according to Equation (10), at the corresponding experimental temperatures [III].

Schmidt et al. [29] reported  $\Delta_f S^\circ(\text{AgBi}_3\text{S}_5, 298.15 \text{ K}) = 105 \text{ J}\cdot(\text{K}\cdot\text{mol})^{-1}$ , which is largely different from the value  $-0.50 \pm 2.78 \text{ J}\cdot(\text{K}\cdot\text{mol})^{-1}$  determined in [III]. To rule out possible calculation errors, we recalculated the entropy of formation from their experimental data  $E_{\text{EMF}}(\text{V}) = 0.285855 + 0.134 \cdot 10^{-3} \cdot T/\text{K}$  for reaction (III) and the literature data of [56]. The  $\Delta_f S^\circ(\text{AgBi}_3\text{S}_5, 298.15 \text{ K}) = -0.928 \text{ J}\cdot(\text{K}\cdot\text{mol})^{-1}$  obtained after recalculation, is in the range of the values obtained with our galvanic cell (G),  $-0.50 \pm 2.78 \text{ J}\cdot(\text{K}\cdot\text{mol})^{-1}$  [III]. Shykhyyev et al. [31] reported (as given in [109])  $S^\circ(\text{AgBi}_3\text{S}_5, 298.15 \text{ K}) = 367.5 \pm 16.5 \text{ J}\cdot(\text{K}\cdot\text{mol})^{-1}$ . Using the standard entropies of the pure substances compiled in [56], we calculated  $\Delta_f S^\circ(\text{AgBi}_3\text{S}_5, 298.15 \text{ K}) = -5.66 \pm 16.5 \text{ J}\cdot(\text{K}\cdot\text{mol})^{-1}$ . The value is in agreement with the results obtained with galvanic cell (G),  $-0.50 \pm 2.78 \text{ J}\cdot(\text{K}\cdot\text{mol})^{-1}$  [III]. However, the standard enthalpy of formation they reported is more negative by  $-90 \pm 7.7 \text{ kJ}\cdot\text{mol}^{-1}$  than the value determined with galvanic cell (G),  $-233.92 \pm 0.88 \text{ kJ}\cdot\text{mol}^{-1}$ . The  $\Delta_f H^\circ(\text{AgBi}_3\text{S}_5, 298.15 \text{ K}) = -323.4 \pm 7.7 \text{ kJ}\cdot\text{mol}^{-1}$  reported by Shykhyyev et al. [31] is also more negative by  $-55 \text{ kJ}\cdot\text{mol}^{-1}$  than the value obtained with galvanic cell (I),  $-268.65 \pm 6.92 \text{ kJ}\cdot\text{mol}^{-1}$ , which is for bismuth-saturated pavonite.

A comparison of the standard thermodynamic properties of pavonite, at 298.15 K, determined in [III] with those of the literature values is shown in Table 6. Standard entropies of pavonite, at sulphur and bismuth saturation, are calculated according to Equation (8); and these values are also compiled in Table 6. The difference between the standard entropies of pavonite saturated with sulphur ( $372.66 \pm 2.78 \text{ J}\cdot(\text{K}\cdot\text{mol})^{-1}$ ) and that of saturated with bismuth ( $336.05 \pm 13.52 \text{ J}\cdot(\text{K}\cdot\text{mol})^{-1}$ ) is  $36 \pm 10 \text{ J}\cdot(\text{K}\cdot\text{mol})^{-1}$ .

**Table 6.** A summary of standard thermodynamic properties of pavonite at 298.15 K and 1 atm. The standard states are: Ag(fcc), Bi(rho) and S(ortho) [III].

Phase	$\Delta_f G^\circ/\text{kJ}\cdot\text{mol}^{-1}$	$\Delta_f H^\circ/\text{kJ}\cdot\text{mol}^{-1}$	$\Delta_f S^\circ/\text{J}\cdot(\text{K}\cdot\text{mol})^{-1}$	$S^\circ/\text{J}\cdot(\text{K}\cdot\text{mol})^{-1}$	Ref.
'AgBi <sub>3</sub> S <sub>5</sub> ' (sulphur saturated)	-233.78 ± 1.70	-233.9 ± 0.88	-0.50 ± 2.78	372.7 ± 2.78	[III]
'AgBi <sub>3</sub> S <sub>5</sub> ' (bismuth saturated)	-257.58 ± 11.0	-268.7 ± 6.92	-37.11 ± 13.52	336.1 ± 13.52	[III]
'AgBi <sub>3</sub> S <sub>5</sub> '	-250.61	-219.30	-0.93 <sup>a</sup>	372.23	[29]
'AgBi <sub>3</sub> S <sub>5</sub> '	-	-219.6 ± 4.20	-	-	[28]
'AgBi <sub>3</sub> S <sub>5</sub> '	-326.4 ± 12.90	-323.4 ± 7.70	-5.66 ± 16.50 <sup>b</sup>	367.5 ± 16.50	[31]
'AgBi <sub>3</sub> S <sub>5</sub> '	-234.04 ± 2.20	-230.90	10.4 ± 7.30	383.6 ± 7.30	[III] <sup>c</sup>

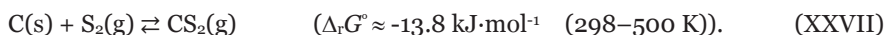
<sup>a</sup> Calculated by combining the  $E_{\text{EMF}}$  vs.  $T$  relations reported in [29] and  $S^\circ$  data of pure elements in [56]. The composition of their sample suggests that the pavonite (AgBi<sub>3</sub>S<sub>5</sub>) studied was at S-saturation.

<sup>b</sup>  $\Delta_f G^\circ$  was calculated from  $S_{988.15}^\circ(\text{AgBi}_3\text{S}_5)$  data in [31] and  $S^\circ$  data of pure elements in [56].

<sup>c</sup> Calculated by the Craig and Barton [32] approximation method, according to Equation (16).

### Results of graphite incorporating galvanic cell (H)

In spite of the effect from phase transition and melting of sulphur [56,99], in the measurement temperature range 299–450 K, the  $E_{\text{EMF}}$  vs.  $T$  relations observed with most of the galvanic cells which contained graphite (cell (H)) can be approximated to be linear, as shown in Figure 12. This may suggest that there could be side reactions due to the presence of graphite in the cathode material. One possible source of error could be the so far unknown contribution of reaction (XXVII) [110] to the overall cell reaction.



Therefore, the correlation in the slope of  $E_{\text{EMF}}$  vs.  $T$  obtained with galvanic cell (G) (299–338 K) and galvanic cell (H) (303–452 K), as shown in Figure 12, may suggest that results obtained with the graphite free galvanic cell (G) can be extrapolated over the temperature range 338–368 K. Thus, the standard Gibbs energies of formation of pavonite in equilibrium with sulphur over the temperature range 338–368.7 K could also be expressed by Equation (20), which was originally calculated from the  $E_{\text{EMF}}$  vs.  $T$  relations in the temperature range 299–338 K. Nevertheless, there are not enough experimental data to correlate reliably the effect of added wt. % C, in the phase assemblage, with the resulting  $E_{\text{EMF}}$  values. More experimental work should be done for this equilibrium.

### 5.3.4 $\Delta_f G^\circ$ values of matildite and schapbachite

By combining the  $\Delta_f G^\circ$  values of reactions (XVIII)–(XXIII) determined in [IV,V] with those  $\Delta_f G^\circ$  values of pavonite (AgBi<sub>3</sub>S<sub>5</sub>) determined in the previous work [III], the Gibbs energies of formation of matildite and schapbachite were calculated as expressed by Equations (27)–(32).  $\Delta_f G_{\text{AgBi}_3\text{S}_5}^\circ$  values determined for pavonite, in the previous work [III], were only below  $T_{\text{tr}} = 368.30$  K at sulphur saturation and in the temperature range 492–594 K at bismuth saturation. Assuming that pavonite exists in one structural form below its incongruent melting point at  $T_{\text{m}} = 1005 \pm 4$  K [65]; the  $\Delta_f G_{\text{AgBi}_3\text{S}_5}^\circ$  values were extrapolated over 368–464 K, at

sulphur saturation, and over 594–699 K, at bismuth saturation, and used in the calculations of Equations (27)–(32).

$$\Delta_f G_{\beta\text{-AgBiS}_2}^\circ = -82.72 \pm 1.1 - (25.08 \pm 3.0) \cdot 10^{-3} \cdot T \quad (325\text{--}356 \text{ K}) \quad (27)$$

$$\Delta_f G_{\beta\text{-AgBiS}_2}^\circ = -81.92 \pm 1.1 - (27.26 \pm 3.0) \cdot 10^{-3} \cdot T \quad (371\text{--}382 \text{ K}) \quad (28)$$

$$\Delta_f G_{\beta\text{-AgBiS}_2}^\circ = -78.48 \pm 1.1 - (36.12 \pm 3.0) \cdot 10^{-3} \cdot T \quad (395\text{--}450 \text{ K}) \quad (29)$$

$$\Delta_f G_{\beta\text{-AgBiS}_2}^\circ = -122.63 \pm 2.3 + (42.0 \pm 5.2) \times 10^{-3} \cdot T \quad (429\text{--}464 \text{ K}) \quad (30)$$

$$\Delta_f G_{\alpha\text{-AgBiS}_2}^\circ = -113.58 \pm 0.4 + (21.76 \pm 0.7) \cdot 10^{-3} \cdot T \quad (474\text{--}543 \text{ K}) \quad (31)$$

$$\Delta_f G_{\alpha\text{-AgBiS}_2}^\circ = -129.50 \pm 0.1 + (51.15 \pm 0.2) \cdot 10^{-3} \cdot T \quad (550\text{--}699 \text{ K}). \quad (32)$$

Using the high-temperature (429–699 K) Gibbs energies of formations of matildite and schapbachite in Equation (30) and Equations (31) and (32), respectively, Gibbs energies of formation reactions below  $T_{\text{tr}} = 368.30 \text{ K}$  were also calculated. The high temperature experimental values from galvanic cell (K) were extrapolated to low-temperatures, with  $\alpha\text{-S}$  as standard state, by reactions (XXIV)–(XXVI) [56,78,99, 107,108] and Equation (9). The least square analysis yields Equation (33) for matildite in equilibrium with bismuth and Equation (34) for schapbachite in equilibrium with bismuth:

$$\Delta_f G_{\beta\text{-AgBiS}_2}^\circ = -126.88 \pm 2.34 + (53.05 \pm 5.2) \times 10^{-3} \cdot T \quad (298\text{--}368 \text{ K}) \quad (33)$$

$$\Delta_f G_{\alpha\text{-AgBiS}_2}^\circ = -112.10 \pm 2.4 + (15.99 \pm 4.6) \cdot 10^{-3} \cdot T \quad (298\text{--}368 \text{ K}). \quad (34)$$

The errors in Equations (33) and (34) were calculated by taking into account the different values of the enthalpies of phase transformation and melting of sulphur and bismuth [56,78,99, 107,108], including the estimated values in [III,V], and the errors in least square fitting of the experimental data. Differences in the literature values of the phase transition temperatures of bismuth and sulphur [56,65,78,99,105,106] are small and insignificant in the  $\Delta_{\text{tr}}G^\circ$  calculations.

The standard Gibbs energies of formation of matildite and schapbachite were also calculated by the Craig and Barton [32] approximation method. By interpolating the data of standard Gibbs energies of the pure binary sulphides  $\text{Bi}_2\text{S}_3$  and  $\text{Ag}_2\text{S}$  given in [56] at the experimental temperatures and using those values in Equation (10), Equations (35)–(40) were obtained. The interpolations of  $\Delta_f G_{\text{Bi}_2\text{S}_3}^\circ$  vs.  $T$  and  $\Delta_f G_{\text{Ag}_2\text{S}}^\circ$  vs.  $T$  data of [56] at the experimental temperatures were done in temperature range 298–700 K, taking into account the temperature regions in which  $\alpha\text{-Ag}_2\text{S}$ ,  $\beta\text{-Ag}_2\text{S}$ ,  $\alpha\text{-S}$ ,  $\beta\text{-S}$ ,  $\text{S(L)}$ ,  $\text{Bi(s)}$  and  $\text{Bi(L)}$  are the stable phases. In the  $\Delta_f G_{\alpha\text{-AgBiS}_2}^\circ$  calculations (Equations (39) and (40)),  $\Delta_{\text{mix}}H^\circ = 12 \text{ kJ}\cdot\text{mol}^{-1}$  reported by Bryndzia and Kleppa [28] were included.

$$\Delta_f G_{\beta\text{-AgBiS}_2}^\circ = -87.86 - (37.58 \pm 19.3) \cdot 10^{-3} \cdot T \quad (325\text{--}356 \text{ K}) \quad (35)$$

$$\Delta_f G_{\beta\text{-AgBiS}_2}^\circ = -89.46 - (33.51 \pm 19.3) \cdot 10^{-3} \cdot T \quad (371\text{--}382 \text{ K}) \quad (36)$$

$$\Delta_f G_{\beta\text{-AgBiS}_2}'^\circ = -92.90 - (24.65 \pm 19.3) \cdot 10^{-3} \cdot T \quad (395\text{--}450 \text{ K}) \quad (37)$$

$$\Delta_f G_{\beta\text{-AgBiS}_2}'^\circ = -92.25 \pm 0.2 - (26.14 \pm 19.3) \cdot 10^{-3} \cdot T \quad (429\text{--}464 \text{ K}) \quad (38)$$

$$\Delta_f G_{\alpha\text{-AgBiS}_2}'^\circ = -84.23 \pm 0.9 - (18.04 \pm 19.3) \cdot 10^{-3} \cdot T \quad (474\text{--}543 \text{ K}) \quad (39)$$

$$\Delta_f G_{\alpha\text{-AgBiS}_2}'^\circ = -92.48 \pm 0.5 - (3.23 \pm 19.3) \cdot 10^{-3} \cdot T \quad (550\text{--}699 \text{ K}). \quad (40)$$

The calculated  $\Delta_f G_{\alpha\text{-AgBiS}_2}'^\circ$  values at each experimental temperature (474–699 K) were extrapolated to low temperatures with  $\alpha$ -S as the standard state of sulphur by reactions (XXIV)–(XXVI) and Equation (9). The least square analysis yields [V]:

$$\Delta_f G_{\alpha\text{-AgBiS}_2}'^\circ = -91.11 \pm 10.1 - (8.34 \pm 18.5) \cdot 10^{-3} \cdot T \quad (298\text{--}368 \text{ K}). \quad (41)$$

Below  $T_{\text{tr}} = 368.30 \text{ K}$ , where  $\alpha$ -S is the stable state of sulphur, the standard Gibbs energies of formation of schapbachite ( $\alpha$ -AgBi<sub>1+x</sub>S<sub>2</sub>) calculated through the analysis of results obtained with galvanic cell (K), Equation (34), are more negative, by -13.7 kJ·mol<sup>-1</sup>, than those estimated through the approximation method of Craig and Barton [32]. If the results obtained by the approximation method of Craig and Barton [32] assumed to represent thermodynamic properties of the stoichiometric  $\alpha$ -AgBiS<sub>2</sub>, the observed differences in  $\Delta_f G^\circ(\alpha\text{-AgBiS}_2)$  values can be interpreted as the stability difference between bismuth-saturated schapbachite ( $\alpha$ -AgBi<sub>1+x</sub>S<sub>2</sub>) (Equation (34)), in the phase region  $\alpha$ -AgBiS<sub>2</sub>-AgBi<sub>3</sub>S<sub>5</sub>-Bi, and stoichiometric schapbachite ( $\alpha$ -AgBiS<sub>2</sub>) (Equation (41)).

### *Sulfidation reactions involving S<sub>2</sub>(g) to produce schapbachite*

Standard Gibbs energies of the pure substances Ag, Bi and S given in [56] over temperature range 400–700 K and standard Gibbs energies of formation of bismuth-saturated schapbachite determined in [V] were combined to calculate  $G_{\alpha\text{-AgBi}_{x+1}\text{S}_2}'^\circ$  values. The calculations were done for each region where Bi(s) and Bi(L) are the stable phases together with S(L).

$$G_{\alpha\text{-AgBi}_{x+1}\text{S}_2}'^\circ = -85.46 \pm 1.35 - (213.0 \pm 2.66) \cdot 10^{-3} \cdot T \quad (474\text{--}543 \text{ K}) \quad (42)$$

$$G_{\alpha\text{-AgBi}_{x+1}\text{S}_2}'^\circ = -75.39 \pm 0.9 - (230.7 \pm 1.4) \cdot 10^{-3} \cdot T \quad (550\text{--}699 \text{ K}). \quad (43)$$

Standard Gibbs energies of sulfidation reactions (XXVIII) and (XXIX) with gaseous pure diatomic sulphur at 1 atm as the standard state were calculated by combining Equations (42) and (43) with the Gibbs energies of the pure substances given in [56].



The calculations yield Equations (44) and (45) for reactions (XXVIII) and (XXIX), respectively.

$$\Delta_{r(\text{XIV})}G^\circ = -243.87 \pm 0.3 + (182.58 \pm 0.5) \cdot 10^{-3} \cdot T \quad (550\text{--}699 \text{ K}) \quad (44)$$

$$\Delta_{r(\text{XVI})}G^\circ = -199.32 \pm 0.3 + (163.64 \pm 0.4) \cdot 10^{-3} \cdot T \quad (550\text{--}699 \text{ K}). \quad (45)$$

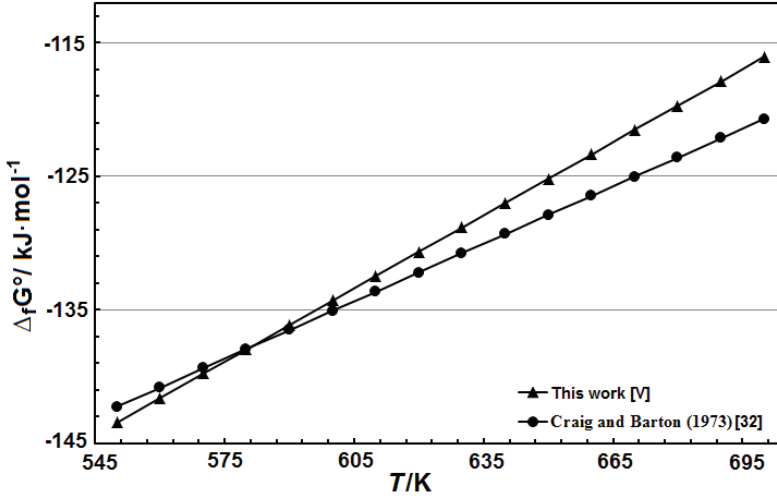


**Figure 18.**  $\Delta_f G^\circ(\alpha\text{-AgBiS}_2)$  vs.  $T$  diagram showing a comparison between calculated values in this work for bismuth-saturated schapbachite and the values reported by Craig and Barton [32] for the stoichiometric schapbachite according to reaction (XXVIII). The standard states are: Ag(fcc), Bi(L) and  $\text{S}_2(\text{g})$  [V].

Assuming thermodynamic functions for reactions (XXVIII) and (XXIX) reported by Craig and Barton [32] represent the formation of the ideal stoichiometric schapbachite ( $\alpha\text{-AgBiS}_2$ ); it might be possible to conclude that above  $T = 580 \text{ K}$  and in the presence of Ag,  $\text{Ag}_2\text{S}$ , Bi(L) and  $\text{S}_2(\text{g})$  the stoichiometric schapbachite ( $\alpha\text{-AgBiS}_2$ ) is thermodynamically more stable than that saturated with bismuth, as shown in Figure 18.

#### Matildite ( $\beta\text{-AgBiS}_2$ )

As Figure 19 shows, the standard Gibbs energies of formation of  $\beta\text{-AgBiS}_{2+y}$  calculated through the analysis of results obtained with galvanic cell (J), Equation (27), are more positive than those of the standard Gibbs energies determined by analysing the results obtained with galvanic cell (K), Equation (33), with  $\alpha\text{-S}$  as standard state. The observed differences in  $\Delta_f G^\circ_{\beta\text{-AgBiS}_2}$  values can be interpreted as the difference between thermodynamic properties of matildite saturated with sulphur (Equation (13)), in the phase region  $\beta\text{-AgBiS}_2\text{-AgBi}_3\text{S}_5\text{-S}$ , and matildite saturated with bismuth (Equation (16)), in the phase region  $\beta\text{-AgBiS}_2\text{-AgBi}_3\text{S}_5\text{-Bi}$  [IV]. The more negative  $\Delta_f G^\circ$  values of matildite in the phase region  $\beta\text{-AgBiS}_2\text{-AgBi}_3\text{S}_5\text{-Bi}$  also suggest that, at the same temperature, bismuth-saturated matildite ( $\beta\text{-AgBi}_{1+x}\text{S}_2$ ) has a lower Gibbs energy than the sulphur-saturated variety. The estimated  $\Delta_f G^\circ$  values for the stoichiometric  $\beta\text{-AgBiS}_2$  through the simplified calculations of Craig and Barton [32], according to Equation (10), lie in between the  $\Delta_f G^\circ$  values of the sulphur-saturated matildite ( $\beta\text{-AgBiS}_{2+y}$ ) and bismuth-saturated matildite ( $\beta\text{-AgBi}_{1+x}\text{S}_2$ ), as shown in Figure 19.

In Figure 19, open diamonds and squares are the experimental data obtained with galvanic cells (J) and (K), respectively. Open circles are calculated values at the experimental temperatures, according to Equation (35). Solid diamonds are the extrapolated values of experimental data obtained with galvanic cell (K) to low temperatures, as expressed in Equation (33).

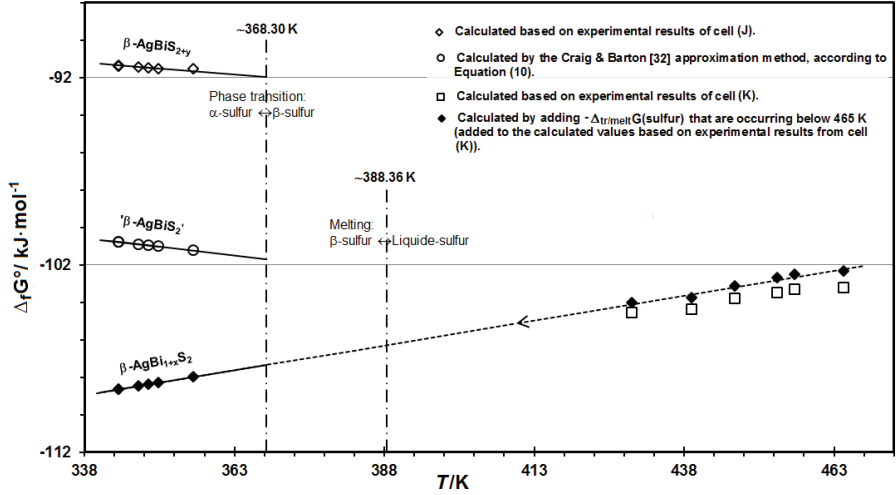


**Figure 19.**  $\Delta_f G^\circ$  vs.  $T$  values of matildite determined in [IV] at bismuth and sulphur saturation as well as those calculated by the Craig and Barton [32] approximation method. The standard states are Ag(fcc), Bi(rho) and S(ortho).

As  $\Delta_f G^\circ$  vs.  $T$  relation of Equation (35) indicates,  $\Delta_f H_{298.15}^\circ(\beta\text{-AgBiS}_2)$  obtained by the Craig and Barton [32] approximation method ( $-87.86 \text{ kJ}\cdot\text{mol}^{-1}$ ) is close to the result observed for sulphur-saturated  $\beta\text{-AgBiS}_{2+y}$  ( $-82.72 \pm 1.1 \text{ kJ}\cdot\text{mol}^{-1}$ ), according to Equation (27). The  $\Delta_f H_{298.15}^\circ(\beta\text{-AgBiS}_2)$  value calculated from the  $\Delta_f G^\circ$  vs.  $T$  relation in Equation (33), for the bismuth-saturated matildite ( $\beta\text{-AgBi}_{1+x}\text{S}_2$ ),  $-126.88 \pm 2.34 \text{ kJ}\cdot\text{mol}^{-1}$ , is clearly more negative than the value calculated for stoichiometric  $\beta\text{-AgBiS}_2$ ,  $-87.86 \text{ kJ}\cdot\text{mol}^{-1}$ .

The calculated  $\Delta_f S_{298.15}^\circ(\beta\text{-AgBiS}_2)$  value,  $37.58 \pm 19.3 \text{ J}\cdot(\text{K}\cdot\text{mol})^{-1}$ , from the  $\Delta_f G^\circ$  vs.  $T$  relation in Equation (35), is more positive than the result observed through the analysis of  $\Delta_f G^\circ$  vs.  $T$  relation in Equation (27),  $25.08 \pm 3.0 \text{ J}\cdot(\text{K}\cdot\text{mol})^{-1}$ , and Equation (33),  $-53.05 \pm 5.2 \text{ J}\cdot(\text{K}\cdot\text{mol})^{-1}$ .

The experimentally determined  $\Delta_f G_{\beta\text{-AgBiS}_2}^\circ$  values based on results obtained with galvanic cell (J) are more positive than the calculated values according to the Craig and Barton [32] approximation method as well as the experimentally determined values based on results obtained with galvanic cell (K), as shown in Figure 20. The average deviation between the values calculated by the Craig and Barton [32] approximation method and experimentally determined  $\Delta_f G_{\beta\text{-AgBiS}_2}^\circ$  values (obtained with galvanic cell (J), at sulphur saturation) at the experimental temperatures is about  $10.2 \pm 0.6 \text{ kJ}\cdot\text{mol}^{-1}$ . As also observed in our previous work [III], in which thermodynamic properties of bismuth saturated pavonite ( $\text{AgBi}_{3+x}\text{S}_5$ ;  $0 < x < 0.14$ ) were studied; the magnitude of the observed deviation may emanate from the differences in thermodynamic properties of the

stoichiometric matildite ( $\beta\text{-AgBiS}_2$ ) and the sulphur saturated matildite ( $\beta\text{-AgBiS}_{2+y}$ ) studied in [IV].

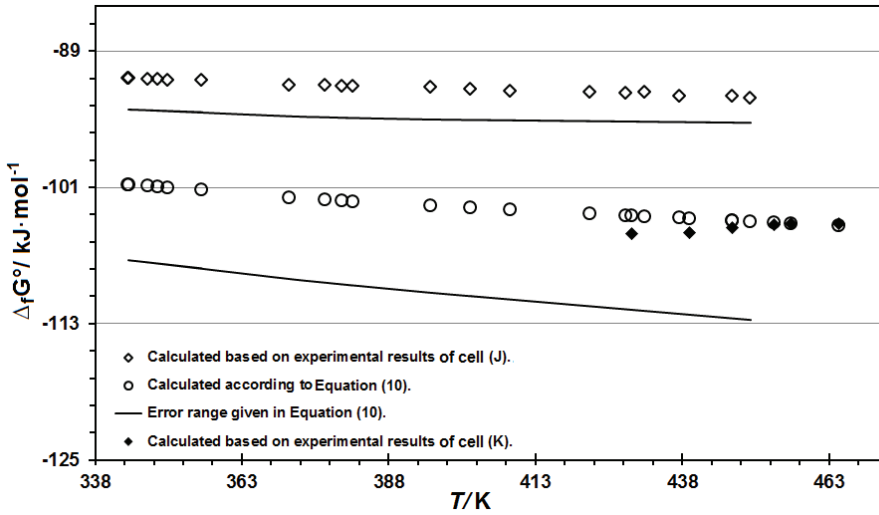


**Figure 20.**  $\Delta_f G^\circ(\beta\text{-AgBiS}_2)$  vs.  $T$  diagram showing a summary of the experimentally determined and calculated values according to Equation (16), at the corresponding experimental temperatures [IV].

In the temperature range 429–464 K, differences between the experimentally determined (Equation (30), at bismuth saturation) and the calculated (Equation (38), stoichiometric) Gibbs energies of formation of matildite are small; even though the slope of the  $\Delta_f G^\circ_{\beta\text{-AgBiS}_2}$  vs.  $T$  relations are different. In our previous work [III], for pavonite saturated with bismuth, these differences in Gibbs energies of formation were significant. The observed larger deviations from the stoichiometric thermodynamic properties of matildite at sulphur saturation and pavonite at bismuth saturation could indicate that sulphur readily dissolves into matildite structure such that the thermodynamic properties of matildite are altered, significantly, whereas bismuth dissolves into pavonite structure more readily.

The standard enthalpy of formation of  $\beta\text{-AgBiS}_2$  ( $\Delta_f H^\circ_{298.15}$ ) determined from the  $E_{\text{EMF}}$  vs.  $T$  relations obtained with galvanic cell (J),  $-82.72 \pm 1.1 \text{ kJ}\cdot\text{mol}^{-1}$ , is close to the value  $-81.83 \text{ kJ}\cdot\text{mol}^{-1}$  which was determined by Schmidt et al. [30], by the EMF-method, and the average value  $-81.7 \pm 6.7 \text{ kJ}\cdot\text{mol}^{-1}$  determined by Bryndzia and Kleppa [28], by the calorimetric method. As in galvanic cell (J) of this work, the cathode materials of Schmidt et al. [30] also incorporated pure sulphur as the third constituent, indicating that the matildite ( $\beta\text{-AgBiS}_2$ ) they studied was also sulphur-saturated. Hence, a fair agreement of  $\Delta_f H^\circ_{298.15}(\beta\text{-AgBiS}_2)$  value is observed in this work [IV] and their work, due to different compositions of matildite. However, the standard entropy of formation of  $\beta\text{-AgBiS}_2$  ( $\Delta_f S^\circ_{298.15}$ ),  $53.95 \text{ J}\cdot(\text{K}\cdot\text{mol})^{-1}$ , reported by Schmidt et al. [30], is more positive than the values obtained with galvanic cell (J) in [IV] ( $25.08 \pm 3.0 \text{ J}\cdot(\text{K}\cdot\text{mol})^{-1}$ ). The average  $\Delta_f H^\circ_{298.15}$  value obtained by analyzing measurement results on the galvanic cell (K) at higher temperatures, according to Equation (33),  $-126.88 \pm 2.34 \text{ kJ}\cdot\text{mol}^{-1}$ , is

higher than the values obtained with galvanic cell (J) and the values determined by Schmidt et al. [30] and Bryndzia and Kleppa [28]. This higher  $\Delta_f H_{298.15}^\circ$  value for matildite in equilibrium with bismuth (in cell (K)) suggests that different compositions of matildite have different standard enthalpies of formation.

Shykhyyev et al. [31] reported (as given in [109]) the standard entropy ( $S_{298.15}^\circ$ ) of  $\beta$ -AgBiS<sub>2</sub> to be  $166.3 \pm 6.8 \text{ J}\cdot(\text{K}\cdot\text{mol})^{-1}$ . Using the standard entropy of the pure elements from [56] and the standard entropy of  $\beta$ -AgBiS<sub>2</sub> reported by Shykhyyev et al. [31], we calculated the standard entropy of formation ( $\Delta_f S_{298.15}^\circ$ ) of  $\beta$ -AgBiS<sub>2</sub> according to them to be  $2.78 \pm 6.8 \text{ J}\cdot(\text{K}\cdot\text{mol})^{-1}$ . This value is more positive, by  $55.4 \pm 6.8 \text{ J}\cdot(\text{K}\cdot\text{mol})^{-1}$ , than the value obtained with galvanic cell (K),  $-53.05 \pm 5.2 \text{ J}\cdot(\text{K}\cdot\text{mol})^{-1}$  (for bismuth-saturated matildite) and more negative, by  $22.3 \pm 6.8 \text{ J}\cdot(\text{K}\cdot\text{mol})^{-1}$ , than the value obtained with galvanic cell (J),  $25.08 \pm 3.0 \text{ J}\cdot(\text{K}\cdot\text{mol})^{-1}$  (for sulphur-saturated matildite). However, the standard Gibbs energy of matildite ( $\beta$ -AgBiS<sub>2</sub>), at 298.15 K, reported by Shykhyyev et al. [31] and the results obtained with the galvanic cell (K) are in fair agreement, as shown in Table 7. The  $\Delta_f H_{298.15}^\circ$  values determined from results obtained with galvanic cell (K), for the bismuth-saturated matildite ( $\beta$ -AgBi<sub>1+x</sub>S<sub>2</sub>),  $-126.88 \pm 2.3 \text{ kJ}\cdot\text{mol}^{-1}$ , and the results reported by Shykhyyev et al. [31],  $-118.6 \pm 3.0 \text{ kJ}\cdot\text{mol}^{-1}$ , are in good agreement. These similarities may suggest that the investigated matildite in the study of Shykhyyev et al. [31] was also at bismuth saturation or bismuth enriched.

Voronin and Osadchii [7] also conducted  $E_{EMF}$  measurements on similar galvanic cell arrangements to our cell (K) and reported  $\Delta_f H_{298.15}^\circ = -86.47 \pm 1.63 \text{ kJ}\cdot\text{mol}^{-1}$  and  $\Delta_f S_{298.15}^\circ = 14.64 \pm 2.4 \text{ J}\cdot(\text{K}\cdot\text{mol})^{-1}$  for matildite. However, their cathode layer (Ag-Bi-S phase assemblages) contained significant amounts of graphite and they did not mention whether they considered the phase transition and melting of sulphur in their extrapolation to room temperature. Nevertheless, their values have also shown the tendency of more negative values of standard enthalpy and entropy of matildite in equilibrium with bismuth than the results obtained with galvanic cells similar to our cell (J), i.e. matildite in equilibrium with sulphur.

The divergent results observed among the calculated values, the literature data and the values obtained from our experimental studies may mainly come from the different compositions of matildite. In our series of experiments, it became clear that thermodynamic properties of matildite in equilibrium with sulphur are different from that of matildite in equilibrium with bismuth. A comparison of the standard thermodynamic properties of matildite ( $\beta$ -AgBiS<sub>2</sub>), at 298.15 K, determined in [IV] with those of the literature values is shown in Table 7.

The difference between the standard entropies of matildite saturated with sulphur ( $188.64 \pm 3.0 \text{ J}\cdot\text{K}^{-1}\cdot\text{mol}^{-1}$ ) and that of saturated with bismuth ( $110.5 \pm 5.2 \text{ J}\cdot(\text{K}\cdot\text{mol})^{-1}$ ) is  $78.2 \pm 6.4 \text{ J}\cdot(\text{K}\cdot\text{mol})^{-1}$ . These differences in standard entropies at slightly different compositions of matildite ( $\beta$ -AgBiS<sub>2</sub>) were also observed in our earlier work [III] at slightly different compositions of pavonite ( $\text{AgBi}_3\text{S}_5$ ).

**Table 7.** A summary of standard thermodynamic properties of matildite at 298.15 K and 1 atm. The standard states are: Ag(fcc), Bi(rho) and S(ortho) [IV].

Phase	$\Delta_f G^\circ/\text{kJ}\cdot\text{mol}^{-1}$	$\Delta_f H^\circ/\text{kJ}\cdot\text{mol}^{-1}$	$\Delta_f S^\circ/\text{J}\cdot(\text{K}\cdot\text{mol})^{-1}$	$S^\circ/\text{J}\cdot(\text{K}\cdot\text{mol})^{-1}$	Ref.
' $\beta$ -AgBiS <sub>2</sub> ' (sulphur saturated)	-90.20 ± 4.7	-82.72 ± 1.1	25.08 ± 3.0	188.64 ± 3.0	[IV]
' $\beta$ -AgBiS <sub>2</sub> ' (bismuth saturated)	-111.05 ± 2.5	-126.88 ± 2.3	-53.05 ± 5.2	110.48 ± 5.2	[IV]
' $\beta$ -AgBiS <sub>2</sub> '	-99.06 ± 5.8	-87.86	37.58 ± 19.3	201.1 ± 19.3	[IV] <sup>a</sup>
' $\beta$ -AgBiS <sub>2</sub> '	-97.92	-81.83	53.95	217.47	[30]
' $\beta$ -AgBiS <sub>2</sub> '	-	-81.7 ± 6.7	-	-	[28]
' $\beta$ -AgBiS <sub>2</sub> '	-124.2 ± 4.4	-118.6 ± 3.0	2.78 ± 6.8 <sup>b</sup>	166.3 ± 6.8	[31]
' $\beta$ -AgBiS <sub>2</sub> '	-90.88 ± 1.7	-86.47 ± 1.63	14.64 ± 2.4 <sup>c</sup>	178.16 ± 2.4	[7]

<sup>a</sup> Calculated by the Craig and Barton [32] approximation method, according to Equation (10).

<sup>b</sup> The standard entropy of formation was calculated from Shykhyyev et al.'s [31]  $S_{298.15}^\circ(\beta\text{-AgBiS}_2)$  data and standard entropy data of the pure elements [56].

<sup>c</sup> The standard entropy of formation was calculated from Voronin's and Osadchii's [7]  $S_{298.15}^\circ(\beta\text{-AgBiS}_2)$  data and standard entropy data of the pure elements [56].

### Schapbachite ( $\alpha\text{-AgBiS}_2$ )

The  $\Delta_{\text{tr}}H^{\beta\rightarrow\alpha}(\text{AgBi}_{1+x}\text{S}_2)$  value,  $7.3 \pm 2.1 \text{ kJ}\cdot\text{mol}^{-1}$ , calculated from the EMF cell in [V] and its  $\Delta_f G^\circ$  vs.  $T$  relations at the polymorphic phase transformation temperature obtained,  $465.55 \pm 5 \text{ K}$ , is in good agreement with the value,  $10.5 \pm 4.6 \text{ kJ}\cdot\text{mol}^{-1}$ , reported by Bryndzia and Kleppa [28] at 468 K, by the high-temperature direct synthesis calorimetric studies.

The experimentally determined  $\Delta_f G^\circ(\alpha\text{-AgBi}_{1+x}\text{S}_2)$  values based on the results obtained with galvanic cell (K) are more negative than the calculated values according to the Craig and Barton [32] approximation method, as can be seen in Figure 21. The difference between the calculated and experimentally determined  $\Delta_f G^\circ(\alpha\text{-AgBiS}_2)$  values at the experimental temperatures increases from 0  $\text{kJ}\cdot\text{mol}^{-1}$  to 10  $\text{kJ}\cdot\text{mol}^{-1}$  with increasing temperature in the range 474–699 K. As also observed in the study of pavonite [III] and matildite [IV] differences in  $\Delta_f G^\circ(\alpha\text{-AgBiS}_2)$  values and the  $\Delta_f G^\circ(\alpha\text{-AgBiS}_2)$  vs.  $T$  slope may emanate from the differences in thermodynamic properties of the stoichiometric schapbachite ( $\alpha\text{-AgBiS}_2$ ) and the bismuth-saturated schapbachite ( $\alpha\text{-AgBi}_{1+x}\text{S}_2$ ) studied in [V]. In our previous work published in [III], similar differences were also observed between the calculated values of the stoichiometric pavonite and the bismuth-saturated pavonite ( $\text{AgBi}_{3+x}\text{S}_5$ ;  $0 < x < 0.14$ ).

From experimental results expressed by Equations (27), (31), (39) and (40), it is possible to conclude that in the temperature range 474–680 K, schapbachite ( $\alpha\text{-AgBi}_{1+x}\text{S}_2$ ) saturated with bismuth is thermodynamically more stable than the stoichiometric schapbachite ( $\alpha\text{-AgBiS}_2$ ). This stabilizing effect of bismuth saturation has also been observed by Damian et al. [111], while studying the decomposition of  $\text{AgPbBiS}_3$  along the tie line  $\text{PbS-AgBiS}_2$ . However, as results in [V] indicate: in the presence of  $\text{S}_2(\text{g})$  above  $T = 580 \text{ K}$  and ambient pressure conditions, the stoichiometric schapbachite is thermodynamically more stable than the bismuth-saturated variety.

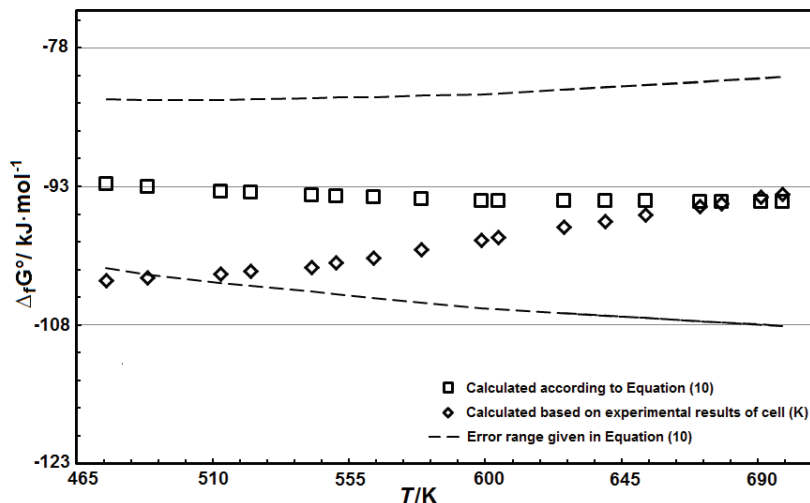


**Figure 21.**  $\Delta_f G^\circ(\alpha\text{-AgBiS}_2)$  vs.  $T$  diagram showing the experimentally determined and calculated values, according to Equation (10), at the corresponding experimental temperatures [V].

The average  $\Delta_f H^\circ(\alpha\text{-AgBiS}_2, 298.15 \text{ K})$  value calculated from the results obtained with the galvanic cell (K) at higher temperatures is  $-112.10 \pm 2.4 \text{ kJ}\cdot\text{mol}^{-1}$ . The average  $\Delta_f H^\circ(\alpha\text{-AgBiS}_2, 298.15 \text{ K})$  value calculated by the approximation method of Craig and Barton [32] is  $-91.11 \pm 10.1 \text{ kJ}\cdot\text{mol}^{-1}$ . Both standard enthalpies of formations calculated from the  $\Delta_f G^\circ$  vs.  $T$  relations are more negative than the average value  $-71.2 \pm 2.1 \text{ kJ}\cdot\text{mol}^{-1}$  reported by Bryndzia and Kleppa [28]. Within the experimental errors of our results and the literature values, the difference between  $\Delta_f H^\circ$  values clearly show that different compositions of schapbachite ( $\alpha\text{-AgBiS}_2$ ) have different thermodynamic properties, and indicate some solid solubility range in it.

As  $\Delta_f G^\circ$  vs.  $T$  relations of Equations (39) and (40) indicate,  $\Delta_f H^\circ(\alpha\text{-AgBiS}_2)$  values calculated by the Craig and Barton [32] approximation method,  $-84.23 \pm 0.9 \text{ kJ}\cdot\text{mol}^{-1}$  (474–543 K) and  $-92.48 \pm 0.5 \text{ kJ}\cdot\text{mol}^{-1}$  (550–699 K), respectively, are more endothermic than the experimentally determined values determined in [V].  $\Delta_f S^\circ(\alpha\text{-AgBiS}_2)$  values calculated by the Craig and Barton [32] approximation method, as expressed in Equations (39) and (40),  $18.04 \pm 19.3 \text{ J}\cdot(\text{K}\cdot\text{mol})^{-1}$  (474–543 K) and  $3.23 \pm 19.3 \text{ J}\cdot(\text{K}\cdot\text{mol})^{-1}$  (550–699 K), respectively, are also more positive than their respective experimental values determined in [V];  $\Delta_f S^\circ(\alpha\text{-AgBi}_{1+x}\text{S}_2) = -21.76 \pm 0.7 \text{ J}\cdot(\text{K}\cdot\text{mol})^{-1}$  and  $\Delta_f S^\circ(\alpha\text{-AgBi}_{1+x}\text{S}_2) = -51.15 \pm 0.2 \text{ J}\cdot(\text{K}\cdot\text{mol})^{-1}$ , respectively.

At 298.15 K, the difference between the standard entropies of the stoichiometric schapbachite, obtained through the approximation method of Craig and Barton [32] and that of bismuth-saturated schapbachite is about  $24.34 \text{ kJ}\cdot\text{mol}^{-1}$ . The differences observed among the approximated thermodynamic functions, the values reported by Bryndzia and Kleppa [28] and our experimental results in [V] may mainly come from the different compositions of schapbachite. A similar difference has been also observed in [III] concerning the stoichiometric pavonite ( $\text{AgBi}_3\text{S}_5$ ) and bismuth-saturated pavonite ( $\text{AgBi}_{3+x}\text{S}_5$ ;  $0 < x < 0.14$ ). A comparison

of the standard thermodynamic properties of schapbachite ( $\alpha$ -AgBiS<sub>2</sub>), at 298.15 K, determined in [V] with those of the literature values is shown in Table 8. The standard entropy of schapbachite was calculated according to Equation (8), based on reaction (XXII).

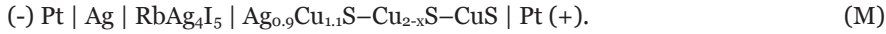
**Table 8.** A summary of standard thermodynamic properties of schapbachite at 298.15 K and 1 atm. The standard states are: Ag(fcc), Bi(rho) and S(ortho) [V].

Phase	$\Delta_f G^\circ/\text{kJ}\cdot\text{mol}^{-1}$	$\Delta_f H^\circ/\text{kJ}\cdot\text{mol}^{-1}$	$\Delta_f S^\circ/\text{J}\cdot(\text{K}\cdot\text{mol})^{-1}$	$S^\circ/\text{J}\cdot(\text{K}\cdot\text{mol})^{-1}$	Ref.
' $\alpha$ -AgBiS <sub>2</sub> ' (bismuth saturated)	-107.33 $\pm$ 3.82	-112.10	-15.99 $\pm$ 4.6	147.53 $\pm$ 4.6	[V]
' $\alpha$ -AgBiS <sub>2</sub> '	-93.60 $\pm$ 15.82	-91.11	8.34 $\pm$ 18.5	171.87 $\pm$ 18.5	[V] <sup>a</sup>
' $\alpha$ -AgBiS <sub>2</sub> '	-	-71.2	-	-	[28]

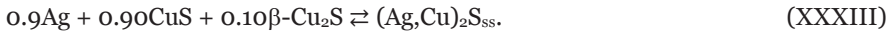
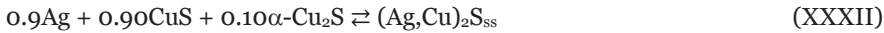
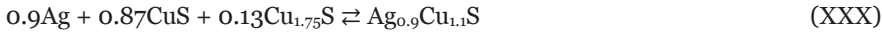
<sup>a</sup> Calculated by the Craig and Barton [32] approximation method, according to Equation (10).

## 5.4 Ag-Cu-S system

In this section, a summary of results obtained in the Ag-Cu-S system, published in [VI], is presented. In the Ag-Cu-S system, thermodynamic measurements were conducted in the temperature range 316–498 K. The cell arrangement on which the measurements were conducted can be represented by a galvanic cell (M).



Based on the literature data and the results of this study, the virtual electrochemical cell reactions of galvanic cell (M) can be explicitly written over temperature regions of the different stable phases as:



### 5.4.1 $E_{\text{EMF}}$ values (cathode: Ag-Cu-S phase assemblages)

The EMF measurements were performed in the temperature range 316–498 K by heating and cooling of the cell. Isothermal equilibrium  $E_{\text{EMF}}$  values were achieved after many days of continuous measurements, in most cases in about a week. For instance, at about 341.5 K the isothermal equilibrium  $E_{\text{EMF}}$  values were observed after 12 days of continuous measurements.

The measured  $E_{\text{EMF}}$  values with galvanic cell (M) at different temperatures together with the only available experimental data in the literature [112] are shown in Figure 22. Below  $T = 345$  K, the  $E_{\text{EMF}}$  values obtained in this study are approximately 0.0046 V less than the values reported by Schmidt et al. [112].

Above  $T = 345$  K, the results reported by Schmidt et al. [112] and our results are in excellent agreement.

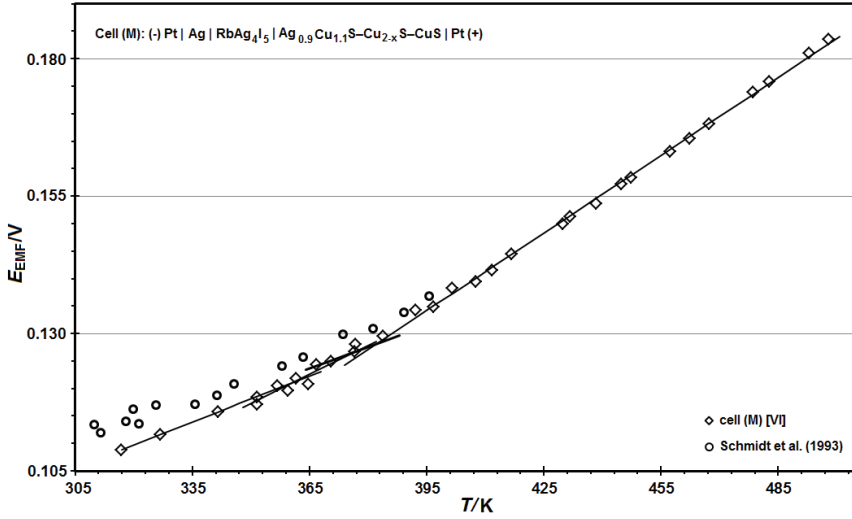


**Figure 22.** A summary of the  $E_{EMF}$  vs.  $T$  relations obtained with galvanic cell (M) together with the literature values [112], the least square fitting of the experimental points in this work are shown with the solid lines [VI].

In our experimental temperature range 316–498 K,  $E_{EMF}$  values continuously increased with increasing temperature. In the temperature range 349–361 K, the slope of  $E_{EMF}$  vs.  $T$  turns upward which is followed by a slight decrease in the slope of  $E_{EMF}$  vs.  $T$ , in the temperature range 366–376 K. Above  $T = 377$  K, the slope of the  $E_{EMF}$  vs.  $T$  plot turns again noticeably upward. All the small angular turns on the  $E_{EMF}$  vs.  $T$  plots can be attributed to phase transformations in the cathode material, i.e., the phase assemblage  $Ag_{0.9}Cu_{1.1}S-Cu_{2-x}S-CuS$ .

#### Analytical forms of $E_{EMF}$ and $T_{tr}$

Least squares linear regression of  $E_{EMF}$  values on temperature values in different temperature regions of phase stabilities were compiled in Table 9. By solving the selected equations in Table 9, simultaneously, two phase transition temperatures were found. The obtained values  $360.7 \pm 4.3$  K and  $376.6 \pm 6.3$  K are in fair agreement with the phase transition temperature of  $Ag_{0.93}Cu_{1.07}S$  to the solid solution  $(Ag,Cu)_2S_{ss}$  ( $T = 363$  K [82]) and the polymorphic phase transition temperature of  $Cu_2S$  ( $T_{tr} = 376$  K [80]), respectively.

**Table 9.** Values of the coefficients a and b, which were calculated by least squares linear regression of  $E_{EMF}$  values on temperature-values [VI].

$E_{EMF}(mV) = a + b \cdot T$			T/K	N
a	b	$R^2$		
20.322	0.2793	0.999	316 -348	3
6.486	0.3536	0.780	349 -361	5
29.897	0.2569	0.978	366 -376	3
-52.06	0.4715	0.998	377 -498	19

### 5.4.2 Thermodynamic functions in Ag-Cu-S system

Gibbs energies of reactions (XXX)–(XXXIII) were calculated directly from the measured  $E_{EMF}$  vs.  $T$  relations according to Equation (3). The results obtained for the reactions (XXX)–(XXXIII) are expressed by Equations (46)–(49), respectively.

$$\Delta_r(\text{XXX})G^\circ = -1.77 \pm 0.02 - [(24.25 \pm 0.06) \cdot 10^{-3}] \cdot T \quad (316\text{--}348 \text{ K}) \quad (46)$$

$$\Delta_r(\text{XXXI})G^\circ = 0.56 \pm 3.35 - [(30.71 \pm 9.41) \cdot 10^{-3}] \cdot T \quad (349\text{--}361 \text{ K}) \quad (47)$$

$$\Delta_r(\text{XXXII})G^\circ = -2.60 \pm 1.25 - [(22.31 \pm 3.36) \cdot 10^{-3}] \cdot T \quad (366\text{--}376 \text{ K}) \quad (48)$$

$$\Delta_r(\text{XXXIII})G^\circ = 4.52 \pm 0.17 - [(40.94 \pm 0.39) \cdot 10^{-3}] \cdot T \quad (377\text{--}498 \text{ K}). \quad (49)$$

$\Delta_r(\text{XXX})G^\circ$  values in Equation (46) combined with those  $\Delta_f G^\circ(\text{Cu}_{1.75}\text{S})$  values, calculated from the results reported by Schmidt et al. [112], and  $\Delta_f G^\circ(\text{CuS})$  values of Barin [56]; Gibbs energies of formation of  $\text{Ag}_{0.9}\text{Cu}_{1.1}\text{S}$  were calculated to be:

$$\Delta_f G_{\text{Ag}_{0.9}\text{Cu}_{1.1}\text{S}}^\circ = -55.1 \pm 0.7 - (26.61 \pm 0.1) \cdot 10^{-3} \cdot T \quad (316\text{--}348 \text{ K}). \quad (50)$$

**Table 10.** A summary of standard thermodynamic properties of stromeyerite ( $\text{Ag}_{0.9}\text{Cu}_{1.1}\text{S}$ ) at 298.15 K. The standard states are: Ag(fcc), Cu(fcc) and S(ortho) [VI].

$\Delta_f G^\circ/\text{kJ}\cdot\text{mol}^{-1}$	$\Delta_f H^\circ/\text{kJ}\cdot\text{mol}^{-1}$	$\Delta_f S^\circ/\text{J}\cdot(\text{K}\cdot\text{mol})^{-1}$	$S^\circ/\text{J}\cdot(\text{K}\cdot\text{mol})^{-1}$	Reference
$-63.03 \pm 0.76$	$-55.09 \pm 0.67$	$26.61 \pm 0.07$	$133.56 \pm 0.07$	This work
$-75.39 \pm 5.81$	$-59.74$	$52.50 \pm 19.16$	$159.45 \pm 19.16$	This work <sup>a</sup>
$-67.50$	$-60.34$	$24.0$	$130.95^b$	[112]

<sup>a</sup> Calculated by the Craig and Barton [32] approximation method (Equation (10)).

<sup>b</sup> Calculated by using the data of Barin [56] and  $\Delta_f S^\circ$  value of Schmidt et al. [112].

The standard Gibbs energies of formation of stromeyerite were also calculated by the Craig and Barton [32] approximation method according to Equation (10). In the calculation  $\Delta_f G^\circ(\text{Ag}_2\text{S})$  and  $\Delta_f G^\circ(\text{Cu}_2\text{S})$  data of Barin [56] were used. The calculation yields Equation (51):

$$\Delta_f G_{\text{Ag}_{0.9}\text{Cu}_{1.1}\text{S}}^\circ = -59.74 - (52.50 \pm 19.16) \cdot 10^{-3} \cdot T \quad (316\text{--}348 \text{ K}). \quad (51)$$

The  $\Delta_f G^\circ(\text{Ag}_{0.9}\text{Cu}_{1.1}\text{S})$  values calculated from our experimental values are in good agreement with both the experimental values reported by Schmidt et al. [112] and the values calculated by the Craig and Barton [32] approximation method. However, the  $\Delta_f S^\circ(\text{Ag}_{0.9}\text{Cu}_{1.1}\text{S}) = 52.50 \pm 19.16 \text{ J}\cdot(\text{K}\cdot\text{mol})^{-1}$  calculated by the simplified approach of Craig and Barton [32] is more positive than the values obtained in this study [VI]. A comparison of the standard thermodynamic properties of stromeyerite, at 298.15 K, determined in this study with those of the literature values was compiled in Table 10.

## 6. Conclusions

Accurate thermodynamic data are essential for reliable quantitative modelling of the stabilities of phases and their chemical behaviour in equilibrium chemical reactions. The solid state EMF method is one of the versatile methods to achieve the necessary thermodynamic data accurately. Due to the discovery of solid state electrolytes; such as AgI and  $\text{RbAg}_4\text{I}_5$ , which are fast ionic conductors of  $\text{Ag}^+$  ions, accurate thermodynamic studies of silver-based systems at low and intermediate temperatures can be realized by the EMF method.

In this thesis work [I–VI], thermodynamic properties of phases and their assemblages in the Ag-Te, Ag-Bi-S and Ag-Cu-S systems below  $T = 700$  K have been studied experimentally by an improved EMF method. The traditional EMF method has been improved for better accuracies and to overcome experimental difficulties in studying those phase assemblages incorporating volatile components. State-of-the-art equipment has been utilized and a new philosophy for constructing the galvanic cell and a new experimental arrangement to control the temperature gradient over the galvanic EMF cell were employed.

The results obtained in the Ag-Te system [I,II] are, generally, in reasonable agreement with some of the available literature values. Thermodynamic properties of the stoichiometric equilibrium phase assemblages;  $\text{Ag}_5\text{Te}_3$ -Te,  $\text{Ag}_5\text{Te}_3$ - $\text{Ag}_{1.9}\text{Te}$ ,  $\text{Ag}_5\text{Te}_3$ - $\text{Ag}_2\text{Te}$  and  $\text{Ag}_2\text{Te}$ - $\text{Ag}_{1.9}\text{Te}$ , have been determined accurately and explicitly *in situ* at low and intermediate temperatures. New experimental data were also obtained and used to determine eutectic, eutectoidic decomposition and phase transition temperatures.

In the Ag-Bi-S system, thermodynamic properties of pavonite, matildite and schapbachite at bismuth- and sulphur-saturation conditions have been experimentally determined. Prior to this thesis work [III–V], the effects of saturation of sulphur and bismuth on the thermodynamic properties of the ternary phases were not known distinctively. In addition, new experimental thermodynamic data of the ternary phases in the temperature ranges that have not been experimentally studied before were obtained. Based on the experimental results, accurate thermodynamic functions for 17 selected equilibrium reactions were derived. Using these thermodynamic data and the literature values the stability of  $\text{AgBiS}_2$  in the presence of gaseous sulphur has also been evaluated.

The obtained thermodynamic properties of sulphur-saturated pavonite are in reasonable agreement with selected literature values and the values calculated by the Craig and Barton [32] approximation method. The standard enthalpy of formation of pavonite reported by Shykhiev et al. [31] does not agree with our results and the other available literature data. However, their standard entropy of pavonite ( $367.5 \pm 16.5 \text{ J}\cdot(\text{K}\cdot\text{mol})^{-1}$ ) is in fair agreement with the result obtained for sulphur-saturated pavonite in this study [III] ( $372.7 \pm 2.8 \text{ J}\cdot(\text{K}\cdot\text{mol})^{-1}$ ).

The obtained thermodynamic properties of matildite are also in a reasonable agreement with selected literature values. Below  $T = 464$  K, new experimental

thermodynamic functions for matildite saturated with bismuth and saturated with sulphur were obtained.

For the first time, thermodynamic functions for schapbachite saturated with bismuth ( $\alpha$ -AgBi<sub>1+x</sub>S<sub>2</sub>) were experimentally determined [V]. In the absence of enough experimental thermodynamic data in the available literature sources, the results obtained at bismuth saturation were compared mainly with the values calculated by the Craig and Barton [32] approximation method. Taking into account compositional differences, the value  $\Delta_{tr}H^{\beta \rightarrow \alpha}(\text{AgBi}_{1+x}\text{S}_2) = 7.3 \pm 2.1 \text{ kJ}\cdot\text{mol}^{-1}$  obtained from  $\Delta_rG^\circ$  vs.  $T$  relations in [V], at  $465.55 \pm 5 \text{ K}$ , is in good agreement with the value  $\Delta_{tr}H^{\beta \rightarrow \alpha}(\text{AgBiS}_2) = 10.5 \pm 4.6 \text{ kJ}\cdot\text{mol}^{-1}$  determined by the high-temperature direct synthesis calorimetry of Bryndzia and Kleppa [28], at  $468.15 \text{ K}$ .

The differences observed among the calculated values, the literature values and the values obtained from our experimental studies mainly came from the different compositions of pavonite, matildite and schapbachite. For instance, the results obtained in our experimental studies of matildite [IV] in equilibrium with sulphur ( $\beta$ -AgBiS<sub>2+y</sub>) and bismuth ( $\beta$ -AgBi<sub>1+x</sub>S<sub>2</sub>) have clearly shown that slightly different compositions of matildite have different thermodynamic properties. From the results obtained in [IV], it can be concluded that at the temperatures studied; even the small compositional variation is energetically significant, resulting in lower Gibbs energies for matildite saturated with bismuth, relative to those saturated with sulphur. In general, the results obtained in the temperature range 298–699 K indicate that pavonite, matildite and schapbachite saturated with bismuth are more stable than those saturated with sulphur. However, our calculations above  $T = 580 \text{ K}$  and ambient pressure conditions show that in the presence of S<sub>2</sub>(g), the stoichiometric schapbachite, or alternatively sulphur enriched schapbachite, is thermodynamically more stable than that of schapbachite saturated with bismuth.

Solid solubility limits for bismuth in the ternary phases of the Ag-Bi-S system were estimated by Craig [65] to be less than 1 mol. %. The solubility limits of sulphur in the ternary phases were not numerically reported, however, the extent of its solubility in AgBiS<sub>2+y</sub> at 623 K can be seen in Figure 2. Future phase equilibria studies including the cathode phase assemblage of this study [III–V] will determine the exact values of  $x$  and  $y$  as a function of temperature.

Thermodynamic properties of the other phases of interest in the silver-based systems, stromeyerite and the solid solution (Ag,Cu)<sub>2</sub>S<sub>ss</sub>, were studied in the temperature range 316–498 K. Below  $T = 348 \text{ K}$ , the standard Gibbs energies of formation of stromeyerite obtained are in good agreement with those experimental values reported by Schmidt et al. [112] and the values calculated by the Craig and Barton [32] approximation method. However, the analysis made by Schmidt et al. [112] did not consider the different phase stability regions of the coexisting phases. For the first time, thermodynamic properties of the solid solution (Ag,Cu)<sub>2</sub>S<sub>ss</sub> were also experimentally determined [VI].

## 7. References

1. F. Tesfaye, P. Taskinen, Phase equilibria and thermochemistry of selected sulfide systems in the pyrometallurgy of Ni and Cu, Aalto University publication series SCIENCE + TECHNOLOGY 5/2012, p. 51. ISBN (printed) 978-952-60-4531-3
2. E.A. Echmaeva, E.G. Osadchii, *Geo. of Ore Dep.* 51 (3) (2009) 247–258.
3. S. Fadda, M. Fiori, G.M. Silvana, Bulgarian Academy of Sciences, *Geochemistry, Mineralogy and Petrology*, Sofia 43 (2005) 79–84.
4. D.W. Pals, P. G. Spry, *Vatukoula, Fiji, Mineralogy and Petrology* 79 (2003) 285–307.
5. L.J. Cabri, *Econ. Geol.* 60 (8) (1965) 1565–1634.
6. J.R. Craig, W.R. Lee, *Econ. Geol.* 67 (1972) 373–377.
7. M.V. Voronin, E.G. Osadchii, *Econ. Geol.* 108 (2013) 1203–1210.
8. J.R. Craig, G. Kullerud, *Mineral. Deposita* 8 (1973), 81–91.
9. J.E. Hoffman, *J. Met.* 41 (6) (1989) 33–36.
10. H. Tashiro, M. Harigaya, Y. Kageyama, K. Ito, M. Shinotsuka, K. Tani, A. Watada, N. Yiwata, Y. Nakata, S. Emura, *Jpn. J. Appl. Phys.* 41 (2002) 3758–3759.
11. J.-H. Kim, D.-Y. Chung, D. Bile, S. Loo, J. Short, S.D. Mahanti, T. Hogan, M.G. Kanatzidis, *Chem. Mater.* 17 (2005) 3606–3614.
12. L.K. Samanta, S. Chatterjee, *Phys. State. Sol. B* 182 (1994) 85–89.
13. T. Thongtem, N. Tipcompor, S. Thongtem, *Mater. Lett.* 64 (2010) 755–758.
14. G.Z. Shen, D. Chen, K.B. Tang, Y.T. Qian, *J. Cryst. Growth* 252 (2003) 199–201.
15. J.Q. Wang, X.K. Yang, W.B. Hu, B. Li, J.M. Yan, J.J. Hu, *Chem. Commun.* 46 (2007) 4931–4933.
16. H. Liu, J. Zhong, X. Liang, J. Zhang, W. Xiang, *J. Alloys Compd.* 509 (2011) 267–272.
17. N.K. Allouche, N. Jebbari, C. Guasch, N.K. Turki, *J. Alloys Compd.* 501 (2010) 85–88.
18. M. Lei, P.G. Li, W.H. Tang, *J. Alloys Compd.* 509 (2011) 5020–5022.
19. J. Yan, J. Yu, W. Zhang, Y. Li, X. Yang, A. Li, X. Yang, W. Wang, J. Wang, *J. Mater. Sci.* 47 (2012) 4159–4166.
20. S.N. Guin, B. Kanishka, *Chem. Mater.* 25 (2013) 3225–3231.
21. A.N. Skomorokhov, D.M. Trots, S.G. Ovchinnikov, H. Fuess, *J. Phys.: Condens. Matter* 19 (2007) 1–12.
22. K. Kiukkola, Galvanic cells in metallurgical thermodynamics, Ph.D. thesis, Massachusetts Institute of Technology (MIT), Boston, USA, 1955, p. 140.
23. K. Kiukkola, C. Wagner, *J. Electrochem. Soc.* 104 (6) (1957) 379–387.
24. N. Valverde, *Z. physik. Chem.* 70 (1970) 113–127.
25. W. Sitte, A. Brunner, *Solid State Ionics* 28-30 (1988) 1324–1328.
26. E.A. Echmaeva, E.G. Osadchii, *Geochemistry, Mineralogy and Petrology*, Sofia 43 (2005) 75–78.

27. D.A. Chareev, E.A. Echmaeva, E. G. Osadchii, *Russian J. of Electrochemistry*, 43 (2007) 694–698.
28. L.T. Bryndzia, O.J. Kleppa, *Econ. Geol.* 83 (1988) 174–181.
29. J.A. Schmidt, A.E. Sagua, A. Robledo, *Mater. Chem. Phys.* 55 (1998) 84–88.
30. J.A. Schmidt, A.E. Sagua, M.R. Prat, *Mater. Chem. Phys.* 61 (1999) 153–155.
31. Yu.M. Shykhyyev, Yu.A. Yusibov, M.B. Babanly, *Thermodynamic properties of system Ag-Bi-S*, *News of Baku University, natural science series 1*, 1995, pp. 93–98.
32. J.R. Craig, P.B. Barton, *Econ. Geol.* 68 (1973) 493–506.
33. R. Schenck, I. Hoffman, W. Knepper, H. Vogler, *Z. Anorg. Allg. Chem.* 240 (1939) 173–195.
34. R. Schenck, P. Von Der Forst, *Z. Anorg. Allg. Chem.* 241 (1939) 145–157.
35. H. Ipsier, A. Mikula, I. Katayama, *CALPHAD* 34 (2010) 271–278.
36. N.B. Hannay (Ed.), *Treatise on solid state chemistry, Reactivity of solids*, Plenum press, New York-London, vol. 3, 1976, pp. 291–292.
37. O. Kubaschewski, C.B. Alcock, *Metallurgical thermochemistry, International Series on Metallurgical Science and Technology*, 5<sup>th</sup> edition, vol. 24, 1979, p. 449.
38. A. Mikula, in: Y.A. Chang, F. Sommer (Eds.), *Thermodynamics of Alloy Formation*, TMS, Warrendale, PA, 1997, p. 77.
39. A. Mikula, *JOM* 59 (1) (2007) 35–37.
40. Z. Moser, K. Fitzner, *Thermochim. Acta* 332 (1) (1999) 1–19.
41. R.E. Aune, P. Fredriksson, S. Seetharaman, *J. of Mining and Metallurgy*, 38 B (2002) 213–227.
42. S.A. Kissin, S.D. Scott, *Am. Mineral.* 64 (1979) 1306–1310.
43. C. Tubandt, *Z. Anorg. Allg. Chem.* 115 (1921) 105–126.
44. M. Tatsumisago, T. Saito, T. Minami, *Thermochim Acta* 280/281 (1996) 333–341.
45. C.B. Choudhary, H.S. Maiti, E.C. Subbarao, *Defect structure and transport properties*, in: E.C. Subbarao (Ed.), *Solid electrolytes and their applications*, Plenum Press, New York–London, 1980, pp. 1–80.
46. M.R. Johan, S.L. Tay, N.L. Hawari, S. Suan, *Int J. Electrochem. Sci.* 6 (2011) 6235–6243.
47. S. Geller, in: S. Geller (Ed.), *Solid electrolytes, Topics in Applied Physics* 21, Springer-Verlag, New York, 1977.
48. W.V. Johnston, H. Wiedersich, G.W. Lindberg, *J. Chem. Phys.* 51 (1969) 3739–3747.
49. S. Hull, D.A. Keen, D.S. Sivia, P. Berastegui, *J. Solid State Chem.* 165 (2002) 363–371.
50. H. Sato, in: S. Geller (Ed.) *Solid electrolytes, Topics in Applied Physics*, Springer-Verlag, Berlin, Heidelberg, New York, 1977.
51. C. Seok, W. Oxtoby, *Phys. Rev. B* 56 (1997) 11485–11492.
52. H. Wiedersich, S. Geller, in: L. Eyring, M. O'Keefe (Eds.), *The chemistry of extended defects in non-metallic solids*, North-Holland, Amsterdam (1970).
53. C. Tubandt, H. Reinhold, *Z. Elektrochem.* 29 (1923) 313–317.

54. B.B. Owens, J.E. Oxley, A.F. Sammells, Application of halogenide solid electrolytes, in: S. Geller (Ed.), *Solid electrolytes, Topics in Applied Physics*, Springer-Verlag, Berlin, Heidelberg, New York, vol. 21, 1977, pp. 67–104.
55. J.W. Patterson, *J. Electrochem. Soc.* 118 (1971) 1033–1039.
56. I. Barin, *Thermochemical data of pure substances, part I and II*, VCH Verlagsgesellschaft, Weinheim/VCH Publishers, New York, 1989.
57. I. Karakaya, W.T. Thompson, *J. Phase Equil.* 12 (1991) 56–63.
58. F.C. Kracek, C.J. Ksanda, L.J. Cabri, *The Am. Mineral.* 51 (1966) 14–28.
59. V.M. Glazov, A.S. Burkhanov, *Izv. Akad. Nauk SSSR, Neorg. Mater.* 16 (1980) 373–391.
60. W. Gierlotka, *J. Alloys Compd.* 485 (2009) 231–235.
61. F. Roesder, *Zeit. Anorg. Chem.* 9 (1895) 31–77.
62. E.W. Nuffidd, *Amer. Min.* 39 (1954) 409–415.
63. H.F. Van Hook, *Econ. Geol.* 55 (1960) 759–788.
64. L.L.Y. Chang, D. Wu, C.R. Knowles, *Econ. Geol.* 83 (1988) 405–418.
65. J.R. Craig, *Mineralium. Depozita.* 1 (4) (1967) 278–305.
66. D. Wu, *Acta Mineralogica Sinica.* 9 (1989) 126–132.
67. B. Gather, R. Blachnik, *J. Less-Common Met.* 70 (1980) 11–24.
68. R. Schenk, H. Pardun, *Z. Anorg. Allg. Chemie* 211 (1933) 209–221.
69. A. Sabbar, A. Zrineh, J.P. Dubes, M. Gambino, J.P. Bros, G. Borzone, *Thermochim. Acta* 395 (2003) 47–58.
70. I. Karakaya, W.T. Thompson, *J. Phase Equil.* 14 (1993) 525–526.
71. M. Hansen, K. Anderko, *Constitution of binary alloys*, 2<sup>nd</sup> edition, McGraw-Hill, New York, 1958.
72. F.C. Kracek, *Trans. Am. Geophys. Union* 27 (1946) 364–374.
73. S. Djurle, *Acta Chem. Stand.* 12 (1958) 1427–1436.
74. J.–C. Lin, R.C. Sharma, Y.A. Chang, in: T.B. Massalski (Ed.), *Binary alloy phase diagrams*, ASM, USA, 1990.
75. H.F. Van Hook, *Econ. Geol.* 55 (1960) 759–788.
76. S. Geller, J.H. Wernik, *Acta Cryst.* 12 (1959) 46–54.
77. D. Wu, *Chin. J. Geochem.* 6 (1987) 216–224.
78. R.H. Davies, A.T. Dinsdale, J.A. Gisby, J.A.J. Robinson, S.M. Martin, *CALPHAD* 26 (2002) 229–271.
79. D.J. Chakrabarti, D.E. Laughlin, Cu-S (Copper-Sulfur), in: T.B. Massalski, H. Okamoto, L. Kacprzak (Eds.), *Binary alloy phase diagrams*, ASM, USA, 1990, pp. 1467–1471.
80. M. Fleet, *Phase Equilibria at High Temperature, Rev. Mineral. Geochem.* 61 (2006) 365–419.
81. D. Wu, *Chin. J. Geochem.* 6 (1987) 225–233.
82. Y.A. Chang et al., *Phase diagrams and thermodynamic properties of ternary copper-sulfur-metal systems (Inra Monograph VII, The Metallurgy of Copper, 1979)*, p. 191.
83. B.J. Skinner, *Econ. Geol.* 61 (1966) 1–26.
84. A.J. Frueh, Jr, *Z. Kristallogr.*, 106 (1955), 299–307.
85. Y. Takuhara, K. Tezuka, Y.J. Shan, and H. Imoto, *J. of Ceramic Society of Japan*, 117 (2009) 359–362.

86. C. García, J.I. Franco, J.C. López Tonazzi, N.E. Walsøe De Reca, *Solid State Ionics* 9-10 (1983) 1233–1236.
87. H. Okamoto, Bi-Pt (Bismuth-Platinum), in: T.B. Massalski, H. Okamoto, L. Kacprzak (Eds.), *Binary alloy phase diagrams*, ASM, USA, 1990, pp. 777–778.
88. F.M. Mustafaev, F.I. Ismailov, A.S. Abbasov, *Izv. Akad. Nauk SSSR, Neorg. Mater.* 11 (1975) 1552–1555.
89. A.J. Freuh, *Am. Mineral.* 46 (1961) 655–660.
90. H. Reinhold, *Z. Electrochem.*, 40 (1934) 361–364.
91. T. Takahashi, O. Yamamoto, *J. Electrochem. Soc.* 117 (1970) 1–5.
92. M.J. Pool, *Trans. Metall. Soc. AIME*, 233 (1965) 1711–1715.
93. G. Bonnacaze, A. Lichanot, S. Gromb, *J. Phys. Chem. Solids* 44 (1983) 967–974.
94. K.C. Mills, *J. Chem. Thermodynamics* 4 (1972) 903–913.
95. M. Gobec, W. Sitte, *J. Alloys Compd.* 220 (1995) 152–156.
96. B. Eichler, H. Rossbach and H. Gäggeler, *J. Less-Common Met.* 163 (1990) 297–310.
97. A.S. Abbasov, F.M. Mustafaev, *Khim. Suyaz Krist. Poluprovodn. Polimet* 235 (1973).
98. R. Castanet, M. Laffitte, *Rev. Int. Hautes. Temp. Réfract.* 11 (1974) 103–107.
99. R. Hultgren, P.D. Desai, D.T. Hawkins, M. Gleiser, K.K. Kelly, D.D. Wagman, *Selected values of the thermodynamic properties of the elements*, ASM., Metal Park, OH, 1973.
100. D. Feng, P. Taskinen, F. Tesfaye, *Solid State Ionics* 231 (2013) 1–4.
101. M. Kano, *J. Phys. E: Sci. Instrum.* 22 (1989) 907–912.
102. D.G. Archer, *J. Chem. Eng. Data* 49 (2004) 1364–1367.
103. F. Wüst, A. Meuthen, R. Durrer, *Die Temperatur-Wärmeeinhaltskurven der technisch wichtigen Metalle Reihe*, *Forsch. Gebiete Ingenieurw. VDI* 204 (1918).
104. I. Itaka, *Variation of the specific heat during melting and the heat of fusion of some metals*, *Science Reports, Tohoku Imp. Univ.* 8 (1919) 99–114.
105. R.C. Sharma, Y.A. Chang, Ag-S (Silver-Sulfur), in: T.B. Massalski, H. Okamoto, L. Kacprzak (Eds.), *Binary Alloy Phase Diagrams*, ASM, USA, 1990, pp. 86–87.
106. Z. Černošek, J. Holubová, E. Černošková, A. Růžička, *J. of Non-Oxide Glasses* 1 (2009) 38–42.
107. J.N. Brønsted, *Z. Physik. Chem.* 55 (1906) 371–382.
108. G.N. Lewis, M. Randall, *J. Am. Chem. Soc.* 33 (1911) 476–488.
109. B. Mahammad, Y. Yusif, B. Nizameddin, *The EMF method with solid-state electrolyte in the thermodynamic investigation of ternary copper and silver chalcogenides*, in: K. Sadik (Eds.), *Electromotive force and measurement in several systems*, *InTech*, 2011, pp. 57–78. DOI: 10.5772/2109
110. L.B. Pankratz, A.D. Mah, S.W. Watson, *Thermodynamic properties of sulfides*, *BuMines Bull.* 689, 1987, pp. 61–64.
111. G. Damian, C.L. Ciobanu, N.J. Cook, F. Damian, *Neues Jb. Miner. Abh.* 185 (2008) 199–213.
112. J.A. Schmidt, A.E. Sagua, *J. Chem. Thermodynamics*, 25 (1993) 1453–1459.



ISBN 978-952-60-5763-7  
ISBN 978-952-60-5764-4 (pdf)  
ISSN-L 1799-4934  
ISSN 1799-4934  
ISSN 1799-4942 (pdf)

**Aalto University**  
**School of Chemical Technology**  
**Department of Materials Science and Engineering**  
[www.aalto.fi](http://www.aalto.fi)

**BUSINESS +  
ECONOMY**

**ART +  
DESIGN +  
ARCHITECTURE**

**SCIENCE +  
TECHNOLOGY**

**CROSSOVER**

**DOCTORAL  
DISSERTATIONS**